TECHNICKÁ UNIVERZITA V LIBERCI
**Fakulta textilní**

# Tkaniny se zvýšenou odolností proti prořezání

## Disertační práce

*Studijní program:*   P3106 – Textile Engineering
*Studijní obor:*      3106V015 – Textile Technics and Materials Engineering

*Autor práce:*        **Muhammad Usman Javaid**
*Vedoucí práce:*      Ing. Jana Salačová, Ph.D.

Liberec 2019

TECHNICAL UNIVERSITY OF LIBEREC
**Faculty of Textile Engineering**

# Knife Stabbing Resistance of Woven Fabrics

## Dissertation

*Study programme:*    P3106 – Textile Engineering
*Study branch:*       3106V015 – Textile Technics and Materials Engineering

*Author:*       **Muhammad Usman Javaid**
*Supervisor:*   Ing. Jana Salačová, Ph.D.

Liberec 2019

# Declaration

I hereby certify I have been informed that my dissertation is fully governed by Act No. 121/2000 Coll., the Copyright Act, in particular Article 60 – School Work.

I acknowledge that the Technical University of Liberec (TUL) does not infringe my copyrights by using my dissertation for the TUL's internal purposes.

I am aware of my obligation to inform the TUL on having used or granted license to use the results of my dissertation; in such a case the TUL may require reimbursement of the costs incurred for creating the result up to their actual amount.

I have written my dissertation myself using the literature listed below and consulting it with my thesis supervisor and my tutor.

At the same time, I honestly declare that the texts of the printed version of my dissertation and of the electronic version uploaded into the IS STAG are identical.

29. 4. 2019                                     Muhammad Usman Javaid

*Dedication*

*I dedicate my work to my wife and kids, who suffered my absence and remain supporting and patient.*

# Acknowledgment

# TABLE OF CONTENTS

# LIST OF FIGURES

# LIST OF TABLES

# List of Symbols / Abbreviations

## Abbreviations

| | |
|---|---|
| QSKPR | Quasi-Static Knife Penetration Resistance |
| DSR | Dynamic Stab Resistance |
| WG | Water Glass |
| KPA | Knife Penetration Resistance |
| PE | Penetration Energy |
| SA | Stacking Angle |
| SRA | Surface Roughness Amplitude |
| SRW | Surface Roughness Wavelength |
| BR | Bending Rigidity |
| LSCM | Laser Scan Confocal Microscope |

## Symbols

| | |
|---|---|
| $tr$ | Knife edge travel during penetration (*mm*) |
| $\mu_s$ | Fabric friction |
| $\mu$ | Coefficient of fabric between two yarns |
| $\alpha$ | Knife penetration angle (*degree*) |
| $\theta$ | Yarn to yarn contact angle (*degree*) |
| $\varphi$ | Yarn axis angle with plane of the fabric (*degree*) |
| $\sigma$ | Yarn tensile strength in (*cN/tex*) |
| $R_{st}$ | Quasi-static knife penetration resistance (*N*) |
| $T$ | Tension in the yarn (*N*) |
| $R$ | Yarn sliding resistance (*N*) |
| $F$ | Force applied (*N*) |
| $Rad$ | Radian |
| $M$ | Moments of rotation (*gf.mm*) |
| $BR$ | Bending Rigidity of fabric (*gf.mm/rad*) |
| $b$ | Bending modulus of yarn |
| $p$ | Pick spacing (*mm*) |
| $\rho$ | Density (*kg/m³*) |
| $l$ | Strained length of yarn (*mm*) |
| $c_0$, $c_1$, $c_2$ | Coefficient of the Fourier function |
| X, x | Distance / displacement (*μm*) |

**ABSTRACT**

This research focused on the stabbing response of woven fabrics. Woven fabric investigated in this work had an equal set of warp and weft Twaron® para-Aramid filament yarns. In this work, isotropy of single sheet and multiple-sheets stacked together was analyzed at different orientations of knife stabbing. During knife stabbing a knife penetration angle (KPA) is formed between the knife cutting axis and warp yarn of the fabric. The study was conducted at five different cutting angles i.e. 0°, 22.5°, 45°, 67.5°, and 90°. Quasi-static knife penetration resistance (QSKPR) and dynamic stab resistance (DSR) of the woven fabrics were studied in this work.

The main objective of this research was to study the behavior of dry woven fabrics whose surface was modified to change their friction. The selection and application of these modifications were made in such a way to keep the comfort and flexibility characteristics minimally affected. We adopted three surface modification techniques; 1) $SiO_2$ deposition, 2) Ozone treatment along with $SiO_2$ deposition and 3) $TiO_2$ deposition. Furthermore, the effect of treatment was characterized against surface topology, anti-stabbing behavior, mechanical, comfort and friction properties of developed fabrics.

This research discovered a new method of $SiO_2$ deposition, using Water Glass (WG) as a precursor. The deposition of $SiO_2$ was investigated and confirmed using Scanning Electron Microscopy (SEM), Fourier Transfer Infra-Red (FTIR) spectroscopy, and Energy-Dispersive X-ray (EDX) spectroscopy. The concentration of WG showed the direct relation for an increase in QSKPR. At 40% solution of WG the QSKPR was observed about 200%.

The QSKPR measured at 67.5° KPA for untreated fabric was found statistically significantly higher than the mean QSKPR measured for all KPAs. Moreover, the QSKPR seems to follow a specific pattern for different KPAs, irrespective of fabric treatment.

The coefficient of friction of fabric surface was well improved by the deposition layer of $SiO_2$. Hence, the yarn pull-out force was increased for treated fabrics as compared to untreated. It was also observed that, treatment with Ozone before depositing $SiO_2$, reduces the adverse effect on comfort and flexibility characteristics of fabric.

The quasi-static stabbing was found to be the complementary response to warp and weft yarns, due to their orthogonal orientation. This response was modelled with the Fourier function, that fits well to the quasi-static stab of different fabrics. It was also observed that the behaviour of this response is directly proportional to fabric's coefficient of friction and inversely proportional to the gap between yarns.

The interaction of the knife and the fabric was recorded on CCD camera, during QSKPR measurements. It was observed that the shape of the knife profile plays a major role. The blunt edge of the knife finds maximum resistance and causes the major peak in the force-displacement curve. While after the complete penetration of blunt edge, individual yarns cut one by one. It is proposed that $SiO_2$ deposition increases inter-fiber friction, as a result the filaments of the yarn behave as single assembly rather as individual filament against the sharp edge of the knife.

Yarn sliding resistance, individual yarn cutting behaviour and yarn pull out force was measured for warp and weft directions of treated and untreated fabrics. It was found that the major response of stabbing resistance depends upon inter yarn friction, while intra-yarn friction accounts for penetration energy of individual yarn.

QSKPR was measured for two sheets, oriented at three stacking angles (SA). The 45° SA was found to exhibit better response of QSKPR than 0°and 90° SA. A modified version of NIJ standard–0115.00 was followed to verify the dynamic stab resistance at 45° SA. It was found that 45° SA exhibits isotropic stab resistance in all KPAs. Furthermore, treated fabrics showed 200% higher stab resistance than untreated fabrics.

## Abstrakt

Tato práce je zaměřena konstrukci a hodnocení vlastností vrstvených textilních struktur s zvýšenou odolností proti pronikání nožů. Každá vrstva je tkaná textilie vyrobená z para-aramidového vlákna Twaron® se stejnou dostavou ve směru osnovy a útku. Je analyzována anizotropie odporu proti pronikání nože jedné i vice vrstev tkaniny. Orientace odporu proti pronikání je charakterizována úhlem penetrace nože (KPA) mezi osou řezání nožem a směrem osnovy tkaniny. Tento úhel byl měněn v pěti směrech řezu, tedy 0°; 22,5°; 45°; 67,5° a 90°. Byla zkoumána kvazi-statická odolnost proti pronikání nože (QSKPR) a dynamická odolnost proti pronikání nože (DSR) tkaninou.

Základním cílem této práce je úprava povrchu vláken tak, aby se změnily jejich třecí vlastnosti. Výběr a aplikaci těchto úprav je třeba provést tak, aby nebyly negativně ovlivněny vlastnosti charakterizující komfort. Byly použity tři postupy modifikace povrchu vláken, které byly detailně ověřovány. Jedná se o depozici oxidu křemičitého ($SiO_2$) na povrch textilie, dále vystavení textilie působení ozónu spolu s depozicí $SiO_2$ a depozici oxidu titaničitého ($TiO_2$) na povrch textilie. Byly sledovány jednak mechanické vlastnosti upravené tkaniny, dále komfortní vlastnosti, odolnost proti bodání nožem a změny povrchu vláken.

Byla vyvinuta nová metoda pro aplikaci $SiO_2$ na povrch textilie s použitím vodního skla (WG) jako prekurzoru. Depozice $SiO_2$ byla analyzována a potvrzená pomocí skenovací elektronové mikroskopie (SEM), infračervené spektroskopie s Fourierovou transformací (FTIR) a spektroskopie rentgenového spektra (EDX). Byla nalezena významná souvislost mezi koncentrací WG a růstem QSKPR. Při koncentrací 40% WG došlo ke zvýšení QSKPR o více než 200%. Navíc se ukázalo, že pro neupravené tkaniny vykazuje QSKPR specifický průběh pro různá KPA.

Depozice $SiO_2$ na tkaninu zvýšila koeficient tření vláken v tkanině. Ukázalo se, že u upraveného vzorku je třeba vyšší síly k rozestoupení přízí v tkanině než u vzorku neupraveného. Zvýšení koeficientu tření vláken ve tkanině s deponovaným $SiO_2$ bylo srovnatelné s tkaninou vystavenou působení ozónu s naneseným $SiO_2$. Nicméně u tkanin s naneseným $SiO_2$ byla zjištěna relativně vyšší ohybová tuhost.

Bylo zjištěno, že kvazi-statické pronikání nože je silně ovlivněno interakcí osnovních a útkových nití, což bylo popsáno modelem na bázi Fourierovy řady. Tento model se dobře hodí pro hodnocení kvazi-statického pronikání nože pro různé tkaniny. Bylo také ověřeno, že kvazi-statické pronikání nože je přímo úměrné součiniteli tření tkaniny a nepřímo úměrné vzdálenosti mezi nitěmi.

Rozdíly v chování upravené a neupravené tkaniny při pronikání nože byly analyzovány pomocí CCD kamery během QSKPR měření. Bylo pozorováno, že klíčovou roli hraje profil nože. Tupá hrana nože zvyšuje odpor a na křivce tlakové síly způsobuje výrazný pík. Naopak po úplném proniknutí tupého kraje nože jsou jednotlivé nitě přeříznuty jedna za druhou. Lze konstatovat, že depozice částic $SiO_2$ zvyšuje tření mezi vlákny uvnitř příze, a proto se vlákna v upravené přízi chovají jako jednolitá masa proti ostré hraně nože.

Byl měřen odpor příze proti prokluzu, chování příze při řezání a síla nutná pro vytažení příze z tkaniny ve směru osnovy i útku v upravené a neupravené tkanině. Vyšší odolnost proti kvazi-statickému pronikání nože vykazuje osnova ve srovnání s útkem v obou textiliích (upravené i neupravené).

QSKPR byla měřena také na dvou vrstvách orientovaných vzájemně pod různým úhlem kladení (SA) tj. 0°, 45° a 90°. Bylo zjištěno, že SA 45° vykazuje relativně lepší odolnost proti kvazi-statickému pronikání nože do tkaniny. Stejné vrstvy případ byly vyhodnoceny pomocí testu podle modifikované normy NIJ-0115.00. Bylo zjištěno, že 45° SA vykazuje nejlepší odolnost proti kvazi-statickému pronikání nože ve všech KPA. Upravené textilní struktury vykazují dvakrát vyšší odolnost proti kvazi-statickému pronikání nože než neupravené.


**Klíčová slova:** odpor proti prořezání; Oxid křemičitý; Oxid titaničitý; Ozón; Aramidy; vrstvené textilní struktury; vodní sklo

# خلاصہ

اس تحقیق میں کپڑے پر چاقوزنی کے ردّعمل کے بارے میں توجہ مرکوز کی گئی ۔ اس کاوش میں مطالعہ کیے جانے والے کپڑے کے تانے اور بانے کی ایک جتنی مقدار کے تھے اور وہ ٹوارون ائیرامڈ کے فلامنٹ ریشوں سے بنائے گئے تھے ۔ اس کام میں یک ورقی اور کثیرورقی دستہ کی ہمسانگردی کا معائنہ کیا گیا ، جبکہ چاقو کی جہت تبدیل کی گئی ۔ چاقو زنّی کے دوران چاقو کے کائٹ کی سمت سے کپڑے کے تانے کی سمت کے درمیان بننے والے زاویے کو چاقو کے دخول کا زاویہ(کے پی اے)کہا گیا ہے ۔ اس تحقیق کو کائٹ کی سمت کو پانچ زاویوں °0 ، °22.5 ، °45 ، °67.5 اور °90 میں تبدیل کیا گیا ۔ اس کام میں کپڑے کی نیم جامد چاقو زنی کی مزاحمت (قیو ایس کے پی آر) اور متحرک چاقو زنی کی مزاحمت (ڈی ایس آر) کا مطالعہ کیا گیا ہے ۔

اس تحقیق کا بنیادی مقصد خشک کپڑے کے رویّے کا مطالعہ کرنا تھا جبکہ کپڑے کی سطح کو اس طرح تبدیل کر کے اس کی رگڑ کو بڑھایا گیا ہو۔ ان تبدیلیوں کا انتخاب اور استعمال اس طرح سے کیا گیا کہ آرام اور لچک کو کم س کم متاثر کیا جائے ۔ تین تبدیلیوں کا مطالعہ کیا گیا۔ ۱)۔ سیلیکان آکسائیڈ کی تہ ۲) اوزون سے بدلواؤ کے ساتھ سیلیکان ڈائی آکسائیڈ کے تہ اور ۳)ٹائٹینیم ڈائی آکسائیڈ کی تہ ۔مزید براں ، تبدیل شدہ کپڑے کے چاقو زنّی کے ردّعمل کے ساتھ اسکے مکانکی ، آرام دہی اور سطح کے خدّوخال کی خصوصیات کا مطالعہ کیا گیا۔

اس کام میں ، وائر گلاس (ڈبلیو جی) کا استعمال کرتے ہوئے ، سیلیکان ڈائی آکسائیڈ کی تہ جمانے کا نیا طریقہ دریافت کیا گیا ہے ۔سیلیکان ڈائی آکسائیڈ کی جمائی گئی اس تہ کی تصدیق سیکننگ الیکٹران مائیکروسکوپ(سیم) ، فورئیر ٹرانسفارم انفرارڈ (ایف ٹی آئی آر) سپیکٹروسکوپی اور بائی انرجی الیکٹران ڈیسپرس ایکسرے (ای ڈی ایکس)سپیکٹروسکوپی سے کی گئی ۔ ڈبلیو جی کے تناسب کا کیو ایس کے پی آرکے ساتھ براہ راست تعلق پایا گیا ۔ڈبلیو جی کا 40 فیصد تناسب پر قیو ایس کے پی آر میں 200 فیصد اضافہ پایا گیا ۔

سادہ کپڑے کی قیو اس کے پی آر جو کہ °67.5 پر ماپی گئ اعداد و شمار کے لحاظ سے اہم طریقہ سے تمام کے پی اے کے اوسط قیو اس کے پی آر سے زیادہ ہے ۔ اور یہ بھی کہ ،قطع نظر کے کہ ،کونسا کپڑا ہے ، قیو اس کے پی آر مختلف کے پی اے کے کے لیے ایک خاص ترتیب کے مطابق ہے ۔

سیلیکان ڈائی آکسائیڈ لگانے سے کپڑے کی رگڑمیں خاطرخواہ اضافہ ہوتا ہے ۔ پس ، سادہ اور تبدیل شدّہ کپڑے سے دھاگا باہر کھینچنے کی مزاحمت میں اضافہ پایا گیا ۔ یہ بھی دیکھا گیا کہ سلیکان لگانے سے پہلے اوزون لگانے سےکپڑے کی آرامدہ اور لچک کی خصوصیات پر برے اثرات کم ہوجاتے ہیں ۔

یہ معلوم ہوا کہ نیم جامد چاقو زنّی کی مزاحمت تانی اور بانی سے مل کر بنتی ہے ۔ اس اثر کو فورئیر فنگشن سے ماڈل کیا گیا ، جو مختلف کپڑوں کی نیم جامد مزاحمت کے ساتھ متفق پایا گیا ۔ یہ بھی دیکھا گیا کہ نیم جامد مزاحمت کپڑے کے ضریب اصطکاک کے براہ راست متناسب ہے اور دھاگو ں کے درمیان فاصلے کے معکوس متناسب ہے ۔

متغیرشدہ اور سادہ کپڑے کے چاقو زنّی کے رویّے کا معائنہ سی سی ڈی ویڈیو سے کیا گیا جو کہ قیو ایس کے پی آر پیمائش کرنے کے دوران بنائی گئ ۔ یہ ایّاں ہوا کہ چاقو کی شکل اہم کردار ادا کرتی ہے ۔چاقو کا کند کنارہ زیادہ تر مزاحمت کا سامنا کرتا ہے اور فورس-ڈسپلیسمنٹ کروو میں بڑی اوج کا باعث ہوتا ہے ۔ تاہم کند کنارہ گزرجانے کے بعد دھاگے ایک ایک کر کے کٹ جاتے ہیں ۔ یہ متعین کیا گیا کہ سیلیکان ڈائی آکسائیڈ کی تہ ریشوں کے درمیان (دھاگوں کے اندر) رگڑ کو بڑھاتی ہے جس سے ریشے چاقو سے مزاحمت کے خلاف ایک ہی گروہ کی طرح کا رویہ اپناتے ہیں نہ کہ ہر ایک ریشہ الگ اگ ۔

دھاگے کی کھسکنے کی مزاحمت ، اکیلے دھاگے کے کٹنے کا رجھان اور دھاگا باہر کھینچنے کی طاقت کی پیمائش سادہ اور تبدیل شدّہ کپڑوں کے تانی اور بانی کے لیے کی گئی ۔یہ معلوم ہوا کہ چاقو زنّی کے خلاف مزاحمت دھاگوں کے درمیان رگڑ پر منحصر ہے ، جبکہ ہر دھاگے کی طاقت ریشوں کے درمیان رگڑ پر منحصر ہے ۔

قیو ایس کے پی آر دو تہی جتھہ کے تہی جتھے کے لیےمختلف تہی زاویوں (ایس اے) ،یعنی کہ °0 ، °45 اور °90 ، پر ماپی گئی ۔45 درجہ ایس اے نے مقابلاًابہتر ہمساندگی پر قیو ایس کے پی آر ظاہر کی جبکہ چاق زنّی کے خلاف مزاحمت سب سے زیادہ تھی ۔ ڈراپ-ٹاور ٹیسٹ ، تبدیل شدہ این-آئی-جے سٹینڈرڈ 0115.00 ، کے مطابق کیا گیا ۔ یہ معلوم ہوا کہ 45 درجہ ایس اےہمساندہ چاقو زنّی تمام کے پی اے پر فراہم کرتا ہے ۔ اور متغیر شدہ سادہ کپڑوں کے مقابلہ میں چاقو زنّی کی دوگناہ زیادہ مزاحمت ظاہر کرتے ہیں ۔

**کلیدی الفاظ:** چاقو زنّی ، سیلیکان ڈائی آکسائیڈ ، ٹائٹینیئم ڈائی آکسائیڈ ، اوزون ، آئیرامیڈ ، بناہوا کپڑا ، سوڈیم سیلیکیٹ ، وائر گلاس۔

# CHAPTER 1
## INTRODUCTION

## 1. Introduction

Protective textiles have become an important branch of technical textiles [1]. Textiles are playing a major role in wearables that assure life safety in various types of critical applications [2]. The introduction of gunpowder has changed the requirement of a body armour. The old solutions for body protection using metal and leather, silk or flak jacket armour became ineffective [3], [4]. Those solutions were no guarantee of life-saving against high-velocity gunfire or was bulky enough to restrict comfortable use [1]. The soft body light-weight armour became possible only after the birth of Kevlar® by DuPont™ in 1970s [5], [6].

In search of the best system of protection against ballistic threats, last few decades have produced considerable research on body protection armour. These armours are lighter than metallic armour solutions and easier to wear and carry. The solution was found in use of polymer-fiber composites, with synthetic fibers of high strength and high moduli like Dyneema®, Twaron®, and Kevlar® and thermoset polymer matrix. These solutions have better bulk properties and distribute the localized energy of impacting bullet to a larger area and dissipates its penetrating energy [7].

The latest requirement imposed on body protection armour is protection against sharp objects. Personal protection, against the attacks of sharp objects like the knife, has become increasingly important especially for police personnel [8]–[10]. The design of bullet resistant protection is different from the armour protecting against sharp objects like a knife or spike. In various condition of body protection against sharp objects and spikes is required. Such kind of attacks are evident where access to gunpowder and firearms is restricted by territory law, for example as in European countries or in prison facilities around the world [11], [12]. Generally, the bullet attacks are for army personals in some critical situation or in the battlefield, were the attack is expected. In contrast, sharp objects' attacks are unexpected, and the required period of protection is incessant and extended [13]. So, wearer's comfort also becomes a pre-requisite

of armour design to produce light-weight and comfortable armour [14]–[17]. Also, the diversity of protection against various types of threats makes it difficult for a single solution to be viable in different kinds of situations. Generally, bullet resistant armour may not protect against knives or spikes or vice versa [18].

The characteristics of fiber-polymer composite inherit from the qualities of fiber and polymer to provide synergy for protection [19], [20]. In this scenario, it becomes important to study the response of stab resistance at the level of textile itself. This work is an effort in this direction and it investigates the interaction of knife and fabric.

# CHAPTER 2
# AIMS AND OBJECTIVES

## 2. Aims and Objectives

### 2.1. To study stab resistance of para-Aramid woven fabrics at various knife penetration directions

Aramids are the one of the major class of fibres used in fiber-reinforced composites/laminates for soft and hard body protective systems [5]. And, it is proven that their longitudinal mechanical properties largely dominate their transverse characteristics. For example, compression, bending, and flexural properties are far weaker than tensile properties [21], [22]. The fiber damage results in delamination, cracking and fibrillation [23], [24]. However, it is preferably used in cut resistant and stab resistant application by commercial body protective products [25], [26]. The impact produced from symmetrical objects, like bullets in case of a ballistic protection and sharp protruded objects like ice-pick in case of a stab resistance, is homogenous and generally perpendicular impact resistance is measured and reported and relative angle change between impacting object and resistance surface is not focused [15]. However, for the case of the stabbing of the knife the impact can be in various directions. It can be a fruitful study to observe how a para-Aramid respond when at least transverse angle of yarn with a knife is changed.

The most frequently followed methods of testing stab resistance performance are a drop-weight tower and quasi-static penetration of a sharp object into target textile protection [28]. In both these cases, the reported work, for textile fabric-based protection, a very small numbers of studies mentioned the measured angle of knife penetration [9] or tried to find out the effect of change in relative angle between attacking object and protecting surface [5, 16, 18]. However, the effect of blade orientation with respect to a single fibre and the single yarn was studied, which proved sensitivity of change in force required to cut the fibres or yarns with a change in cutting angle [30]–[34]. Cutting resistance is itself an intrinsic property of material but the orientation of fibrous assemblies in textile structure, their geometry and interaction of

these elements within, can play a major role to improve cutting resistance. If we need to observe the cutting characteristics of textiles we need to see anisotropy at the material level (polymer and fibre level) and at textile structure level (yarn and fabric level). Since material level anisotropy is already highlight, there is a need to observe how woven fabric behave against change in orientation of knife stab.

## 2.2. To observe the interaction of knife and yarns of the fabrics

Out of the two methods of stab resistance measurements, the quasi-static method of loading provides the possibility of controlled perpendicular penetration. The provision of a pneumatic platform to hold the fabric in position, provides the ability to control the penetration at the specific orientation of knife blade with respect to the warp of the fabric. The results of stabbing are reproducible and provide the ability to record the interaction of knife and yarns of fabric on camera. While, the drop-weight tower is the accepted method of stab testing by NIJ, only measures if protection fails or not for given energy of penetration.

## 2.3. To observe the effect of change in friction on the stab resistance of fabrics

The force of friction is the major resistance against yarn movement and absorption of impact energy when no binding agent holds the yarns of fabric together. To change the friction between the surface of the yarn of woven fabrics were modified. But to keep the characteristics of soft body protection, the surface of fabrics was modified with minimal effect on their comfort properties, like air permeability and bending rigidity. The most economical ways of changing the surface for increased friction were adopted.

## 2.4. To observe the effect of stacking orientation and knife penetration direction

The orientation of different sheets in a stack, of multiple-layer laminate, can superimpose warp and weft of different sheets or can distribute them in different directions. It

would be beneficial to observe if the super-imposing or distributing warp and weft of different sheets in multiple-sheets helps to improve stab resistance.

# CHAPTER 3
# STATE OF THE ART

# 3. State of the Art

## 3.1. What is Stabbing?

The penetration of a sharp edge object into the attacked body is referred as stabbing; the penetration direction is perpendicular, and the stabbing tool can be a knife, sharp piece of glass or a sharp object like an ice pick, [35] the stabbing action is illustrated in Figure 1(a).

These objects have a very diminutive tip with increasing diameter or width of the object along its length. Consequently, the tip finds the smallest possibility of penetration and makes the structure of the penetrated objects split apart, upon further penetration. The energy exerted by attacking objects is divided in: 1) opening the structure and 2) in increasing the depth of penetration. In case, attacking object has sharp edges present along the length, it triggers fracture of fibers/yarns.

Along with the profile of the object also important is the energy of the penetrating object. This energy is related to the momentum carried by the object, so the mass and the velocity of the impacting object are important characteristics to study stab resistance [17], [36], [37].

Stabbing involves impacting the sharp object vertically to penetrate through the attacked body. The knife can have one or both edges sharp to cut through [35]. The knife tip angle, sharpness, thickness and penetration velocity can affect the damage produced [38], [39]. Different types of cutting involve different modes of failure mechanics, for example, cutting a fabric with scissors involves tension-shear mode, stabbing a knife across the fabric placed on a table involves shear-compression mode and slashing a gripped fabric involves tension-shear mode [40]. Impact loading is influenced by both intrinsic (tensile strength, elastic modulus, elongation to break) and extrinsic (interfacial friction between fibers and yarns) properties of a material [19].

Vertical Penetration

Sharp cutting edge is introduced along the penetrating length of knife. Therefore, knife edge and penetrated surface are perpendicular.

(a)

(b)

(c)

(d)
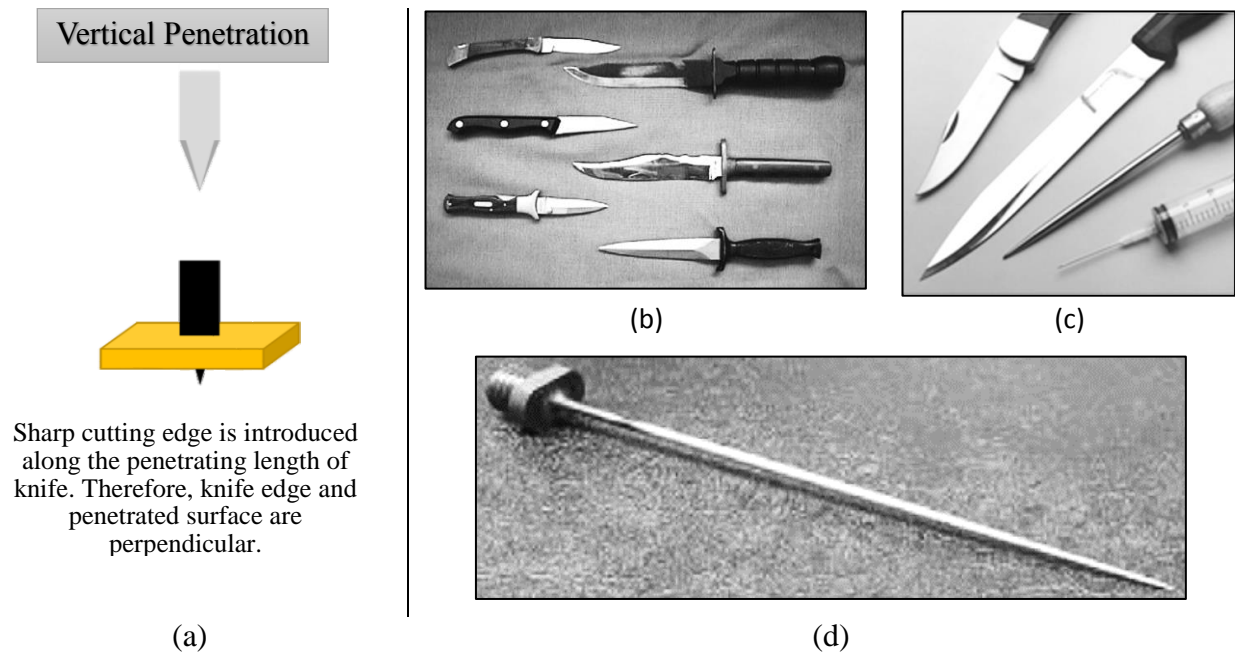
*Figure 1: (a) Knife Stabbing Action, (b) Various types of knives used for stabbing* [41]*, (c) Various type of stab threats* [16] *(d) Example of icepick* [13]

## 3.2. Types of Actions During Stabbing:

Close observation of knife edge and fabric interaction reveals that the knife plays following actions during fabric stabbing:

I.      Upon impact, the knife pushes the yarns towards its direction of penetration. The yarns are stressed and start advancing along knife. Displaced yarns observe a force similar like yarn pull-out.

II.     The tip of the blade lands on fabric either between the yarns or over a yarn. It creates the gap first by displacing the yarns, called yarn slippage, and then by cutting them called yarn fracture [42]–[44].

III.    Once one layer of fabric is penetrated, the knife keeps interacting with next stacking sheets. The overall response of protecting system is combined response of all individual stacking sheets of protective textile.

## 3.3. Stabbing Instruments

The foremost objective of the stabbing is to penetrate the attacked body for maximum damage. Therefore, the tool used to attack can include from very precisely engineered weapon

to very rough, handmade, self-improvised objects. Stabbing instruments can be of different shape, size and technique. Some illustration of these objects can be found in Figure 1(b).

### 3.4. Structure and properties of para-Aramids

One of the most popular high-performance fibre used for the protective application is poly(para-phenylene terephthalamide) (PPTA), available with commercial names like Kevlar® and Twaron® [7]. They are aromatic polyamides known as para-Aramids, that also includes *"a manufactured fiber in which the fiber forming substance is a long chain synthetic polyamide in which at least 85% of the amide (−CO−NH−) linkages are attached directly to two aromatic rings"* [5], [6]. Para-Aramids are high tenacity, high modulus fibres, they are gel spun from liquid crystalline solution, with a known structure as shown in Figure 2, and few of their mechanical properties are given in Table 1.
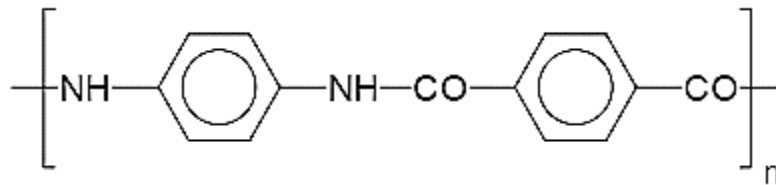


*Figure 2: Polymeric Structure of Twaron® (poly-para-Phenylene-terephthalamide) (PPTA)*

Table 1: Para-Aramids Mechanical Properties [5]

| Type of Fibber | Tenacity (*mN/tex*) | Initial modulus (*N/tex*) | Elongation at break (*%*) |
|---|---|---|---|
| Kevlar® 29 | 2030 | 49 | 3.6 |
| Kevlar® 49 | 2080 | 78 | 2.4 |
| Kevlar® 149 | 1680 | 115 | 1.3 |
| Twaron® | 2100 | 60 | 3.6 |
| Twaron® High-Modulus | 2100 | 75 | 2.5 |

Para-Aramids were first produced for tire reinforcement [5], [6], [30] they are very anisotropic fibres in nature and split readily when mechanically fractured [30], [34]. They are highly crystalline and have long straight chain molecules aligned parallel to the fiber axis. In transverse direction to the fiber axis, they have Van der Wall's and hydrogen bonding which accounts for fibrillization and anisotropy of fibre mechanical character. These fibres show

plastic deformation on compression that is the reason for their higher cutting strength and, therefore, is used in high impact protective textiles. [23]

The structure of PPTA crystal lattice is shown in Figure 3. It is observable that transverse plane, AB, having amide linkage, has a fewer density of covalent bonds than the plane, CD, having rings. Also, the amide linkage in the plane, AB, has a higher number of hydrogen bonding and, therefore, are firmer than the layer above and below to this plane (above and below the paper). That is the reason of anisotropy in a direction perpendicular to the fibre axis. Although fibre is highly crystalline and oriented at fine structure level, axial pleating of crystalline sheets exists in radial orientation as shown in Figure 4.

| | |
|---|---|
|  |  |
| *Figure 3: Showing molecular packing of PPTA crystal (a) hydrogen bonding in AB plane and absence in CD plane, (b) showing separate sheets when viewing along chains* [23] | *Figure 4: Radial pleated structure of para-Aramids* [23] |
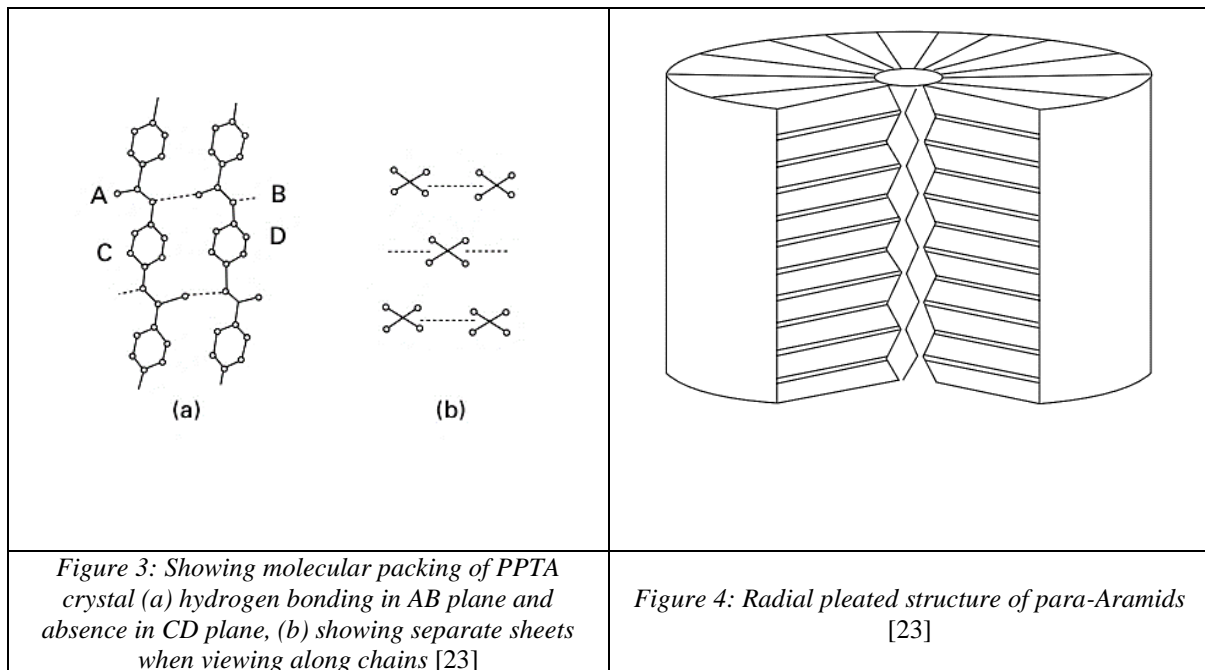
## 3.5. Commercial products of para-Aramids

The body protective armour applications are famous for using para-Aramid textiles. [28], [45], [46]. They provide superior impact and cut resistance properties and are extensively used in ballistic and stab protestation system both in research and in commercial products.[5] The famous manufacturer of Dupont™ for Kevlar® and Teijin™ for Twaron® have their respective ballistic protection system based on para-Aramid fibres. From, Teijin® it involves

ComForte ™ and AT Flex® for bullet protection vest with anti-trauma and SRM® and Mircroflex® for stab and spike resistance [25]. And, from Dupont Kevlar® XP™ for Soft Body Armor protection against bullets and Kevlar® Correctional™ to protecting against stab [26], [47].

### 3.6. Ballistic Resistance versus Stab Resistance

A ballistic resistant textile system requires the distribution of impact energy to dissipate along the stress wave, produced in the textile. A system with higher sound velocity through the medium, $c$ $[m/s]$, can better resist against ballistics threats, as is evident from Equation 1. To meet such requirement the fabrics used in these systems required adequate amount of yarn packing to produce the stress waves at higher speed [18]. Along with these requirements the ballistics system requires to impregnate the woven fabric in resin system to produce composite / laminates, that results harder, inflexible armour. Therefore, comfort and flexibility properties are severed. This phenomenon limits the length of use of such a protective system, mobility and performance of wearer is questioned. [48], [49]

$$c = \sqrt{\frac{E}{\rho}}$$

*1*

Here $c$ is the velocity of sound ($m/s$) in the medium, $E$ the elastic modulus ($N/m^2$ ), and $\rho$ the mass density ($kg/m^3$ ). This equation is valid for ideal solid with isotropic elasticity.



Ballistic fabrics enable yarn motions and do not prevent punctures

Dense, tightly woven fabrics restrict yarn motions and prevent defeat punctures
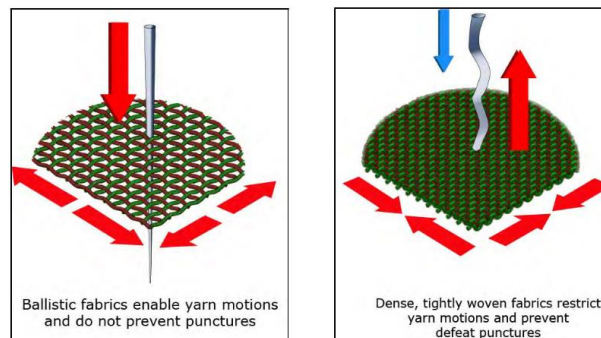
*Figure 5: Fabric requirement of Ballistic versus Stab resistant system* [18]

On the other hand, fabric requirement for anti-stabbing application is higher packing of yarns to resist against protruded and sharp objects, as illustrated in Figure 5. Therefore, not suitable for ballistic protection application unless multiple levels of protection are developed for various kind of threats separately.

It was mentioned by Shin & Shockey that higher sharpness of cutting edge of penetrating instrument cause cutting of fibres before tensile failure of the fibre [50]. As an application of impact load is concern, stabbing is a multi-directional phenomenon rather unidirectional or bidirectional phenomenon, because maintaining same initial modulus in all the direction is not possible.

### 3.7. Surface Modification Technologies Used to Enhance Stab Resistance

To increase the impact resistance of para-Aramid fibres against stabbing, their surface is modified. Following are some famous techniques followed to do so.

#### 3.7.1. Hard Particles Coating

The ceramics are the hardest martials. They are coated on the fabric surface to provide a layer of very hard surface yet maintaining the flexibility of the fabric. Few of such method can be found in literature that claim to improve stabbing resistance of protecting textile [51], [52]. However, depending upon the thickness such coating adds a considerable weight.  Most used ceramics for body protection systems are Alumina, SiC, $TiB_2$ and $B_4C$ [53], [54].

Gadow and Niessen [52] employed ceramic oxides and refractory cement by thermal spraying to increase the stabbing resistance of para-Aramid fabrics. While Gurgen and Kushan coated SiC particles with shear thickening fluid to enhance the stab resistance [20]. These particles increase the surface hardness of the textile and reduces the damage caused by the sharp edge of the impactor by turn it blunt.
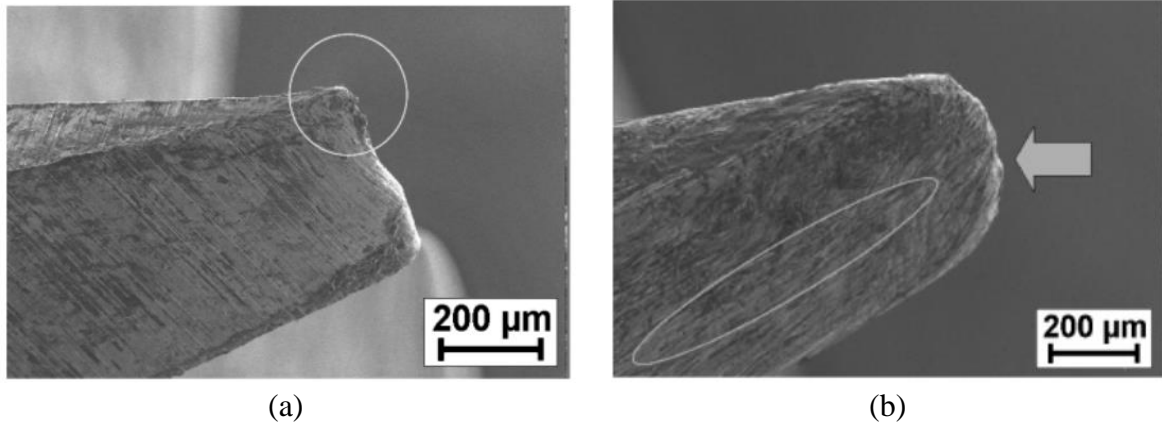
*Figure 6: Knife edge before (a) and after (b) six penetrations in ceramic coated textiles, reproduced from*
[52]

### 3.7.2. Shear Thickening Fluid (STF)

The basic principle of use of Shear Thickening Fluid (STF) is the ability of a non-Newtonian fluid to increase its viscosity with increasing rate of strain, in high impact resistant applications [55]–[60]. It is believed that beyond a certain strain rate of shearing, particles of the suspension group together to form hydro-clusters, those increase the viscosity drastically [61], [62]. For such STF, a colloidal suspension is required to be made between solid particles and an inert liquid. The particles can be of various kinds like silica, ceramic, carbonates, calcium, etc and liquids can be water, Ethylene-glycol, poly-Ethylene glycol etc [42].
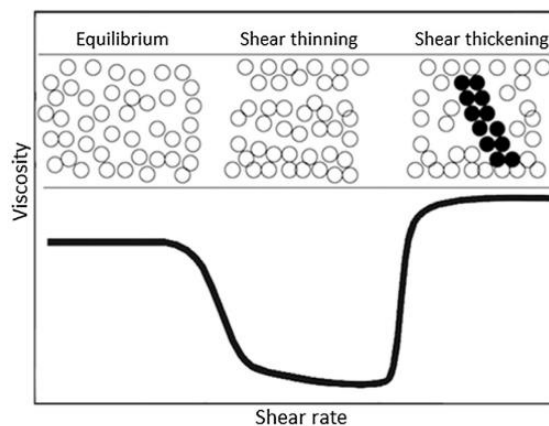


*Figure 7: Illustrating the behaviour of different suspensions showing shear thickening and thinning, reproduced from* [63]

A large number of scientific publication can be found to employee STF technique to enhance the stab resistance of protective textiles [13], [15], [16], [20], [63]–[67]. It has been

established that application of STF increases the friction characteristics, between the fibres in the yarns, between the yarns in the fabric and at the surface of the fabric [20], [67], [68]. The major role of STF is in restricting the movement of yarns and increasing the energy absorbing capacity against spikes and knife attacks. Another, view found in literature is the energy absorption of STF applied fabrics is due to their increased plastic flow and deformation [69].

### 3.7.3. Surface modification by different particles

Increasing the inter-yarn friction is an effective way of improving soft-body armour performance without losing its flexibility characteristics. The surface of fibres is modified to the smallest level. In this regard application of nanoparticles, nanowires or nanolayers are major investigated method. These methods increase the performance of armour many times without much addition to weight.

Hwang et al. [7] developed a method of growing ZnO nanowires on the surface of aramid fibres and found to achieve highly reduce immobility between yarns surface. Consequently, they reported about 23 times increase in energy absorption and about 11 times increase in peak load for yarn pull-out test.

## 3.8. Role of Inter-yarn friction on impact loading

It has already been established that friction plays a very important role in resistance against impact loading [7], [70]–[72]. Increasing inter yarn friction can improve the performance against impacting load without added weight [71], [73]. A study has also highlighted the importance of yarn to knife and yarn to yarn friction during stab resistance [74]. The cutting force is dependent on the frictional coefficient and the normal force at the point of cutting during knife penetration [75]. There is another study about the cutting behaviour of knife/blade when it slides normally through the fabric. The outcome of the study reveals that there are two types of friction; macroscopic gripping friction and friction at the blade tip due to cutting of material. As the energy required to break the molecular chains is much smaller,

most of the energy is dissipated in friction. Normal load produces friction at the edge of the blade. If the coefficient of friction between the blade tip and cutting point is increased the cutting resistance is reduced. But generally, the lateral gripping force is higher due to which the cutting resistance of the material is higher. Elastic modulus, the structure of material and velocity of the cutting blade significantly affect the friction and the resulting cutting resistance [31].

**3.9. Anisotropic behaviour of High Modulus fibres against sharp blades**

Mayo & Wetzel examined the failure stress of various organic and inorganic high performance single fibres when cut with the sharp blade, while cutting angle was changed from transverse to longitudinal orientation. They showed that the failure stress of both type of fibres was decreased by increasing the cutting angle while inorganic fibres exhibited less sensitivity to change in failure stress with the increase in longitudinal angle, Figure 8(a). It was also concluded that inorganic fibres fail in isotropic fracture while organic fibres, like para-aramids, had mixed mode of failure that involved cut failure, longitudinal and transverse tensile failure and transverse shear failure, owning to their structural anisotropy. [30], [33] Similar, studies on high performance Zylon® yarn [40] and Zylon®, Spectra® and Kevlar® yarns [32] concluded the similar results of the drastic decrease in yarn fracture energy as the knife cutting angle shifts from transverse direction to longitudinal direction, shown in Figure 8(b).



(a)                    (b)
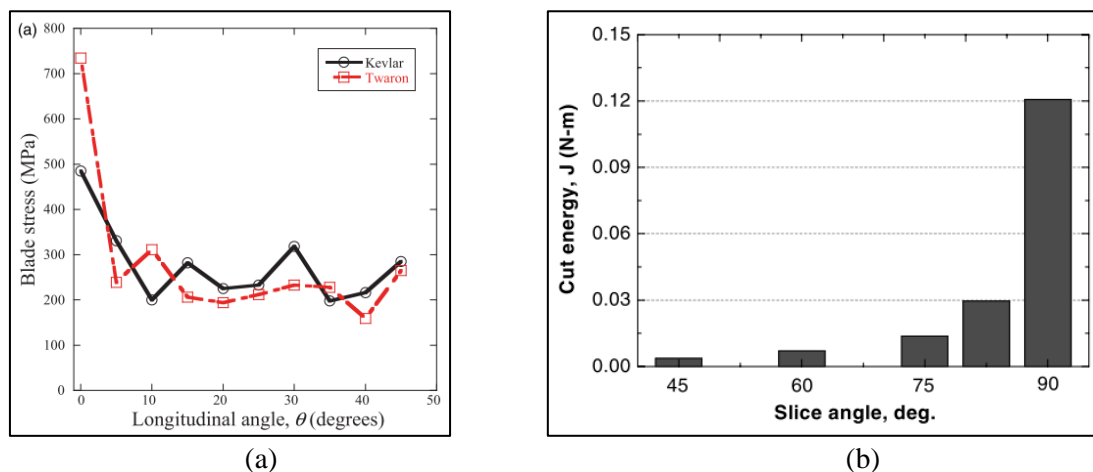
*Figure 8: (a) Cut resistance of single fiber para-Aramids measured at different cutting angles by Mayo & Wetzel [30], (b) Effect of Yarn cutting angle on cutting energy measured by Shin & Shockey [40]*

### 3.10. Importance of Blade Orientation in Cutting Resistance of Fabric

Most of the research conducted to measure the stab resistance of woven fabrics does not mention the knife penetration angle. Either fabric is loaded without mentioning the knife penetration angle [76], [77] or one angle is selected [9] and comparison of different angle is not made. However, very few studies mentioned the effect of change in knife orientation with respect to protective fabric.[27], [29] These studies showed that changing relative angle between knife penetration direction and surface of textile significantly affect the resistance of protective textile [78]. However, such study that involves observing the knife's transverse orientation with respect of warp and weft of fabric is not yet performed. This suggests investigating if such anisotropic behaviour of stab resistant in such orientation of knife and fabric is present.

### 3.11. Effect of plies orientation textile resisting against impacting load

Importance of orientation of plies in resisting against ballistic impact situation is already established. The literature established this fact either numerically [79], [80] or/and experimentally. It has been shown that plies oriented at an angle can absorb up to 20% higher amount of impact energy than aligned plies. There is an optimum level of plies orientation that improves this impact resistance [80]. However, the effect of orientation of plies on stab resistance could be a good area of study. It can verify the benefits of angle plied achieved in ballistic impact for knife stabbing resistance.

### 3.12. Various methods of stab testing

#### 3.12.1. Drop-tower (drop-weight) testing

Drop-tower testing is specified by NIJ Standard 0115.00 [81]. It is the globally accepted standard method of testing anti-stabbing performance of body armour. It is one of the test methods developed by American National Institute of Justice for protective armours. The drop-tower test is believed to simulate the stabbing action and

can reproduce the impact energy, be controlling the mass and height of the impactor. This standard strictly defines the sharpness of the blade, different energy levels, characteristics of backing material to simulate body, and shape and material of different impactors.

Drop-tower is a good method for evaluating the anti-stabbing performance. But the result only indicates if some protection is safe for specified energy level or not. This method is not good for studying the mechanism of stabbing and response of protecting surface. For studying the interaction of impactor and textile a method with controlled penetration method is required [27].

3.12.2. Quasi-static stab testing

The quasi-static stab testing is frequently adopted method for the measurement of stabbing response, in the lab. This method gives better control over different aspects of penetration that includes:

I. Consistent penetration direction and speed,

II. Recording of force-displacement or force-time curve and penetration energy,

III. Possibility of capturing interaction of knife and fabric on video and

IV. Repeatable results.

The quasi-static stab testing method can be followed using a universal testing machine [13]. The machine equipped with load cell can record resistance and depth of stabbing. The impactor can be mounted in the cross-head of the machine.

However, due to the absence of acceleration the impact simulation is not as in reality [80]. The rate of loading in quasi-static stab testing is of order of 50-500 mm/min while rate of dynamic stab can go up to 9.2 m/s [78]. Therefore, the quasi-static stab resistance measured will always be higher than stab resistance measured with drop-

tower method. Furthermore, no standard has been established for quasi-static stabbing method, therefore, the reported results in literature are not directly comparable.

3.12.3. Biaxial measurement device

The biaxial method is used to load the specimen in biaxial tension while impactor penetrates. In this method the tension in specimen and resistance measure by impactor both can be recorded. In quasi-static stab testing the penetration resistance is measure by impacting instrument. Biaxial testing method can be superior to quasi-static testing as it can provide better understanding of specimen response while it is being impacted. A biaxial testing setup is shown in Figure 9.
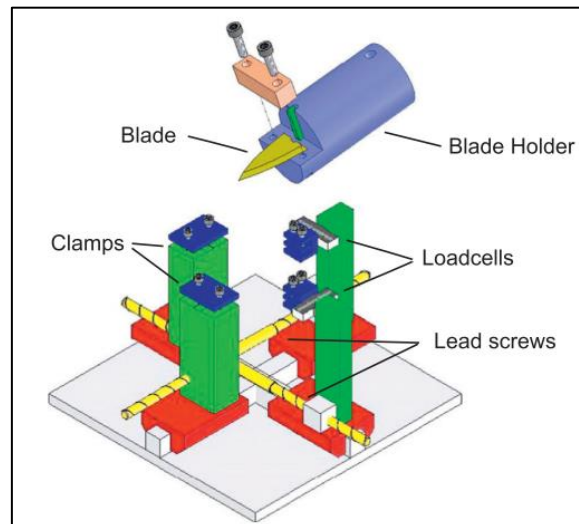


*Figure 9: Biaxial Stab testing device, reproduced from reference* [78]

## 3.13. Prediction Models

Sadegh and Cavallaro, presented a model of ballistic penetration into the fabric sheet with the constraint of undemageable yarns. The fabric was suppose to have higher crimp of warp than weft yarns. The model predicts the work done ($W$) required for bullet of diameter ($D$) to penetrate into the fabric when impacting force of bullet ($F$), yarn to yarn sliding resistance ($R$), and yarn pull-out resistance ($T$) is known. [70]

20

If there are $n$ number of yarns (cross-over points, Figure 10 e) and have $\mu$ coefficient of friction between them, according to this model the sliding resistance of yarns in x and y directions can be given by:

$$R_x = 2n\mu \sin\left(\frac{\theta_x}{2}\right)\left[2\sum_{i=1}^{n+1} T_{ix} - \left(T_{1x} + T_{(n+1)x}\right)\right] + n\mu F_i$$

2

$$R_y = 2n\mu \sin\left(\frac{\theta_y}{2}\right)\left[2\sum_{i=1}^{n+1} T_{iy} - \left(T_{1y} + T_{(n+1)y}\right)\right] + n\mu F_i$$

3

And, yarns' pull-out resistance can be given as:

$$\frac{T_1 + \left(\frac{F_i}{\theta}\right)}{T_{n+1} + \left(\frac{F_i}{\theta}\right)} = e^{\mu n\theta}$$

4

So, work done required by bullet to penetrate the fabric is:

$$W = \left(R_x D_x + R_y D_y\right) + 2n\left(T_{1x}\Delta_x + T_{1y}\Delta_y\right)$$

5
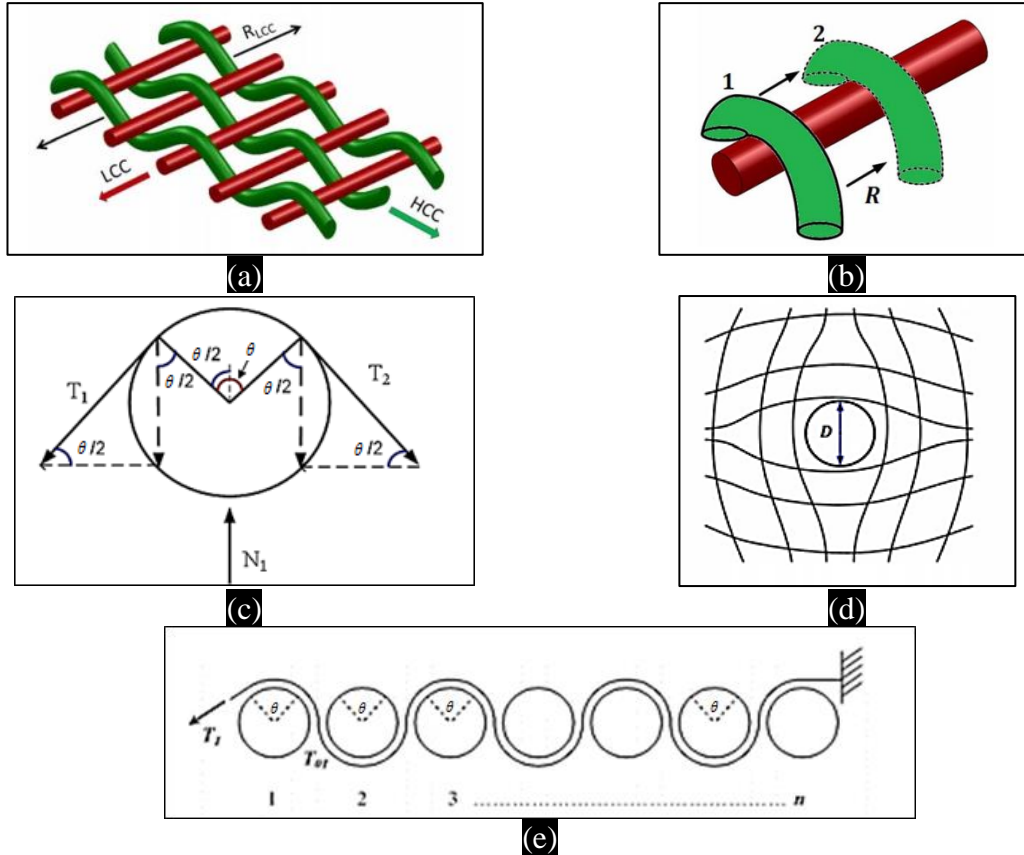


Figure 10: Illustration from refrence [70], (a) showing crimp imbalce between warp and weft yarns, (b) yarn sliding resistance, (c) Free-body diagram for single cross-overand yarn tension, (d) penetration of bullet into the fabric, and (e) yarn pull-out resistance and contact angle of each interlacement

### 3.14.    Yarn Pull-out Force

Yarn pull-out can be a good method of measurement of inter-yarn friction with in the fabric. There are three techniques used to measure this method. [82]

1.  Bottom Clamped [83], Figure 11(a)

2.  Side Clamped, Figure 11(b)

3.  Dynamic Pull-out, Figure 11(c)&(d)



(a)

(b)

(c)

(d)
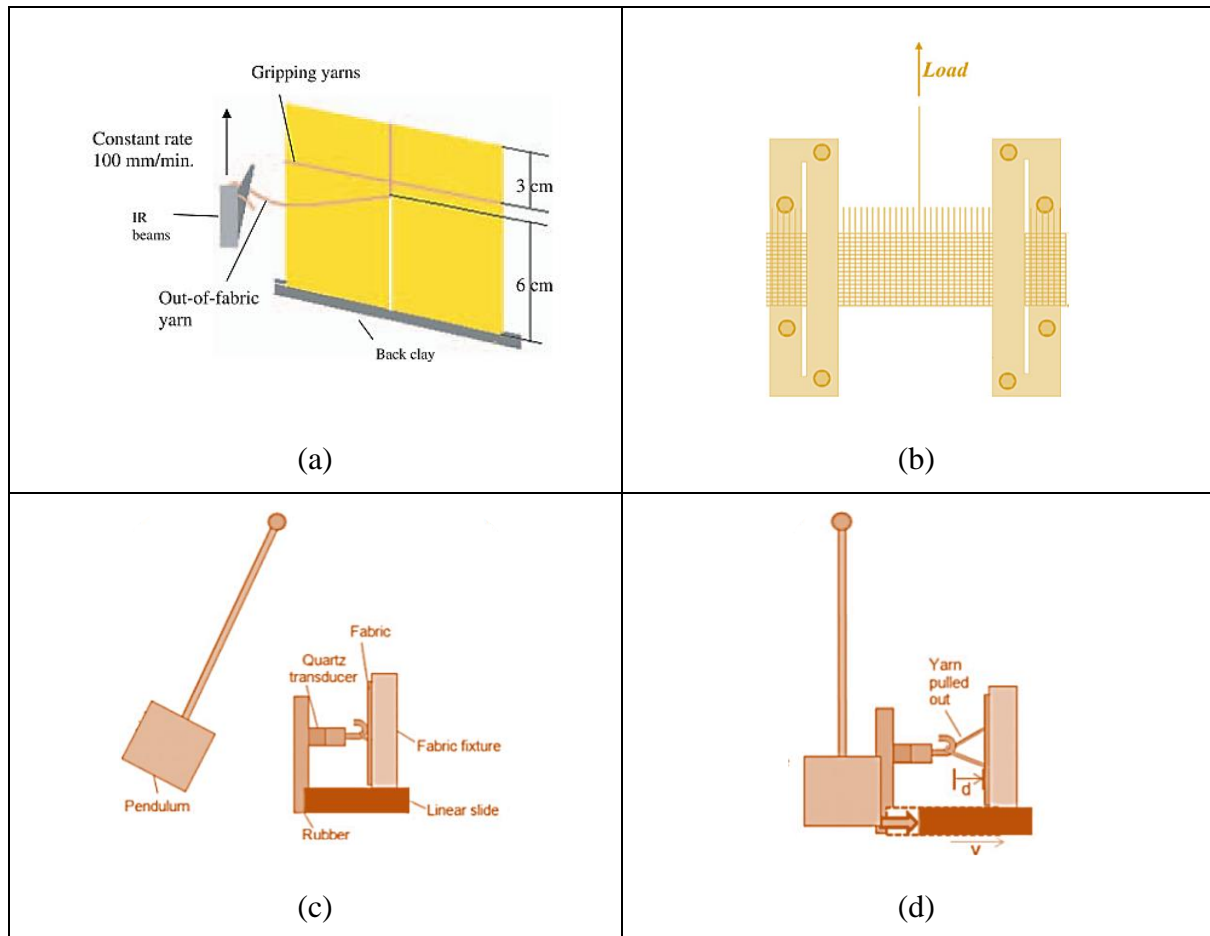
*Figure 11: Schematic drawings of different methods of yarn pull-out from the fabric, reproduced from* [82], [83]

If bending modulus of yarn ($b$), yarn axis angle with plane of the fabric ($\varphi$) and yarn pick spacing ($p$) are know the force applied on each yarn ($F_{pullout}$) can be found using relation as found in [84], Equation 6:

$$F_{pullout} = \frac{8\,b\,\sin\varphi}{p^2}$$

*6*

# CHAPTER 4
## MATERIALS AND METHODS

## 4. Materials and Methods:

### 4.1. Materials:

#### 4.1.1. Fabric

Woven fabric investigated in this research was composed of high modulus multifilament Twaron® 2200 yarns, with linear density of 1620 *dtex* (1000 filaments, 5.86 *TPM*). The weave of the fabric was 1/1 plain and a balanced construction, with equal yarn linear density and equal set of warp and weft was used. The style of the fabric was KK220P and it was sourced in loom state from G. Angeloni srl Italy. The greige fabric was having an areal density of 220 *g/m²*. [85]

*Table 2: Fabric Parameters*

| ID | Warp / Weft Yarn | Weave | Warp Sett (*ends/cm*) | Weft Sett (*picks/cm*) | Areal Density (*g/m²*) | Thickness (*mm*) |
|---|---|---|---|---|---|---|
| Off-Loom | Twaron ® 2200 (1000 f) 1620 *dtex* | 1/1 Plain | 6.45 | 6.34 | 220 | 0.28 |
| Neat | | | 6.41 | 6.40 | 218 | 0.32 |

The detailed specifications of Neat fabric are given in Table 2. The optical micrographs of treated and untreated fabrics are shown in Figure 12.



(a)          (b)          (c)
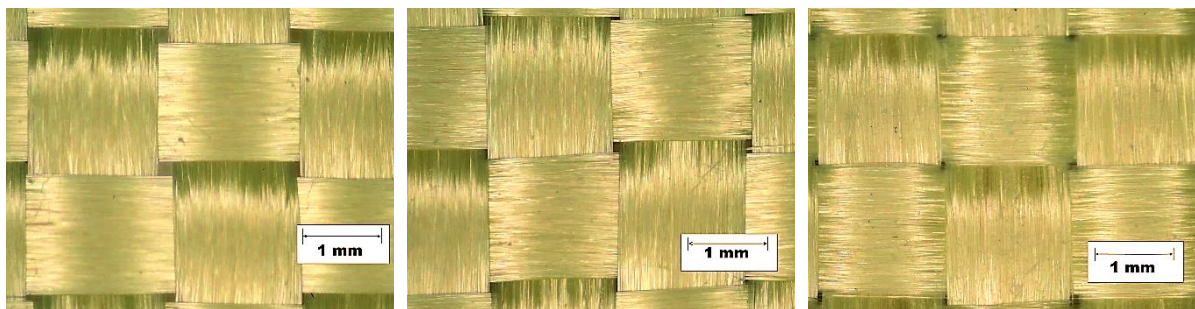
*Figure 12: Microscopic image of (a) Neat, (b) S3 and (c) S4 fabrics*

### 4.1.2. Water Glass

Sodium Silicate aqueous solution (36-40% concentration) is a low-cost product, available in market, known as Water Glass, is used as source of $SiO_2$. It contains Sodium Oxide ($Na_2z$) and Silicon dioxide (Silica, $SiO_2$). It is an industrial product and is used in various industries like detergent, paper pulp bleaching, municipal and waste water treatment, concrete, abrasive and adhesive [86].

The water glass (VODNÍ SKLO Vízuveg of KITTFORT, CAS: 1344-09-8) is used as a precursor of $SiO_2$ in the current study. It has been reported to be a silica source [87]. It is alkaline in nature and precipitates into $SiO_2$ when reacted with weak acid, like acetic acid. A generalize reaction of $SiO_2$ deposition can be given as:

$$Na_xSi_yO_z \xrightarrow{H^+} SiO_2 + Na^+$$

$$(1)$$
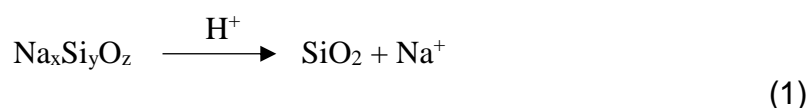
### 4.1.3. Titanium dioxide ($TiO_2$)

Titanium dioxide used in this work is (AEROXID® $TiO_2$ P25 by EVONIK INDUSTRIES) a hydrophilic fumed powder. It has high purity ($TiO_2 \geq 99.50\%$) and high specific surface area of 35-65 $m^2/g$. It consists of primary aggregate of partials with an approximate partial size approximate 21 nm and density 4 $g/cm^3$. Anatase to Rutile weight ratio of 80/20 [88], [89].

## 4.2. Methods

The summery of methods followed in this work is shown as tree diagram in Figure 13.
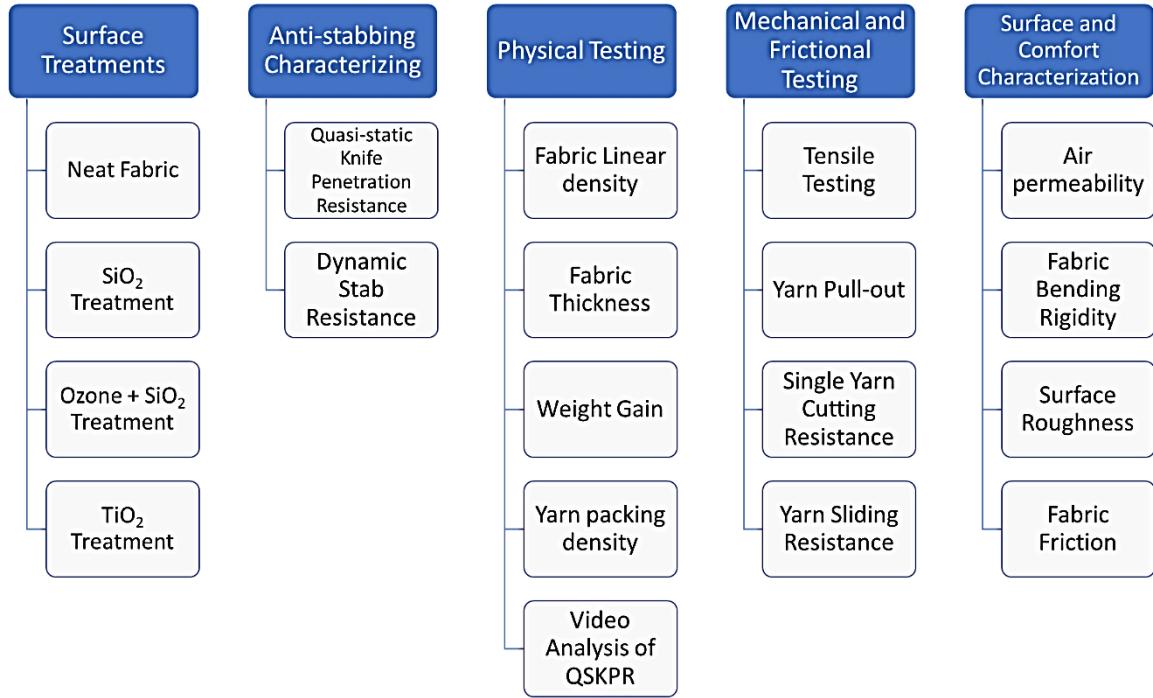


*Figure 13: Summery of methods followed in this work*

### 4.2.1. Surface Modifications

#### 4.2.1.1. Neat Samples Preparation

Before any chemical application the surface of raw samples was made clear from process add-ons that may have been applied on the fabric surface. For this purpose, different trials were made and finally Methanol washing was chosen as sufficiently effective method. So, 99.99% Methanol, ($CH_3OH$) (P-Lab Czech Republic), washing was conducted for 3 *min* in a vibrating bath (at 150 *rpm*), with a bath ratio 1:50. Afterwards, samples were rinsed and dried. The fabric samples in this state are called "Neat" samples and used as "untreated" fabric for comparison with surface modified samples. Neat samples are denoted with "N" in this work. The process of methanol washing is illustrated in Figure 14(a).
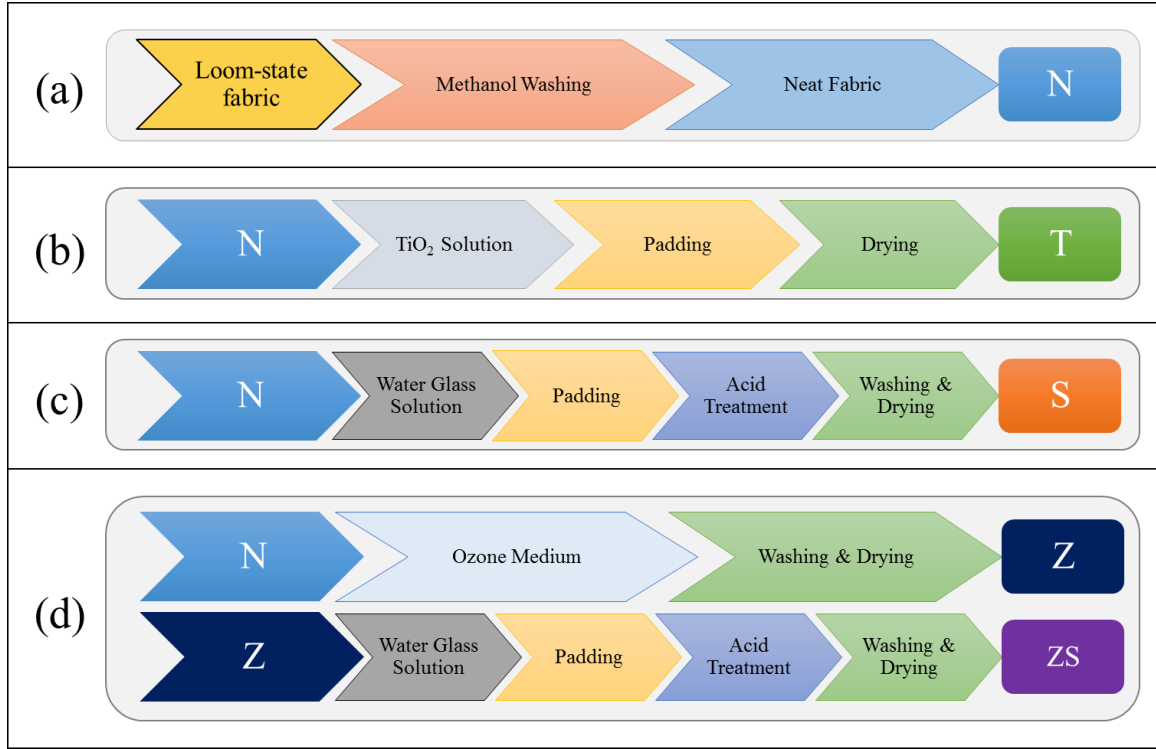
*Figure 14: Steps of surface modifications for different techniques, (a) Methanol Washing steps for Neat samples, (b) Steps followed for TiO₂ Treatment, (c) Steps followed for SiO₂ treatment, and (d) Steps followed for Ozone pre-treatment and post-treatment with WG*

### 4.2.1.2. Surface Modification by SiO₂

WG, used in this work, was 40% aqueous solution of Sodium Silicate. It was diluted to different concentrations to produce S1, S2, S3 and S4 samples, details can be found in Table 3. Each of these sample was immersed in Sodium silicate solution. And was padded at squeezing pressure of 1 *bar* at linear speed of 1 *m/min,* to gain a wet pick up of 50±10%. The samples were then immersed in 5 *g/l* Acetic acid for 15 *min*, a bath ratio of 1:20 was maintained enough to dip the samples well in the solution. To facilitate the reaction and deposition of SiO₂ the container was continuously shaken at 150 *rpm*. After that it was rinsed and hot-air oven dried. An illustration can be found in Figure 14(c).

*Table 3: Different concentrations of Sodium silicate solution*

| Sample Identification | S1 | S2 | S3 | S4 |
|---|---|---|---|---|
| Water Glass Conc. | *4%* | *8%* | *20%* | *40%* |

### 4.2.1.3.  Surface Modification by Titanium dioxide

Aqueous solution of hydrophilic $TiO_2$ was prepared with the help of sonification. The concentration of $TiO_2$ was increased from 0.01 *g/l* to 0.5 *g/l* in five different solutions as identified in Table 4. Each sample was dipped in respective solution of $TiO_2$ with a liquor ration of 1:25. Roller padding was followed with nipping pressure of 1 *bar*, followed by hot-air oven drying at $100°C$ for 10 *min*, the process is illustrated in Figure 14(b).

*Table 4 Details of different TiO₂ Solutions*

| Sample Identification | T1 | T2 | T3 | T4 | T5 |
|---|---|---|---|---|---|
| TiO₂ Concentration (g/l) | 0.01 | 0.05 | 0.1 | 0.25 | 0.5 |

### 4.2.1.4.  Ozone Application

Ozone medium was prepared from distilled water in which weighted fabric samples were immersed. The oxygen was concentrated by Kröber O2 (Kröber Medizintechnik GmbH, Germany) at 3.0 *l/min* flow rate. The Ozone gas was generated by Ozone Generator TRIOTECH GO 5LAB-K (Czech Republic), and its concentration was monitored by LONGLIFE TECHNOLOGY LF-2000. At the end of the stream flow Ozone gas was destroyed. The set-up of application of the Ozone medium is illustrated in Figure: 15.
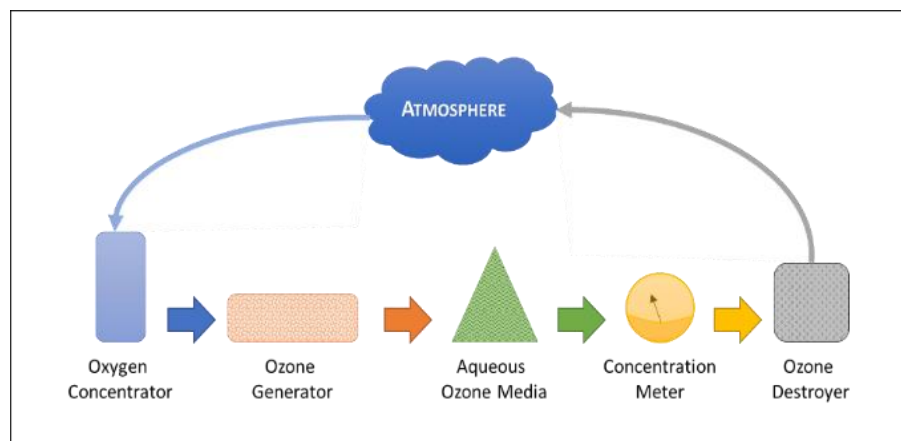


*Figure: 15 Illustration of Ozone Medium Set-up*

28

Neat fabric samples were exposed to the Ozone in the aqueous medium, for 60 and 120 *min*. To check the combined effect of Ozone and WG, 120 *min* ozone treated samples were, also, deposited with $SiO_2$ (*following the same procedure as described in 4.2.1.2 for Neat samples*). The details of exposure time of these samples are given in Table 5 and treatment steps are shown in Figure 14(d).

Table 5: Details of Ozonized and $SiO_2$ Deposited Samples

| Sample Identification | 1Z | 2Z | 2ZS3 | 2ZS4 |
|---|---|---|---|---|
| Ozone Medium Exposure (*min*) | 60 | 120 | 120 | 120 |
| Water Glass Concentration | - | - | 20% | 40% |

4.2.2. <u>Stab Resistance Measurements</u>

*4.2.2.1.  Details of Knife and Measurement Procedure of Quasi-Static Knife Penetration Resistance (QSKPR)*

The testing procedure, for the measurement of quasi-static knife penetration resistance, was in accordance to recently reported method followed by various researchers. [28], [75], [90], [91].



|     |     |     |
|-----|-----|-----|
| (a) | (b) | (c) |
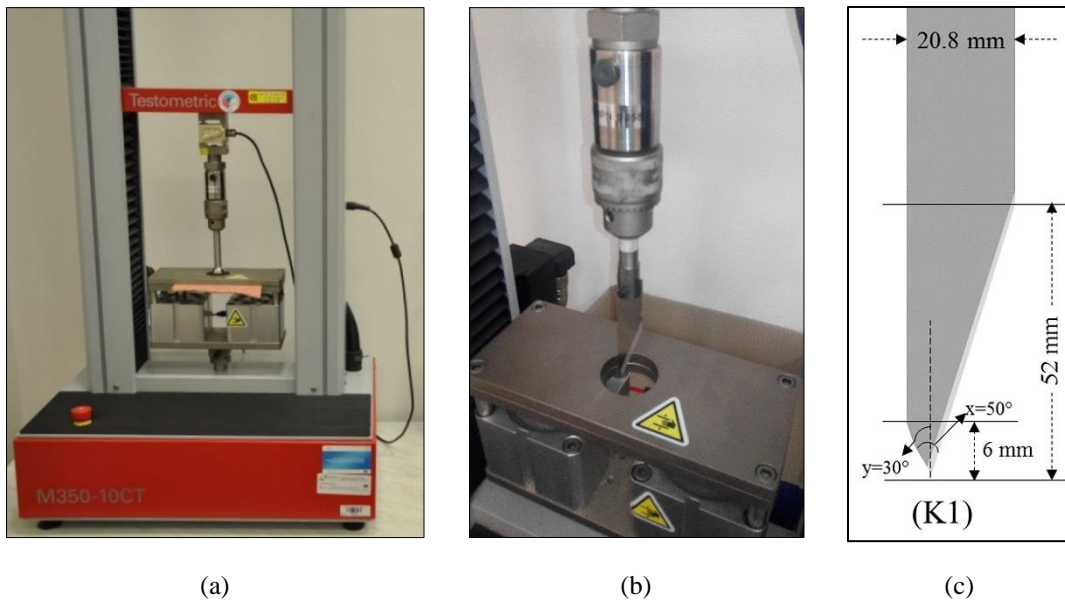
*Figure 16: (a) Universal Testing Machine (TESTOMETIC M350-10CT), (b) Cross-head installed with knife and (c)* Geometry of CKB-2 (K1)

Universal testing machine TESTOMETIC M350-10CT, shown in Figure 16(a), was used to penetrate the fabric samples quasi-statically at constant rate of penetration of 8.33 mm/s. The fabric held in a pneumatically operated platform at 7.5 *bar* with inner diameter of circular opening of 45.55 *mm*. Samples were pre-tensioned at 1 *N* force. Samples size of each fabric sample was 100 *mm* x 100 *mm* ±5 *mm*. The knife was held in cross-head with 1000 *N* load cell and was vertically penetrated the fabric for 42 *mm*. Its response in terms of force-displacement curve was recorded and force at peak resistance was noted.

The knife material, shape and sharpness directly effects the response of the fabric. [11], [32], [40], [52], [78] Owing to this important factor the knife used in this procedure, was wood crafting stainless steel knife, namely CKB-2 of OLFA Japan. To obtain consistent shape and sharpness for different measurements, commercially available knives were utilised.

The shape of knife can be observed, as K1, in Figure 16(c). It is visible that one edge of knife is sharp and other side is blunt. The first 6 *mm* of the tip of knife profile has inclination on both direction with 50° angles while after this tip the blunt side is parallel to the length of knife. While sharp edge has 15° inclination for a maximum vertical length of 52 *mm*. Maximum width of knife is 20.8 *mm* and thickness of 1.2 *mm*. One important observation must be noted here that width of the knife (that causes cut in the fabric) increases rapidly for first 6 *mm* due to both-sided inclinations, however, after that knife profile width increases in single-side corresponding to 20° angle of inclination. To keep the knife to knife sharpness variation, on average, one knife was used for a set of 18-24 samples, with equal probability of selection among different KPAs.
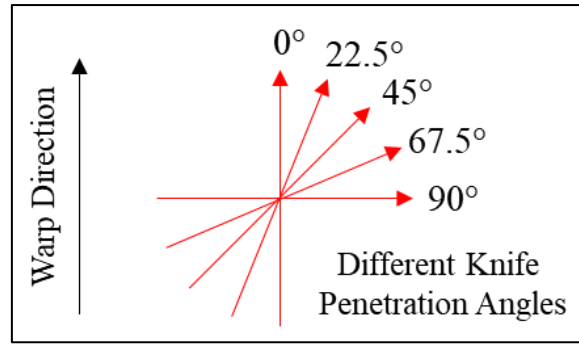
*Figure 17: Illustration of different Knife Penetration Angles*

The QSKPR was tested for five different Knife Penetration Angles (KPA= $\alpha$ = 0°, 22.5°, 45°, 67.5°, and 90°), as illustrated in Figure 17. KPA here refers to the angle made between axis of warp yarn length and blade cutting axis, while blade penetrates the fabric vertically downwards, as illustrated in Figure 18. For each KPA at least 10 samples were tested for single sheet stack and 6 samples for multiple sheet stack, and mean results were computed.
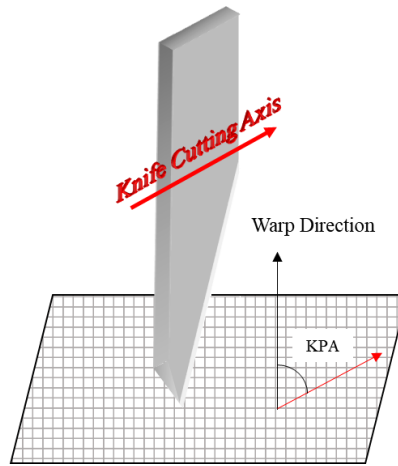


*Figure 18: Illustration of knife cutting axis*

### 4.2.2.2.    Video Analysis Setup

The interaction of knife and fabric samples during QSKPR measurement was recorded on video using SONY HDR-SR12E camera at 25.0 *fps*. A setup was developed to reflect rare side of fabric penetration to focus at camera lens, as shown in Figure 19.
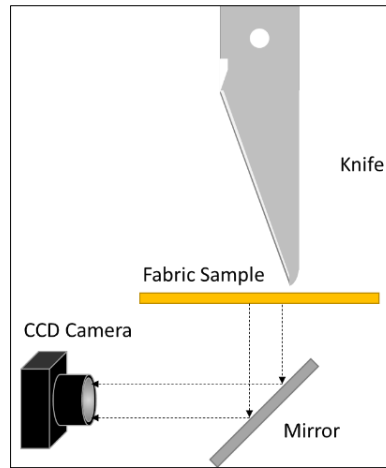
*Figure 19: Camera Set-up for tracking knife penetration*

Each frame of recorded video was separated into an image file using MATLAB program. These images were analysed to observe the interaction of knife with each yarn fractured. By using image analysis software, Digimizer, knife edge displacement and strain of each yarn was measured before rupture. Then comparison of Neat and S4 fabrics was conducted.

### 4.2.2.3.    Dynamic Stab Resistance (DSR) Measurement Procedure:

DSR was performed following the modified version of NIJ Standard–0115.00 [81]. The drop-weight tower testing equipment was used, as shown in Figure 20(a), and damping material layers shown in Figure 20(b). K1 knife was used to penetrate for DSR, consistent with QSKPR measurements. The effect of change in knife penetration angle on stabbing resistance was observed, while density of the samples was kept similar. Change in penetration depth for two potential energies, of dropping knives 0.74 *J* and 1.47 *J*, was compared.

*Table 6: Dynamic stab resistance Samples details (95% confidence interval in parenthesis)*

| Fabric ID | Sheets | Stacking Angle | Areal Mass ($g/m^2$) | Thickness (*mm*) | Fabric Density $\rho$ [$kg/m^3$] |
|---|---|---|---|---|---|
| N | 8 | 45° | 1765 | 2.60 (±0.02) | 678.85 |
| S4 | 8 | 45° | 1812 | 2.73 (±0.04) | 663.74 |

The drop-weight measurement equipment was available with laser distance measurement device with high accuracy. The knife was dropped under gravity from two fixed heights of 10 *cm* and 20 *cm*. The data was recorded by a custom written program in National Instrument Software that acquires the data from load cell, distance measurement sensor and accelerometer and presents data for acceleration, drop distance, resistance force with sampling rate of 50 *µs*.



(a)                                           (c)
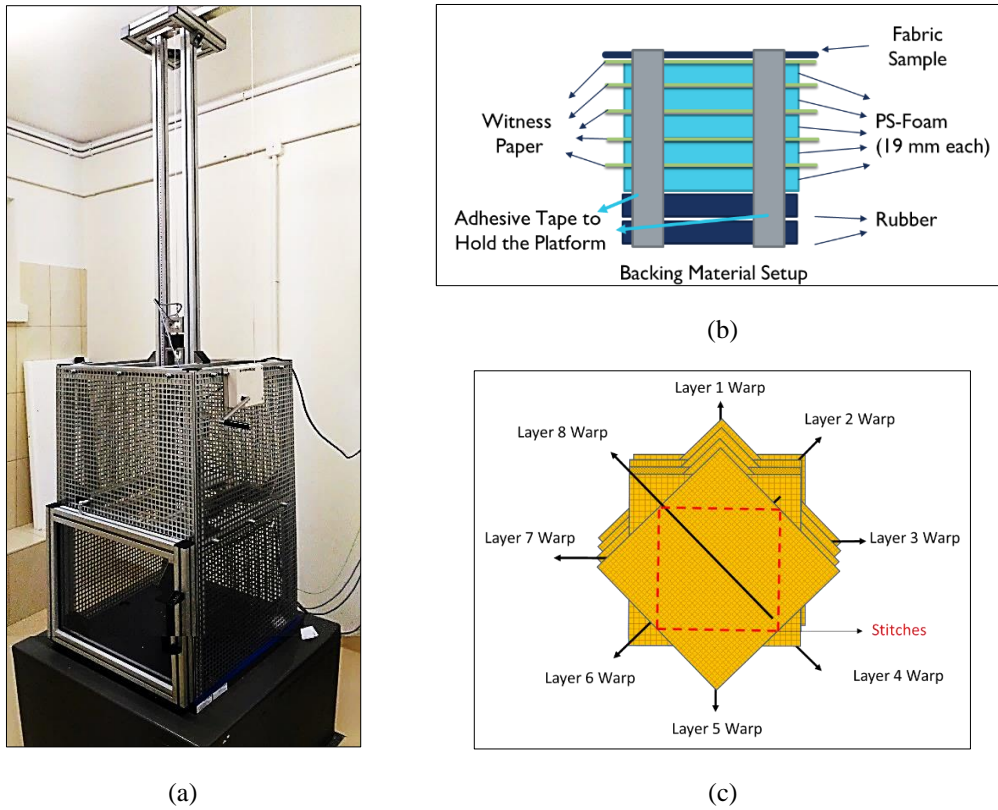
*Figure 20: (a) Drop-weight measurement set-up for DSR, (b) Backing / Damping material arrangement and (c) Illustration of 8 sheets stacking orientation*

DSR of different samples were compared for KPA of 0°, 45° and 90°. Eight sheets of single layer fabric sample were placed one over another at 45° stacking angle and were sewed, illustrated in Figure 20(c). The details are available in Table 6.

### 4.2.3. Imaging and Topography Analysis

#### 4.2.3.1. Fourier Transformation Infra-Red (FTIR) spectroscopy

To verify the chemistry of the deposited layer, the treated samples were analysed for Fourier Transform Infra-Red (FTIR) spectroscopy. A Thermo Fisher FTIR spectrometer, model Nicolet iN10, was used in this work.

### 4.2.3.2. Scanning Electron Microscopy (SEM)

Fabric samples were also scanned for their surface topological differences using Scanning Electron Microscope (SEM) VEGA TESCAN TS5130 at 20 *KV* for 2000X magnification. Fibres removed from post-penetrated fabric samples in quasi-static knife penetration resistance testing were also scanned to observe the plastic deformation mode.

### 4.2.3.3. Energy-Dispersive X-ray (EDX) Spectroscopy

To observe the atomic composition of deposited layer, EDX was performed at 20 *KV*. The atomic composition of treated and untreated surfaces was determined. The peaks of the detected elements were obtained, and percentage composition was computed.

### 4.2.3.4. Optical Microscopy

Optical microscopy was conducted to observe the surface changes and structural parameters. For the structural measurement image analysis was performed. To obtain the fabric cross-sectional images, fabric samples were immersed in epoxy resin, cured, dissected and polished. Afterwards, microscopic images were taken under different lighting conditions.

### 4.2.3.5. Laser Scanning Confocal Microscopy (LSCM)

To observe the microscopic changes at knife cutting edge, it was 3D scan using LSCM. Laser scanning helped generates three-dimensional surface map. Scanned data was analysed for roughness at tip of knife edge and change in its

sharpness after stabbing.

### 4.2.4. Mechanical Characterization

#### *4.2.4.1.    Tensile Testing*

The tensile strength of warp and weft yarns removed from different fabric samples was recorded. Measurements were made following the ASTM D2256 standard; on Universal Testing Machine TIRATEST. Samples gauge length was 20 *cm* with loading speed of 100 *mm/min*. 20 samples were tested for each selected set of yarns.

#### *4.2.4.2.    Yarn Pull Out*

To observe the interaction of individual yarn with interlacing yarns yarn pull out test was carried out. The method followed is in accordance with already available in literature [36]. The details are described as follows:
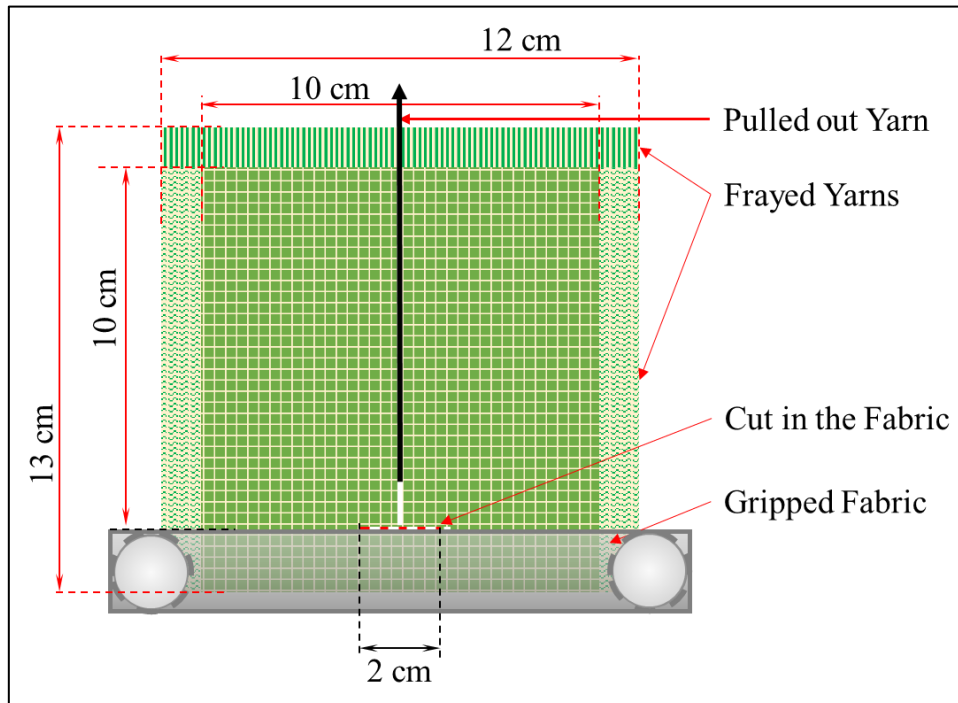


*Figure 21: Description of yarn pull-out setup*

A rectangular sample of size $12 \times 13$ *cm²* was taken. Fabric was unravelled 1 *cm* from three sides, skipping the side that is to be gripped, as shown in Figure

21. A cut of 2 *cm* was made, as shown by red dashed line, at distance of 2 *cm* from edge, to make the pulling yarn's one end free. The cut was made exactly at the centre, which makes sliding end of pulling yarn free. The pulling yarn was gripped in tensile machine's jaw from frayed side of sample. Force-displacement curve was plotted for complete pull-out of yarn. At least 10 samples for each fabric direction, warp and weft, was measured. The average resistance offered by each interlacement was also computed.

### 4.2.4.3. Individual Yarn Cutting Resistance



(a)                                                        (b)
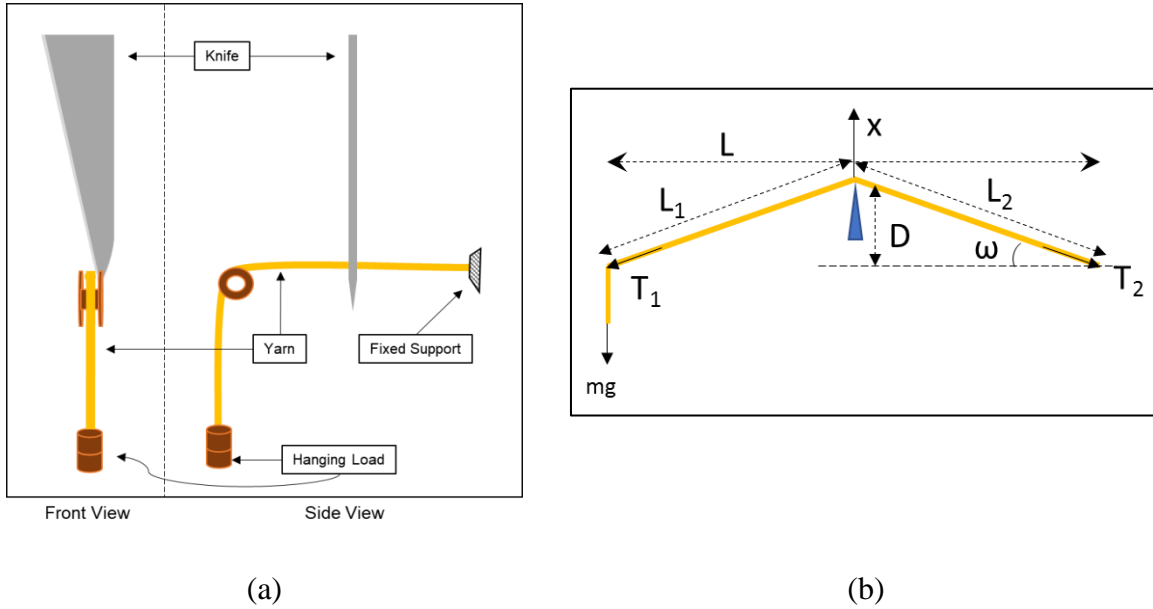
*Figure 22: (a) Illustration describing setup for individual yarn cutting resistance measurement and (b) Free body diagram for resolution of forces at yarn rapture point*

To find out cutting resistance of single yarn, warp and weft yarns were removed from Neat and S4 fabrics. A custom-made yarn holder was used to present the yarn to universal testing machine. One end of each yarn was tied with the fixed support and other was hanged through a free pully with a constant load. The yarn with constant tension, 2.18 *N*, was introduced in front of the sharp edge of knife. The knife was fitted to cross-head of the universal testing machine through a 50 *N* load cell that was operated at 8.33 *mm/s*. The force and displacement were noted

for each individual yarn for its complete cutting. In this way yarn cutting resistance for known yarn tension was recorded. The setup is shown in Figure 22(a) and free-body diagram in Figure 22(b). The details of testing results can be found in section 0. The objective was to observe the force and energy required to cut individual yarns, at constant yarn tension.

### 4.2.4.4. Yarn Sliding Resistance

The penetration of knife into the fabric cause formation of a slit that is made by cutting the yarns coming in way of the knife edge. If there is no fracturing of the yarns by knife, the knife penetration would only displace the yarns. It is the sharp edge of the knife that cut through the yarns before displacing the yarn to a considerable distance. Through video analysis it was observed that extent of each yarn sliding before cutting by knife is between 1 to 2 *mm* (Figure 51(b)) before it is fractured. So, an experiment was designed to see the resistance offered by different fabrics when yarns in the fabric are displaced without fracturing.
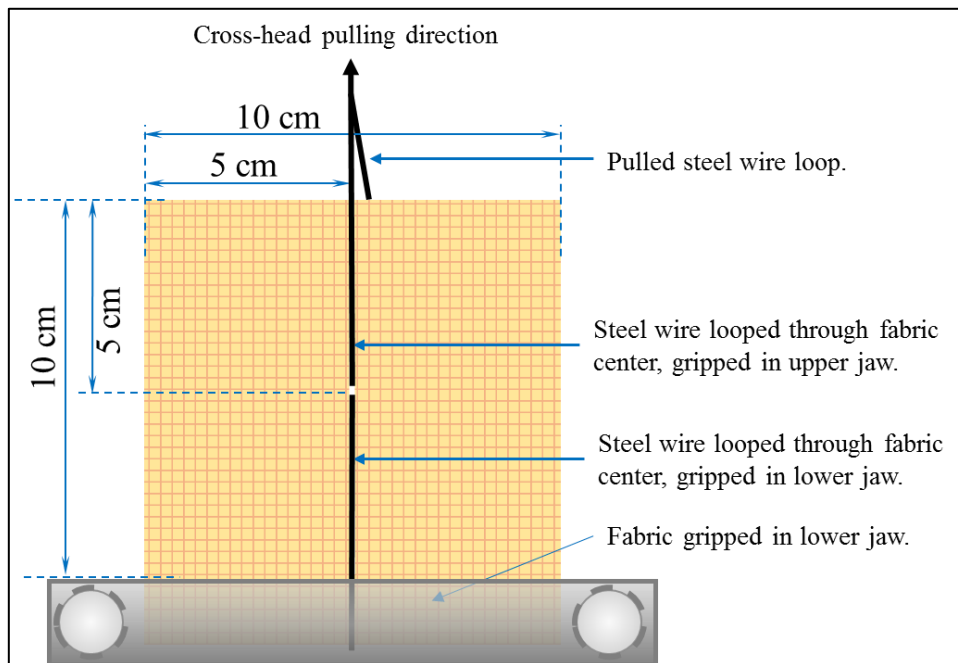


*Figure 23: Yarn sliding resistance measurement setup [83]*

In this devised method, a very fine (0.1 *mm*) thickness steel wire was used to

hold the lower part of the fabric while a loop, of the same wire, was passed through the fabric to be fixed in the upper jaw of universal testing machine. The bottom 1 *cm* of fabric sample was fixed in lower jaw along with the fixed wire. The sample size was 10 × 11 *cm*. The setup devised is illustrated in Figure 23. Each fabric sample was displaced to maximum 10 *mm* distance and force-displacement response was recorded. The cross-head was operated at constant speed of 100 *mm/min*, with a load cell of 100 *N*. The results of yarn sliding resistance can be found in section 4.2.4.4.

### 4.2.5. Comfort and Friction Characterisation

#### 4.2.5.1. *Air Permeability*

Air permeability of different samples were measured using air permeability tester (FX-3300) following the standard method ISO9237.

#### 4.2.5.2. *Surface Feel and Comfort Properties*

Effect on comfort and fabric touch characteristics was analysed using M293 Fabric Touch Tester of SDL Atlas (Figure 25). Fabric bending rigidity, thickness, surface friction, and surface roughness were measured. Measurements was made at face and back of the samples and average was recorded.

#### 4.2.5.3. *Bending Rigidity*

To define softness features of a fabric its bending characteristics are described. A curve of bending moment (*gf.mm*) versus bending angle (*radians*) is shown in Figure 24. With the help of this figure bending rigidity was defined as the average moment needed to bend one radian of the fabric during middle 60% of bending process. So, bending rigidity is defined as in Equation 7: [92]

$$BR = \frac{M_D - M_C}{Rad_D - Rad_C}$$
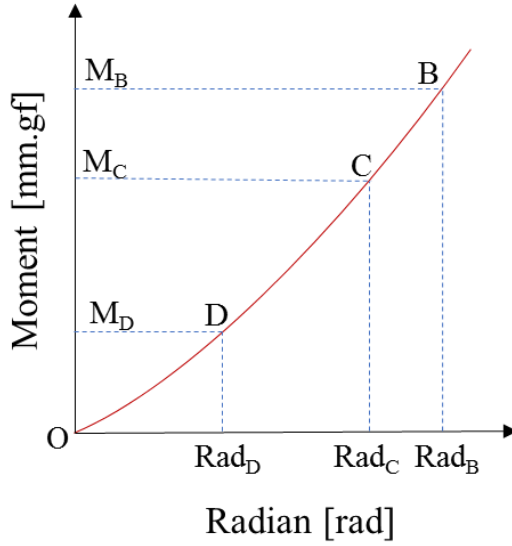
*Figure 24: Definition of BR Measurements*



*Figure 25: Fabric Feel Tester (SDL Atlas)*

### 4.2.5.4.    Fabric Friction

To analyse the change in surface friction the Fabric Touch Tester of SDL Atlas was used. Six measurements of each type of fabric were made at face and back and average was recorded. The average kinetic friction force was measured using Equation 8: [92]

$$Average\ Kinetic\ Friction = \mu_s = \frac{f}{N} = \frac{1}{N(b-c)} \int_c^b F\,dx$$

### 4.2.5.5.    Surface Roughness

The surface roughness data is received as wave format so to define surface roughness amplitude and wavelength of the wave form is measure and defined as below.
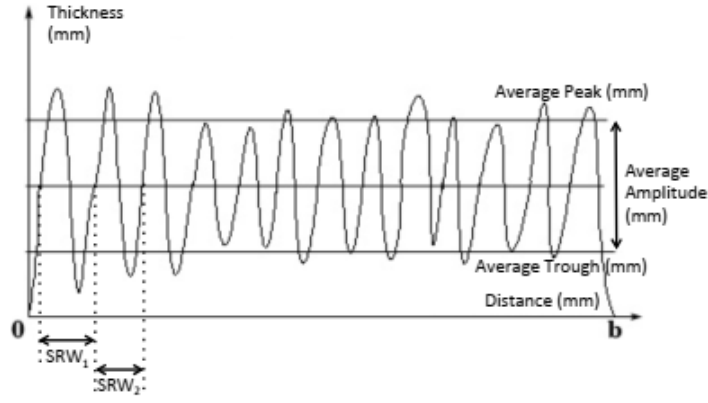
*Figure 26: Definition of surface roughness*

Average peak height and average peak trough was computed and from these values average distance between peak and trough values were computed, for every three waves, and named as *surface* roughness *amplitude (SRA)*. Average moving distance between every three waves is called *surface roughness wavelength (SRW)* [92].

$$SRA \ = \ \bar{H}_k - \ \bar{H}_o \ = \frac{1}{x\prime} \sum_{x=1}^{x\prime} H_{kx} - \frac{1}{x\prime} \sum_{x=1}^{x\prime} H_{ox}$$

*9*

$$SRW \ = \ \frac{1}{G} \sum_{x=1}^{G} |X_{kx} - X_{ox}|$$

*10*

Here $H_{kx}$ and $H_{ox}$ are the measured peak and trough value, respectively, (in *mm*) of the roughness wave when sample has moved a distance $x$. While, $x\prime$ is the maximum distance moved during the measurement. $X_{kx}$ and $X_{ox}$ are the distances (in *mm*) moved when the peak and trough values are found. $G$ is the total counts of groups of three successive intersections.

**CHAPTER 5**
**RESULTS & DISCUSSIONS**

# 5. Results and Discussions:

All the results mentioned in this work represents the mean values of the corresponding measurements. The error bars in figures and values in parenthesis represent the 95 % confidence interval (CI), unless specifically mentioned otherwise.

## 5.1. Comfort Characterization:

### 5.1.1. Air permeability

Air permeability of various fabrics was measured using the procedure mentioned in section 4.2.5.1. The results are shown in Figure 27 and Table 7. The error bars are showing 95% confidence interval. The higher air flow through ozone treated samples in comparison to Neat fabric indicates that Ozone treatment makes structure more open. While air permeability of $SiO_2$ deposited fabric reduces significantly. Therefore, it can be inferred that increasing amount of deposited $SiO_2$ fills the fabric pours and fabric become less permeable to air.
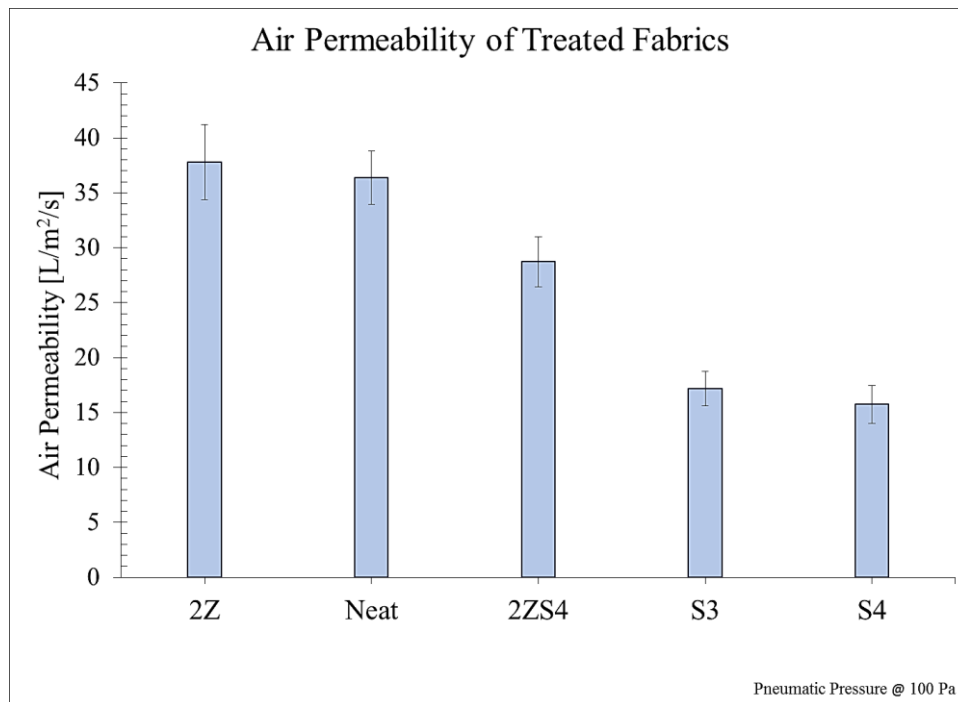


*Figure 27: Air permeability of various treated fabrics*

Table 7: Air permeability of different fabric samples

| Air Permeability (L/m$^2$/s) at 100 Pa | | | | |
|---|---|---|---|---|
| **2Z** | **Neat** | **2ZS4** | **S3** | **S4** |
| 37.80 (3.41) | 36.39 (2.43) | 28.72 (2.27) | 17.19 (1.58) | 15.73 (1.72) |

### 5.1.2. Bending Rigidity

The bending rigidity was measured using Fabric Touch Tester as described in section 4.2.5.3. The bending rigidity of various fabrics were measured at face and back of each fabric, in warp and weft directions. The mean bending rigidity, along warp and weft direction, of various fabrics is shown in Figure 28 and Table 8. The error bars are showing 95% confidence interval. It is apparent that $SiO_2$ treatment made fabrics more rigid, while ozonized fabric, even after treatment with $SiO_2$, is found to be most flexible of all treated and untreated fabrics.
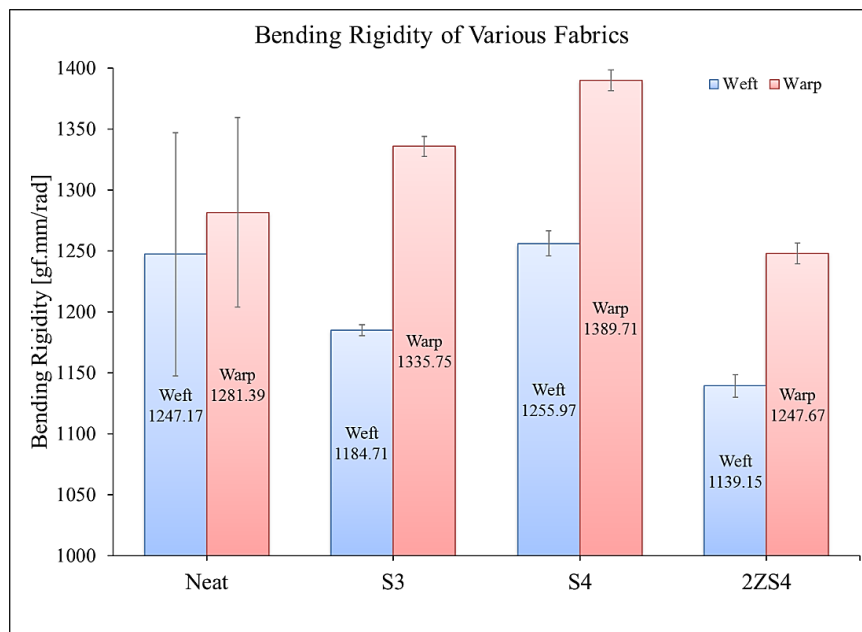


*Figure 28: Bending rigidity of treated and untreated fabrics*

Table 8: Bending Rigidity of different fabrics

| Direction | Fabric Bending Rigidity (gf.mm/rad) | | | |
|---|---|---|---|---|
| | **Neat** | **S3** | **S4** | **2ZS4** |
| **Warp** | 1281.39 (77.74) | 1335.75 (8.24) | 1389.71 (8.40) | 1247.67 (8.40) |
| **Weft** | 1247.17 (99.68) | 1184.71 (4.33) | 1255.97 (10.21) | 1139.15 (9.31) |

### 5.1.3. Coefficient of Friction

The coefficient to friction of various fabrics were measured using Fabric Feel Tester as described in section 4.2.5.4, the average measured values in warp and weft direction can be found in Figure 29 and Table 9. The error bars are showing 95% confidence interval. It is evident that the application of $SiO_2$ has increased the coefficient of friction. The order of increase in friction from least to highest friction is like: Neat $\rightarrow$ S3 $\rightarrow$ 2ZS4 $\rightarrow$ S4. Here S4 and 2ZS4 fabrics are showing significantly higher coefficient of friction in comparison to the Neat fabric.
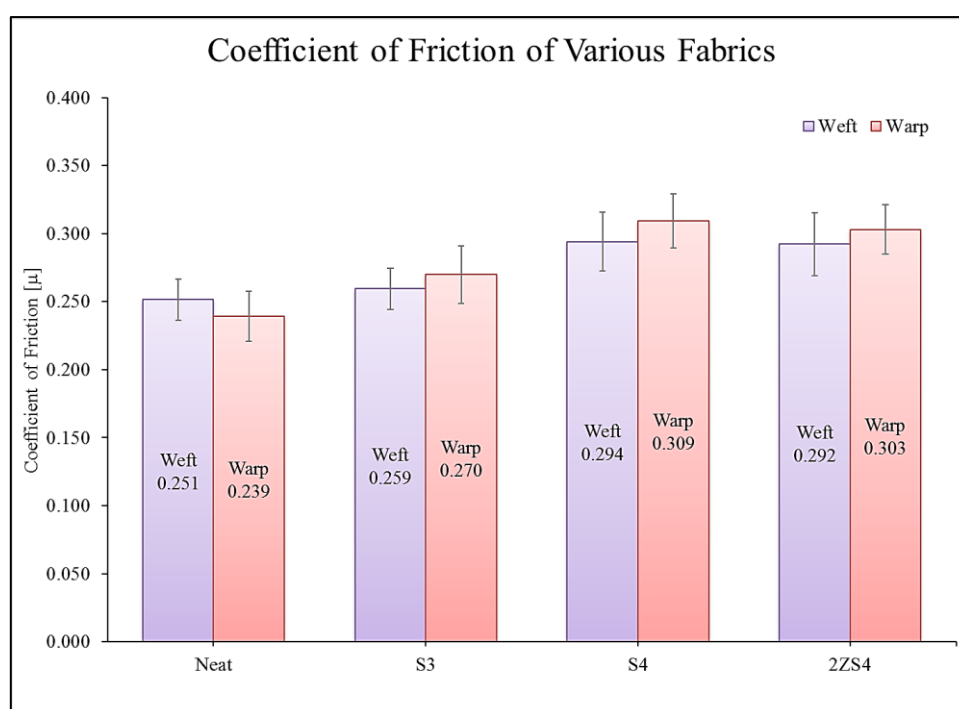


*Figure 29: Change in coefficient of friction from Neat to treated fabrics*

*Table 9: Coefficient of Friction for different fabrics*

| Direction | Fabric Coefficient of Friction | | | |
|---|---|---|---|---|
| | **Neat** | **S3** | **S4** | **2ZS4** |
| **Warp** | 0.239 (0.018) | 0.270 (0.021) | 0.309 (0.020) | 0.303 (0.018) |
| **Weft** | 0.251 (0.015) | 0.259 (0.015) | 0.294 (0.022) | 0.292 (0.023) |

### 5.1.4. Surface Roughness

The surface roughness was measured using Fabric Feel Tester as described in section 4.2.5.5 and results are shown in Figure 30. The error bars are showing 95% confidence interval. From the results it can safely be said that there is not much change in roughness of the fabric samples before and after treatment, however, weft of Neat and S3 shows some variability in the wavelength of waviness.
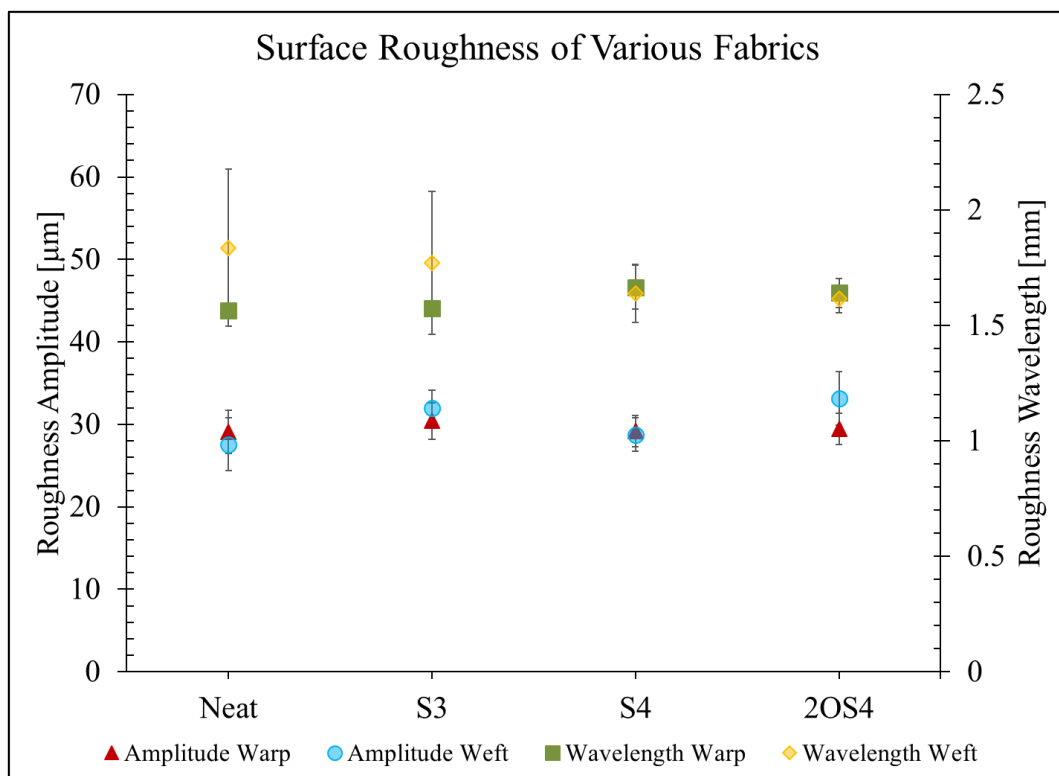


*Figure 30: Surface roughness in terms of waviness amplitude and wavelength*

## 5.2. Physical Characteristics of Fabrics

The changes in physical characteristics of fabrics were noted for treated and untreated fabric samples. The areal mass, fabric thickness, warp/weft linear density, yarn packing density, and fabric density (mass/volume) of these fabrics can be found in Table 10.

<div align="center">*Table 10: Parameters of treated and untreated fabrics*</div>

| Fabric | Warp / Weft Set | | Yarn Packing Density | | Areal Mass | Fabric Thickness | Fabric Density, $\rho$ |
| | | | Warp | Weft | | | |
| | [Ends/cm] | [Picks/cm] | [%] | [%] | [g/m²] | [mm] | [kg/m³] |
|---|---|---|---|---|---|---|---|
| **Neat** | 6.41 (0.02) | 6.40 (0.02) | 93.35 (0.16) | 65.15 (0.66) | 218 (7.09) | 0.32 (0.04) | 681.25 (80.84) |
| **S3** | 6.44 (0.12) | 6.29 (0.18) | 60.75 (0.21) | 58.28 (0.85) | 225 (15.4) | 0.29 (0.02) | 775.86 (92.71) |
| **S4** | 6.47 (0.2) | 6.45 (0.18) | 95.47 (0.99) | 78.35 (0.71) | 234.5 (12.81) | 0.27 (0.08) | 868.51 (112.81) |
| **2ZS4** | 6.49 (0.05) | 6.45 (0.15) | 91.45 (1.32) | 83.03 (1.15) | 227 (18.3) | 0.31 (0.016) | 732.26 (96.32) |

All data showing mean values and parenthesis are showing 95% confidence interval.

The packing densities of yarns were computed using relation shown in Equation 11). The confocal laser microscope was employed to take the cross-sectional images of fabric cured in epoxy resin. The Digimizer software was used for image analysis, to measure the cross-sectional areas of fibres and yarns. These cross-sections of treated and untreated fabrics are shown in Figure 31.

$$Yarn\ Packing\ Density = \frac{Fiber\ cross\ sectional\ area\ \times\ Numbers\ of\ fibers}{Yarn\ cross\ sectional\ area} \times 100$$

*11*
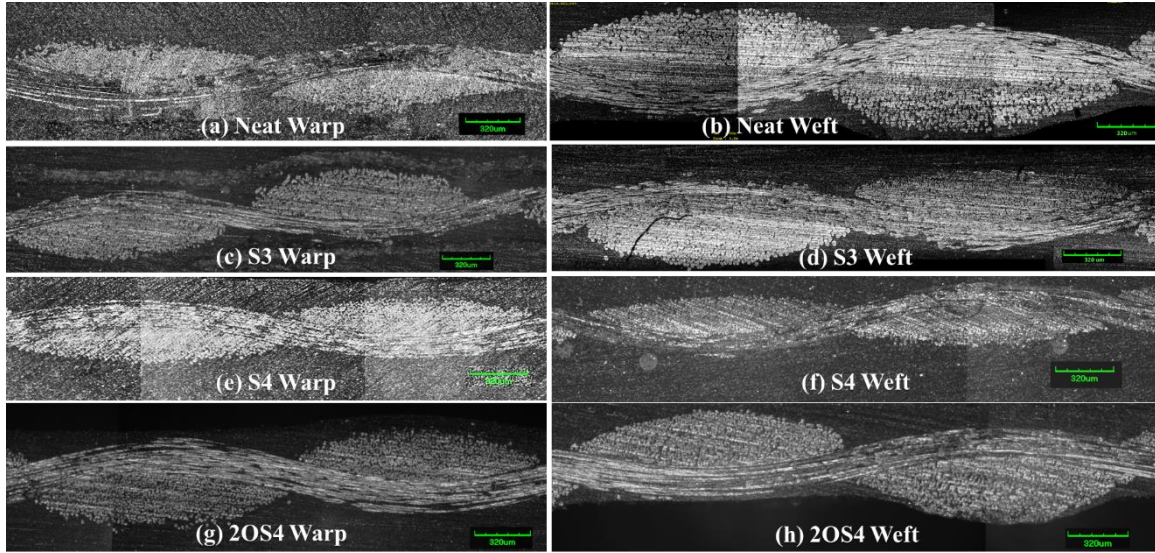


*Figure 31: Cross-sectional images of warp and weft yarns of treated and untreated fabrics.*

From the Table 10 and Figure 31, it is evident that warp yarns are more flat, compact, and less pores than corresponding weft yarns for all the fabrics. Application of WG and padding process has made the S4 fabric most compact in both warp and weft directions, achieving highest fabric density. While shape of weft yarns and their packing densities are contributing to fabric thickness.

## 5.3. Change in knife sharpness

The knives penetrated in single fabric sheet were scanned on LSCM. Change in tip diameter of the virgin and penetrated knives were examined. The data obtained from surface scan of knives was analysed for observing change in tip diameter, each knife

was scanned at its tip for vertical length of 630 $\mu m$. Edge diameter for each 5 $\mu m$ of vertical length was averaged, for 6 samples each 100 $\mu m$ apart. Then mean of all measurements is reported as edge diameter, found in Table 11. For the measurement of edge roughness of the knives the variation of definite thickness of the knives is shown in Figure 32. The variation in heights measured as CV% is computed and can be found in Table 11.



(a)

(b)

(c)                                        (d)
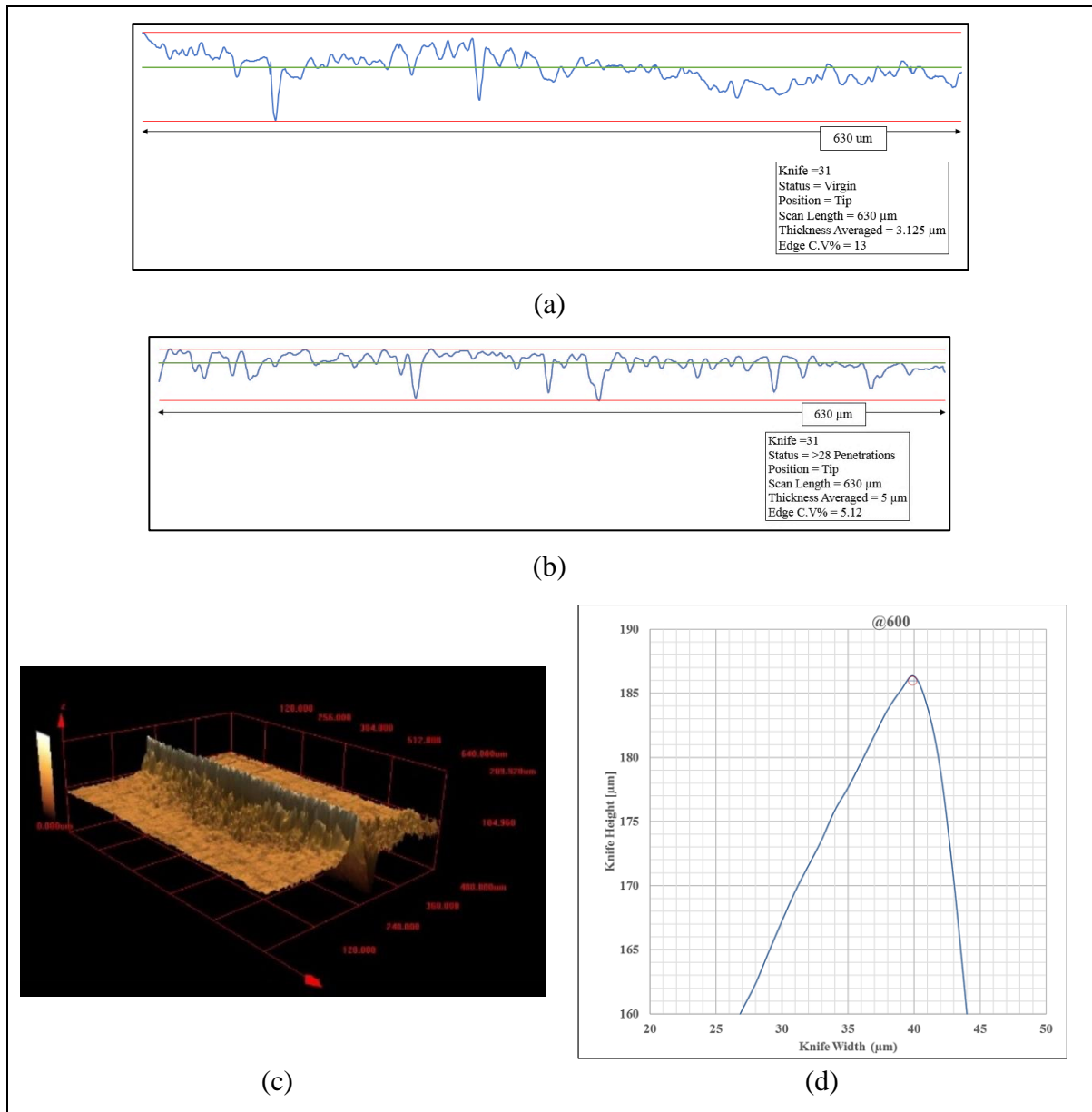
*Figure 32: Surface scan data in graphical format for edge variations of (a) virgin knife (b) same knife after penetrations (c) 3D surface scanned image, and (d) is showing cross-sectional view of knife for edge diameter measurement.*

*Table 11: Measurement of mean edge diameter and roughness of virgin and penetrated knives*

| Blade Type | Edge Diameter (μm) |
|------------|--------------------|
| Virgin | 1.35(0.88) |
| Penetrated | 2.05 (0.043) |

It is observed that the edge diameter of penetrated knives was increased showing increase in its bluntness.

## 5.4. Effect of Different surface modifications on QSKPR and Penetration Energy

### 5.4.1. Silicon dioxide Deposition

Neat fabric was treated with WG in four different concentration (4%, 8%, 20% and 40%) using padding rollers followed by acid treatment to deposit $SiO_2$ layer as described in section 4.2.1.2. Each fabric was tested for QSKPR in three different KPA (0°, 45° and 90°) and their mean QSKPR and penetration energy at peak resistance was computed.

It was founded that, on increasing the concentration of WG directly proportional increase was observed in QSKPR and penetration energy (PE) at peak resistance, as shown in Figure 33. The coefficient of the first order polynomial model fitted to the data (Equation 12), along with goodness of fit, can be found in Table 12.

$$f(x) = p_1 x + p_2$$

*12*

For statistical treatment and calculations, the least squares criterion was used. This criterion is based on the assumption of errors normality, independence and constant variance.
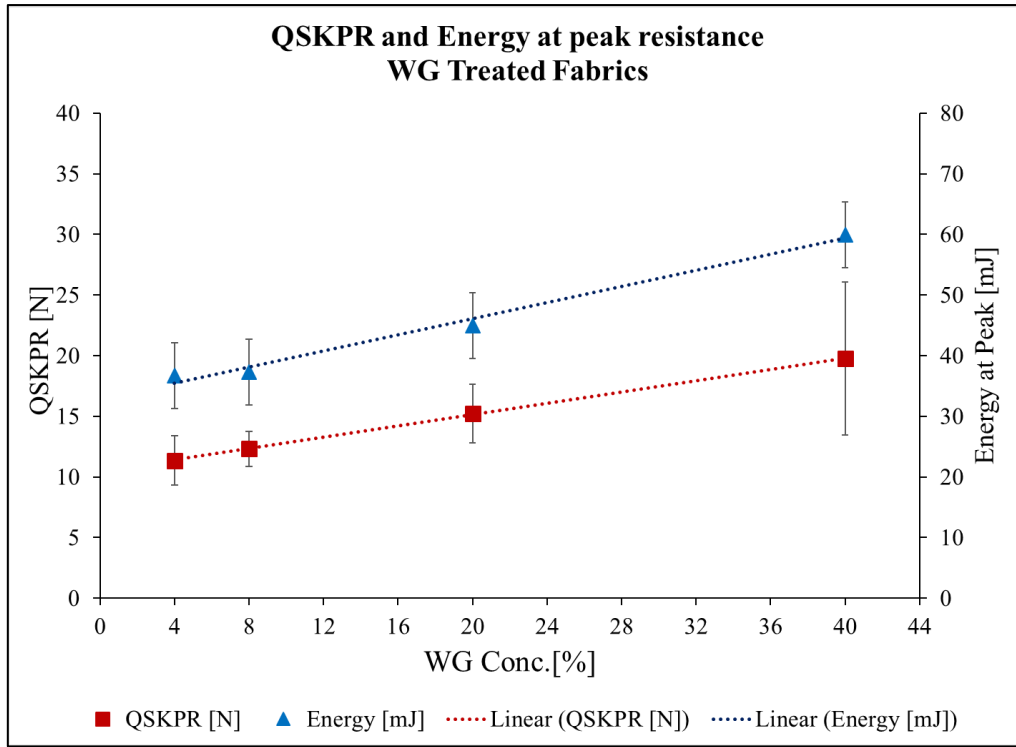
*Figure 33: Effect of WG treatment on QSKPR and Energy at peak resistance*

*Table 12: Coefficients of 1st degree polynomial fit for QSKPR and PE vs WG Conc. and goodness of fit*

| Coefficients of Model (upper & lower bound of 95% CI) | $p_1$ | | $p_2$ | |
|---|---|---|---|---|
| QSKPR | 0.233 (0.221, 0.246) | | 10.47 (10.19, 10.75) | |
| PE | 0.666 (0.456, 0.876) | | 32.75 (27.95, 37.54) | |
| Goodness of fit | SSE | R-square | Adjusted R-sq. | RMSE |
| QSKPR | 0.0131 | 0.9997 | 0.9995 | 0.0810 |
| PE | 3.745 | 0.9893 | 0.984 | 1.368 |

It is judged that on increasing the concentration of WG results higher amount of SiO$_2$ deposition, as is evident from weight gain of up to 8% for S4, as in given in Table 10 and also can be seen in SEM images in Figure 34(b) & (c). The deposition of SiO$_2$ makes yarn stiffer and increase the fabric's coefficient of surface friction. Also, the air permeability results showed the pours are filled with deposited layer which reduced the air permeability significantly for SiO$_2$ deposited fabrics. Also, fabric density (mass per unit volume) increased due to the higher compactness of the fabric. All these parameters are adding to increase the QSKPR and PE at peak resistance.
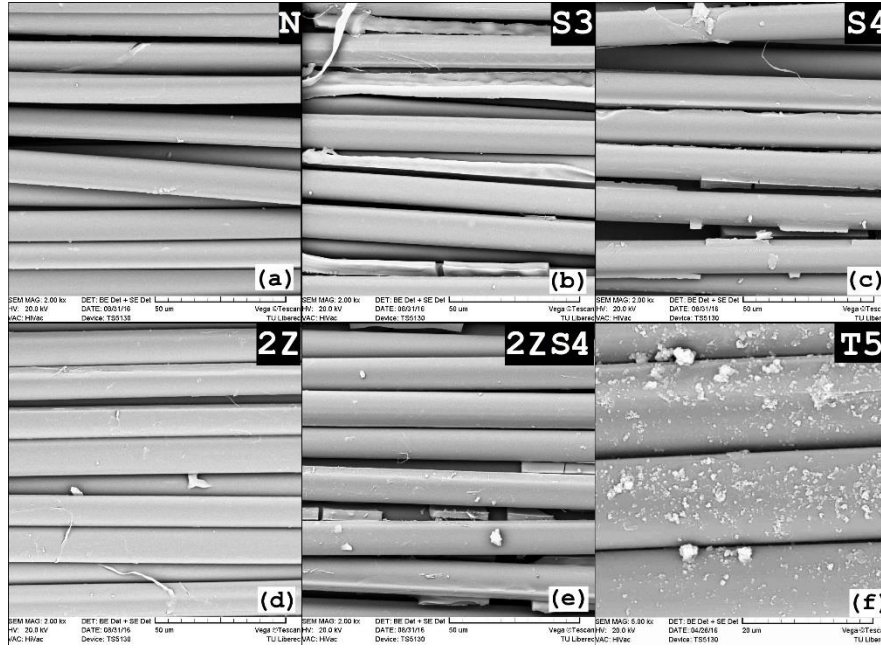
*Figure 34: SEM images of different treated samples showing surface topography of (a) Neat, (b) S3, (c) S4, (d) 2-hour Ozone treated, (e) Ozone and WG treated and (f) Titanium dioxide treated fabric samples*

### 5.4.2. Ozone and WG Treatment

It is believed that Ozone treatment can affect the para-Aramid [93]. Therefore, Neat samples were exposed to aqueous ozone medium for 60 and 120 minutes. The Ozon treatment setup and procedure is described in section 14.2.1.4. The results of these treatments as comparison of fabric treated with Ozone only and with Ozone and WG are shown in Figure 35 and effect of WG concentration on 2ZS4 fabric is shown in Figure 36 and their coefficient of first order polynomial fit (Equation 12) and goodness of fit in Table 13.

*Table 13: Coefficients of 1st degree polynomial fit, for QSKPR and PE vs WG Conc. and goodness of fit, for 120 min Ozone Treatment*

| Coefficients of Model (upper & lower bound of 95% CI) | $p_1$ | | $p_2$ | |
|---|---|---|---|---|
| QSKPR | 0.2489 (-0.4823, 0.9802) | | 12.68  (-6.205, 31.56) | |
| PE | 2.139  (-0.05399, 4.333) | | 39.55  (-17.08, 96.18) | |
| Goodness of fit | SSE | R-square | Adjusted R-sq. | RMSE |
| QSKPR | 2.65 | 0.9493 | 0.8985 | 1.628 |
| PE | 23.84 | 0.9935 | 0.9871 | 4.882 |
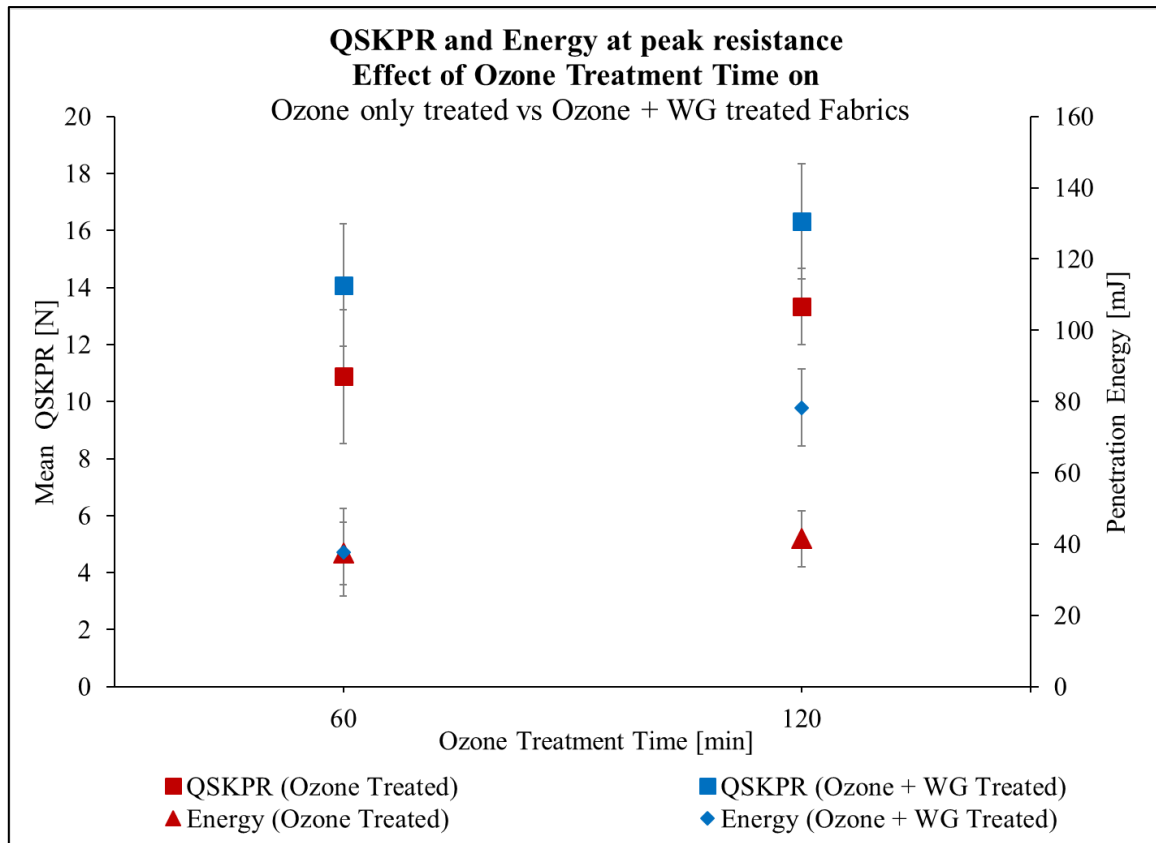
*Figure 35: Effect of Ozone treatment time on Ozonized only and Ozone + WG treated fabrics*
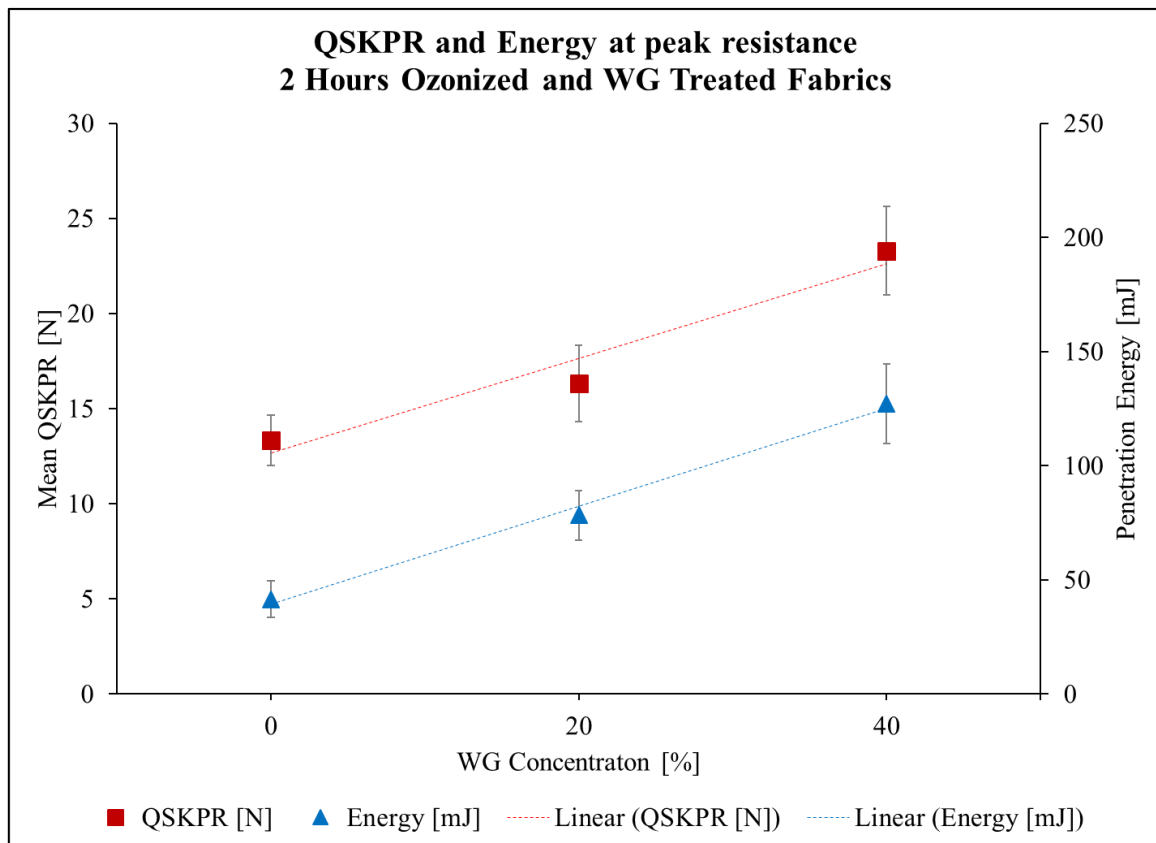


*Figure 36: Effect WG concentration on QSKPR and Penetration Energy of Ozonized and WG treated fabrics*

Ozone treated samples did not showed any physical changes at the fibre surface, as is observable in SEM images shown in Figure 34(d), unchanged flat surface is resembling the Neat fibres as seen in Figure 34(a). The ozone treatment improved the comfort and mechanical properties, as discussed in section 5.1.2, but its stab resistance performance was not significantly improved, as shown in Figure 35. However, ozonized samples were also treated with WG and fabric with both treatments showed proportional increase in QSKPR and penetration energy as WG concentration was increased, as shown in Figure 36. Although, only WG treated fabrics had better QSKPR but ozonized and $SiO_2$ deposited samples had comparable QSKPR, as found in Figure 40, with better comfort properties. It can be observed that 2ZS4 has comparatively less air permeability and lesser bending rigidity, as shown in Figure 27 and Figure 28 respectively.

### 5.4.3. Titanium dioxide Treatment

$TiO_2$ was applied to the neat fabric by pad-dry technique, in five different concentrations from 0.01 *g/l* to 0.5 *g/l*. Treated fabric samples were investigated for their mean QSKPR, that was examined for three different KPA i.e. 0°, 45° and 90°. Mean QSKPR and Energy at peak resistance for treated samples is compared in Figure 37. It is evident that increasing the concentration of $TiO_2$ on fabric surface is not improved QSKPR or Energy at peak resistance.

*Table 14: Coefficients of 1st degree polynomial fit for QSKPR and PE vs TiO2 Conc. and goodness of fit*

| Coefficients of Model (upper & lower bound of 95% CI) | $p_1$ | | $p_2$ | |
|---|---|---|---|---|
| QSKPR | 2.441 (-1.608, 6.491) | | 10.12 (9.084, 11.15) | |
| PE | -4.148 (-39.48, 31.19) | | 35.16 (26.14, 44.17) | |
| Goodness of fit | SSE | R-Sq. | Adj. R-Sq. | RMSE |
| QSKPR | 0.7746 | 0.551 | 0.4013 | 0.5081 |
| PE | 58.98 | 0.04445 | -0.2741 | 4.434 |
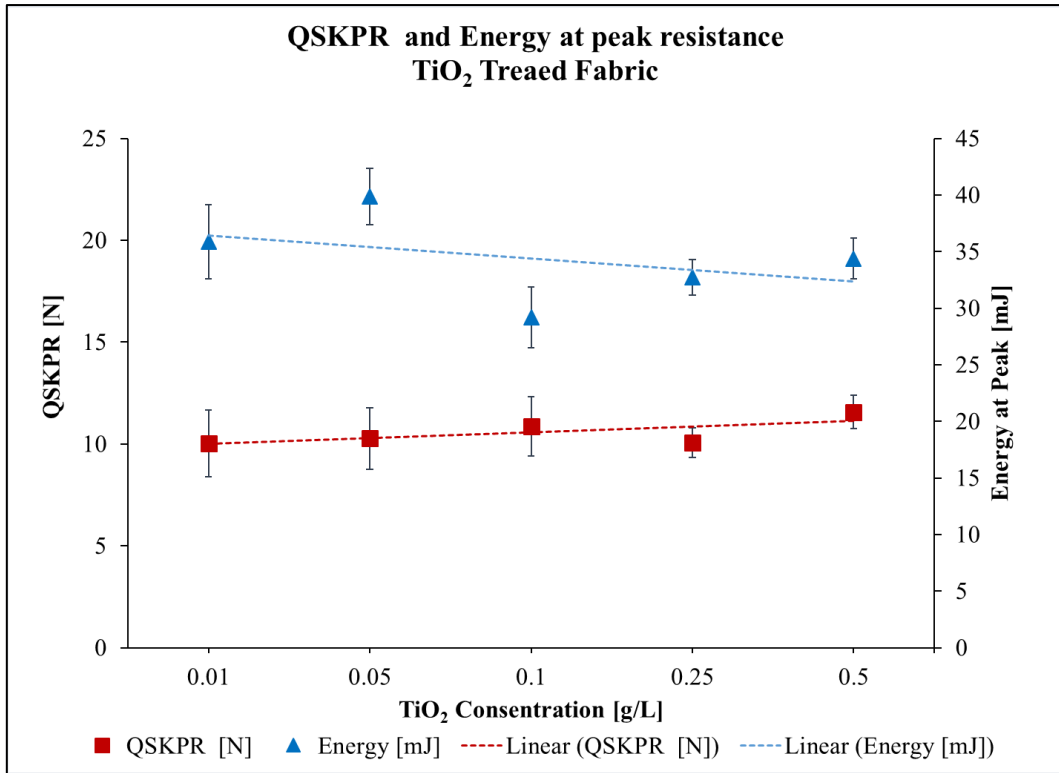
*Figure 37: Effect of increasing TiO₂ concentration on QSKPR and Energy at peak*

It was supposed to improve QSKPR by producing an interface with fibbers' surface and enhance the surface friction of the fabric. To investigate the reason of ineffectiveness of TiO$_2$ treatment, surface topology was observed under SEM, as shown in Figure 34(f). It was verified from the SEM images that the interface between TiO$_2$ particles and filaments' surface was absent. The particles were placed on the surface of the fibres without adhesion with the surface. It was assumed that increasing the density of these particles, by increasing concentration of TiO$_2$ was not resisting the knife penetration rather these particles was causing the mobility of the penetrating knife. Consequently, it is observable that on increasing the concentration of TiO$_2$ the QSKPR is not improving and PE had a negative slope.

To improve the interface of TiO$_2$ with para-Aramid fibres it was necessary to introduce chemical binders that would result in loss of comfort and flexibility

characteristics. Therefore, would be against the goal of this work. This research work investigated other methods of surface modifications further.

## 5.5. Deposition of the SiO₂ Layer

The deposition of $SiO_2$ layer was verified by following surface analysis techniques.

### 5.5.1. <u>SEM images:</u>

The physical presence of the deposited layer was observed in SEM images as shown in Figure 34(a), (b) and (c), for Neat, S3 and S4. Fabric surface topologies, of these fabrics, are confirming the physical presence of the deposited layer. For S3 and S4 samples, the deposited layer is apparent not only on the fibres surface but also in the gaps between fibres. Additionally, S4 sample shows the irregular edges of the deposited layer. In contrast, the untreated Neat sample has the smooth and clear surface.

### 5.5.2. <u>FTIR Spectroscopy</u>
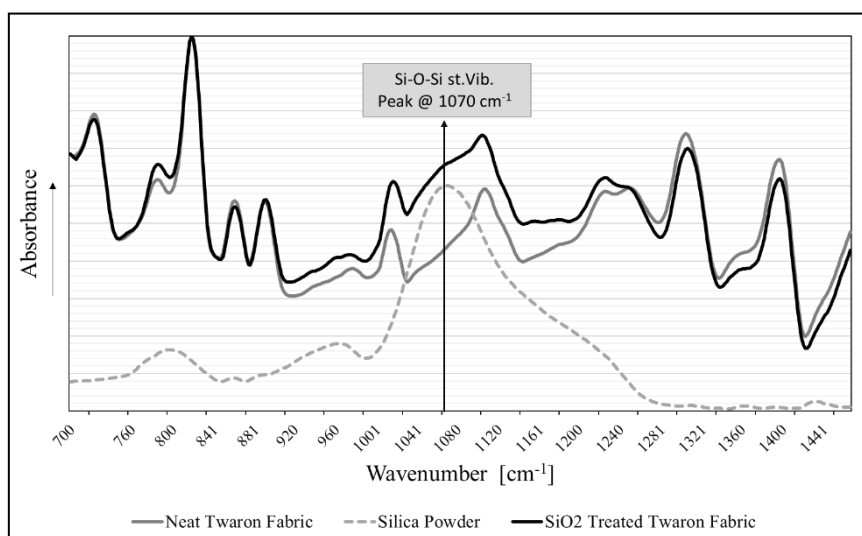


*Figure 38: FTIR spectra of untreated and treated samples and silica powder*

The FTIR spectra of treated and untreated samples are shown in Figure 38. The peak between 1000 to 1100 cm$^{-1}$, for silica powder curve, is due to the characteristic stretch vibration of Si-O [94]. The differences, in the curves of the untreated and the treated samples indicate the changes occurred after $SiO_2$ layer deposition. This change

is noticeable in curve of treated fabric where silica powder peak overlaps Neat fabric at 1070 cm$^{-1}$, as shown in the Figure 38.

### 5.5.3. EDX Analysis

The atomic composition of treated and untreated surfaces was determined by EDX analysis. The peaks of the detected elements can be found in Figure 39 and the percentage of different atoms partaking is given in the Table 15. The presence of Na and Si atoms were found only on treated samples while the comparative occurrence of Si and O atoms were found to be maximum on S4 samples and concentration of Na has reduced on S4 samples as compared to S3.
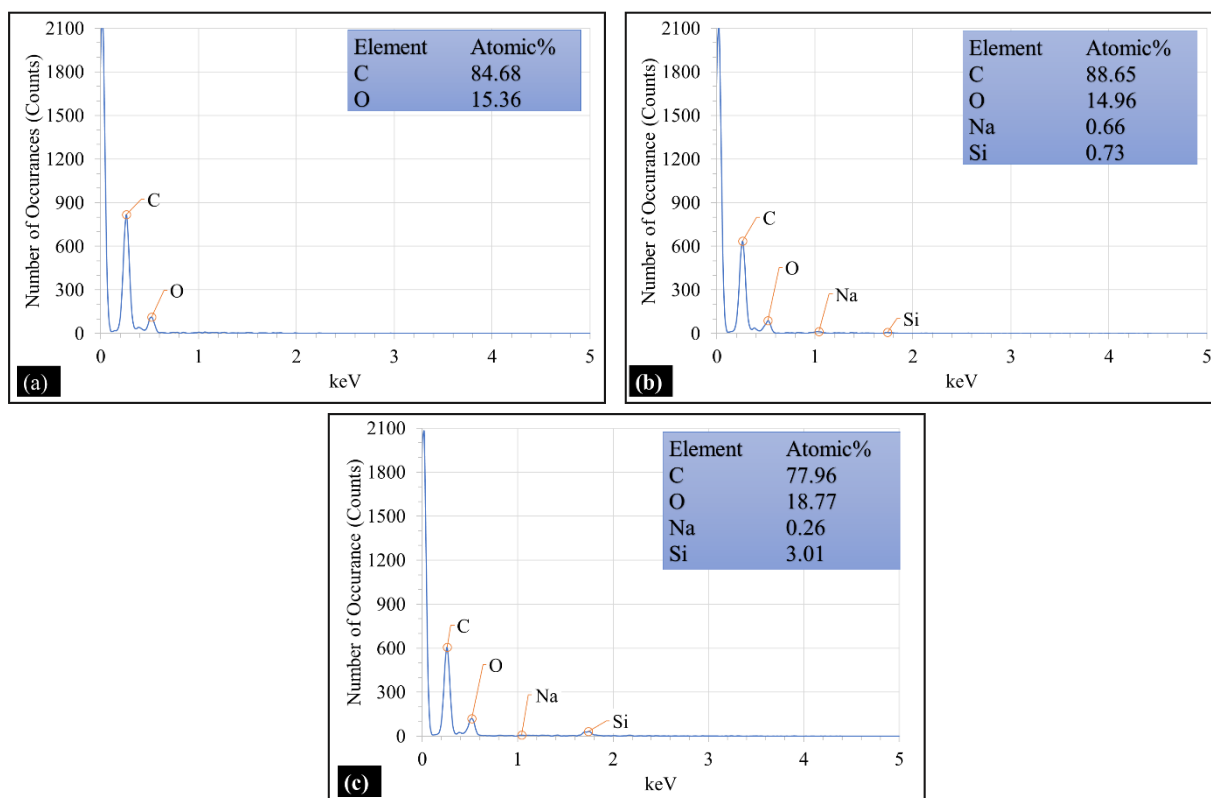


*Figure 39: EDX analysis of (a) Neat, (b) S3 and (c) S4 samples.*

The evidences obtained from SEM, FTIR and EDX analysis confirm the deposition of SiO$_2$ on the surface of treated samples, that can be summarised as:

1. The physical presence of the deposited layer is observable in SEM images,

2.  The presence of Si-O stretch vibration peaks in FTIR spectroscopy curves and

3.  The presence of Si, O and Na atoms as evident by EDX.

*Table 15 Element Analysis by EDX*

| Fabrics | Atomic (%) | | | |
|---|---|---|---|---|
| | C | O | Na | Si |
| N | 84.64 | 15.36 | - | - |
| S3 | 83.65 | 14.96 | 0.66 | 0.73 |
| S4 | 77.96 | 18.77 | 0.26 | 3.01 |

## 5.6. Change in surface friction

The coefficient of surface friction of different samples was also analysed, and the results are given in Table 16. The values in parenthesis show the Student's t-Distribution at 95% confidence interval. The coefficient of friction is found to be increased in order of S4>2ZS4>S3>N. It may indicate that the deposition of $SiO_2$ causes the surface to become irregular and coarser and hence resulting in the higher coefficient of friction for fabric surface. Furthermore, a greater amount of deposition of $SiO_2$ on treated samples resulted in a greater increase in frictional coefficient (as evident from Table 16).

*Table 16: Coefficient of friction of different fabrics*

| Fabrics Type | Neat | S3 | S4 | 2ZS4 |
|---|---|---|---|---|
| **Mean Coefficient of Friction, $\mu_s$** | 0.24(0.02) | 0.26(0.02) | 0.31(0.02) | 0.30(0.01) |

5.6.1.  <u>The effect of surface friction changes on QSKPR:</u>

The comparison of QSKPR force of treated and untreated samples at different penetration angles is expressed in Figure 40. The error bars represent the Student's t-Distribution at 95% confidence interval. The mean values of each fabric tested at all selected angles are represented with the horizontal line.
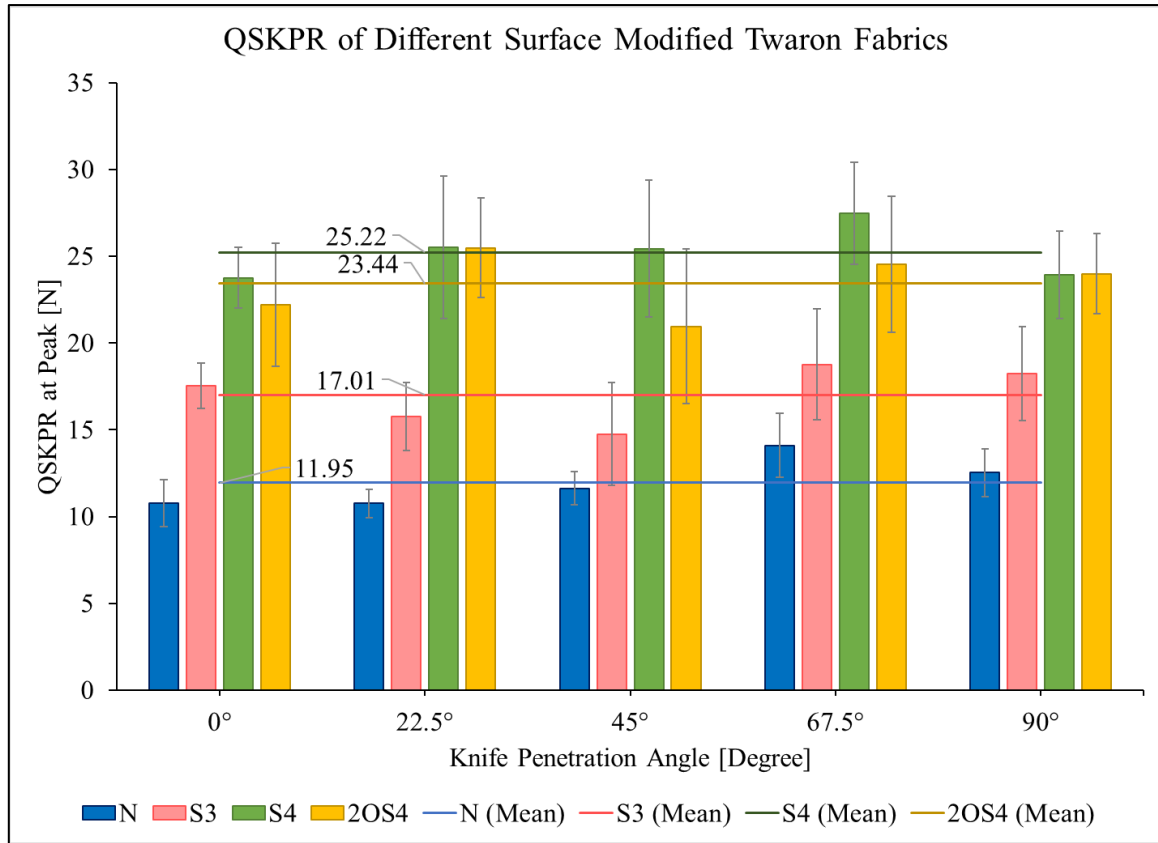
*Figure 40: QSKPR of different surface modified fabrics*

The bar chart establishes the statistically significant increase in penetration resistance, in the order of S4>2ZS4>S3>N. There is more than two-fold increase in mean penetration resistance from 11.88 *N* for Neat fabric to 25.55 *N* for S4 fabric. The reason of this behaviour may be due increase in frictional coefficients of treated samples which resulted in the higher knife penetration resistance. The key observations of the Neat fabric failure against the knife penetration were yarn to yarn sliding, lack of fibres gripping and partial yarn cutting. This may be reasoned to the open-structure of fabric, lack of fibre binding forces and lack of warp-weft friction. However, the behaviour of S4 sample was changed, where failure occurred due to the individual yarn cutting in one or fewer steps without yarn slippage. It may be associated with the increase in friction and knife load distribution to the neighbouring yarns. Comparison of force-displacement curves of Neat and S4 samples indicate this behaviour, as presented in Figure 41.

Close observation of the force-displacement curves discloses two facts:

1. Total numbers of peaks have reduced, for full penetration of 42 *mm*.

2. Peaks for S4 sample were relatively higher than Neat fabric, which can be related to more yarns responding simultaneously i.e. more load distribution from single yarn to neighbouring yarns because of reduced yarn slippage.

These phenomena are evident in cases when the knife does not cut the warp or weft normally i.e. in cases of penetration angles of 22.5°, 45°, and 67.5°. For other cases, at the penetration angles 0° and 90°, the number of peaks for S2 and Neat samples are same. Sparse density of yarns causes individual yarn presentation to the knife sharp edge.
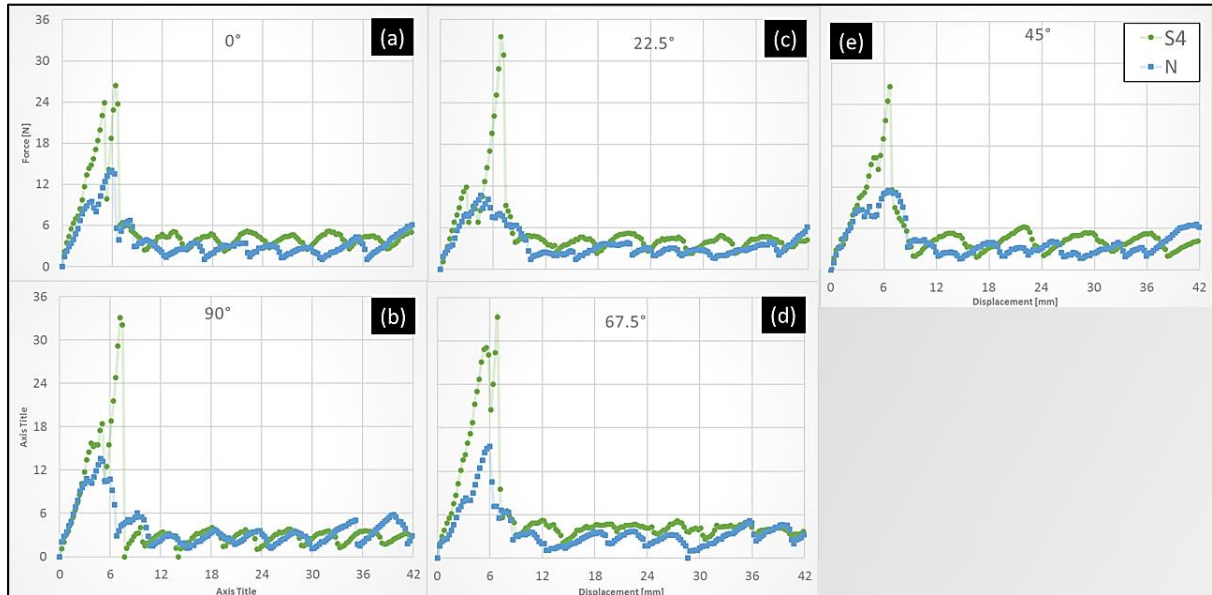


*Figure 41: Force-displacement curves of Neat and S4 samples at different knife penetration angles (best of various samples)*

### 5.6.2. The Relation of QSKPR with the amount of deposition and friction

Another analysis made from Figure 40 is that the QSKPR increases linearly with the increase in amount of $SiO_2$ deposition on the fabric surface. This is true for all the penetration angles. In the similar manner, it is also found that the QSKPR is related to fabric surface friction. To investigate the relation, mean surface frictions were plotted against mean QSKPR for Neat, S3 and S4 samples, as shown in the Figure 42. The vertical

and horizontal error bars are showing 95% confidence interval of QSKPR and fabric friction, respectively. It is clear there is a strong dependence of variable $R_{st}$ (QSKPR) on the independent variable $\mu_s$ (coefficient of surface friction). So, for the given amount of $SiO_2$ deposited in this study, it can be stated that:

$$R_{st} = f(\mu_s)$$

*13*

1st degree polynomial linear model fitted, is shown in Equation 12 and the coefficients of the model and goodness of fit of this model are shown in Table 17.
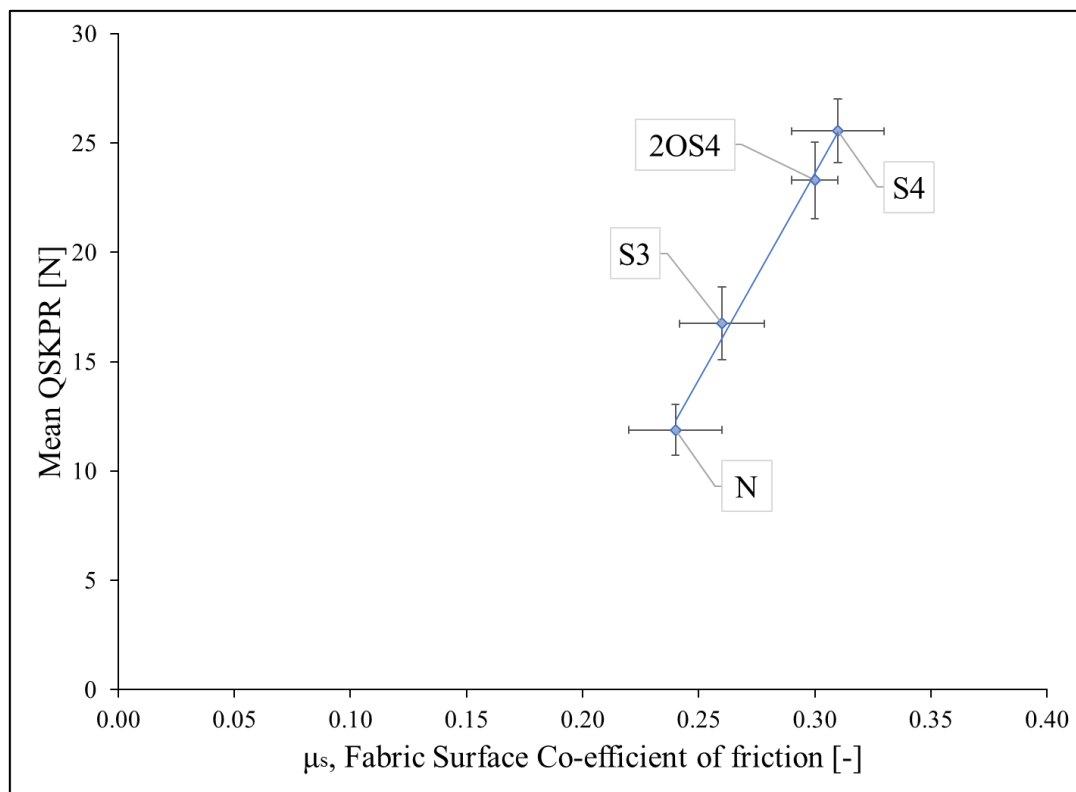


*Figure 42: Effect of change of surface friction on QSKPR*

*Table 17: QSKPR vs Fabric Friction fitted model coefficients and goodness of fit*

| **Coefficients of Model** **(95% confidence lower &** **upper bounds)** | **$p_1$** | | **$p_2$** | |
|---|---|---|---|---|
| | 188.1 (142.9, 233.4) | | -32.84 (-45.46, -20.22) | |
| **Goodness of fit** | **SSE** | **R-Sq.** | **Adj. R-Sq.** | **RMSE** |
| | 0.724 | 0.9938 | 0.9907 | 0.6017 |

## 5.7. The effect of KPA on QSKPR

The effect of the penetration angle on QSKPR is presented in Figure 40. The Neat

fabric shows the increase QSKPR with the increase in penetration angle from 0° to 90°, with the highest resistance at 67.5° penetration angle. The similar behaviour is observed for the surface modified fabrics.

However, it should be noted that the higher penetration resistance at the 67.5° penetration angle is not statistically significantly different, for any fabric type. Only for Neat fabric, the penetration resistance for this angle is statistically significantly different from the means all Neat samples (as seen horizontal blue line in Figure 40). This analysis was performed for t-distribution test at 95% confidence level and given in Table 18. Moreover, all fabrics show comparatively higher penetration resistance at 67.5° KPA as is evident in Figure 40 except 2ZS4.

*Table 18 One-way Analysis of Variance (ANOVA) for QSKPR of Neat fabric at 67.5°*

| Angle | Neat fabrics mean resistance | Mean resistance at 67.5• | P |
|---|---|---|---|
| 67.5° | 11.88 | 14.1 (12.25, 15.95) | 0.017 |

### 5.7.1. Orientation of yarns at different penetration angles

The differences between the penetration resistance forces at different penetration angles can be linked to the orientation and availability of yarns to the knife edge. In Figure 43(a), the knife edge travelling at different penetration angles are shown with dotted lines. There can be three possibilities with respect to the knife travel (tr) for each consecutive yarn cutting:

1. At penetration angles 0° and 90°, one direction yarns, either wefts or warps are cut, and knife travels a distance equal to one pick spacing, denoted here with 'p', as shown in Figure 43(b) as $t_0$ and $t_{90}$. This distance is the smallest of three cases but as compared to knife travel, the warp and weft density is sparse, and the knife edge does not face consistent resistance from fabric. This is the reason that the QSKPR drops to zero after each yarn cutting, before the next yarn starts resistance against

knife, as evident in Figure 41(a) and Figure 41(b).

2. For 45° penetration angle as seen in Figure 43(c), the knife engages warp and weft in orthogonal pairs. The distance travelled is √2p for each next pair. This is the maximum distance for all three cases. Also, yarn to yarn slippage is highest among all cases. That is the reason, QSKPR force-displacement curves shows higher numbers of peaks, and relatively least resistance is observed at 45°. And in the case of higher yarn to yarn friction, as in S4, the number of smaller peaks has reduced, as evident in Figure 41(e).
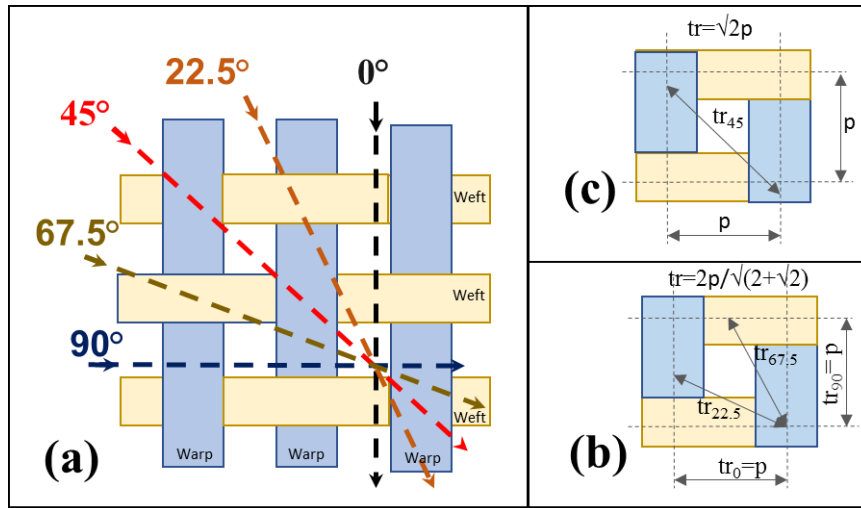


*Figure 43: (a) Illustration of the path, knife edge travels at different KPA, (b) yarn to yarn distance and knife travel (t) at 0°, 90°, 22.5° and 67.5° and (c) at 45°*

3. In the case of 22.5° and 67.5° penetration angles the knife edge travels a distance of $\frac{2p}{\sqrt{2+\sqrt{2}}}$, as clear in Figure 43(b), that is nearly equal to one pick spacing, 1.083p. And both warp and weft yarns offer the resistance simultaneously, although more resistance is offered by yarn that is cut near to its transverse direction. The knife travelling finds less gaps and relatively more steady fabric response is exhibited as is evident from QSKPR force-displacement curves, apparent by fewer peaks and less bumps as shown in Figure 41(c) and Figure 41(d).

The dominated higher resistance at 67.5° as compared to 22.5° and at 90° than 0°

angles may be linked to the higher mechanical strength of warp yarns.

The distance knife should travel for each penetration angle is negatively relating the QSKPR, that can be expressed as:

$$R_{st} = f\left(\frac{1}{tr}\right)$$

### 5.7.2. Warp and Weft complementary cutting behaviour

There seems to be the complementary response of warp and weft when penetration angle changes. This is also supported by the post-penetration fibre damage analysis, removed from damaged Neat fabric samples (Figure 44). It was observed that transverse knife penetration caused maximum load sharing as evident from plastic deformation at 0° and 90° penetration angles, as given in Figure 44(a) and Figure 44(b). Since warp yarns are also showing cracking, fibrillation and fibre rupture along the length, which may be attributed to higher stress at break of warp yarns than weft yarns. This finding is supported by the fact that the tensile strength exhibited by warp yarns, of any fabric, is higher from their respective weft yarns. The ultimate tensile strength of yarns removed from different fabrics is shown in Figure 45. The an-isotropic cutting behaviour of textile fibres and yarns is already recorders [30], [32], and it is known that woven fabric show anisotropy for their mechanical characteristics, when examined at off-axis from warp or weft directions.[95]
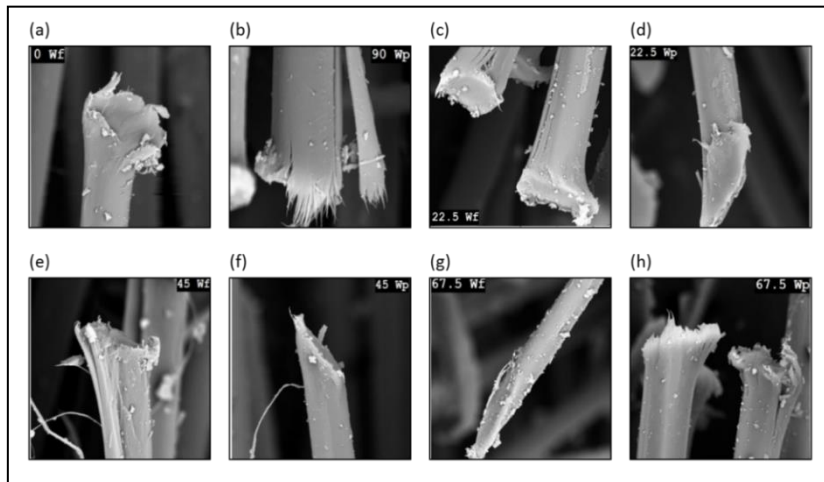


*Figure 44: SEM images of fibres removed from post-penetrated fabric samples.*
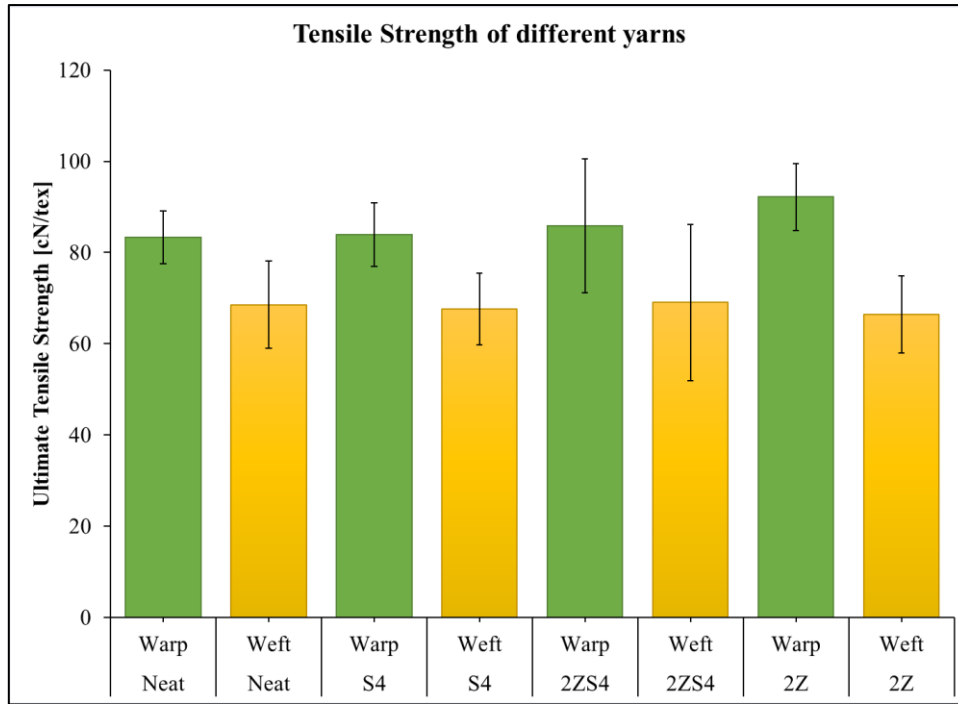
*Figure 45: Comparison of the ultimate tensile strength of warp and weft yarns, removed from respective fabric*

For all the other cases the tip of damaged warp and weft yarns is in accordance with the angle at which knife cut the respective warp or weft yarn. The fibre that is cut at an angle closer to the transverse direction, shows higher plastic deformation, cracking and fibrillation. When the cutting angle decreases to lower penetration angles, a clear sharp edge is observed at the tip of the damaged fibre and plastic deformation mechanisms also diminish.

The orthogonal orientation of warp and weft makes the QSKPR complementary to 90° i.e. the sum of cut angles of warp and weft fibre is 90°. So, the fibres cutting at the smaller angle contribute less resistance than cutting at the higher angle. When yarns with the higher tensile strength are cut at higher angle, more QSKPR is exhibited [35]. This angle dependence of QSKPR can be expressed as:

$$R_{st(warp)} = f(\sigma_{warp} sin\alpha)$$

*15*

$$R_{st(weft)} = f(\sigma_{weft} sin\beta)$$

*16*

Considering orthogonal orientation of warp and weft:

$$\angle\alpha \perp \angle\beta$$

$$\Rightarrow sin\beta = cos\alpha$$

Therefore, the Equation 16 becomes:

$$R_{st(weft)} = f(\sigma_{weft}cos\alpha)$$

*17*

For fabric response, combining equation 15 and 17:
:

$$R_{st} = R_{st(warp)} + R_{st(weft)}$$

$$R_{st} = f\left((\sigma_{warp}\,sin(\alpha)) + (\sigma_{weft}\,cos(\alpha))\right)$$

*18*

Here, $R_{st}$ is QSKPR measured in $N$, $\sigma_{warp}$ and $\sigma_{weft}$ are the warp and weft ultimate

tensile strength in measured in *cN/tex* and α is the knife penetration angle in degrees.

### 5.7.3. Fourier function fitting:

Fourier function, Equation 19, was fitted to the mean QSKPR at different KPAs of

treated and untreated fabrics. Figure 46 shows the fitting results. The fitted equation

coefficients are shown in Table 19 and variance and goodness of fit, for different fabrics,

in Table 20.

$$f(\alpha) = c_0 + c_1\,cos(\alpha.w) + c_2\,sin(\alpha.w)$$

*19*

$\alpha$ here is the KPA and $w$ is the period, which can be up to $2\pi$, for this measurement

$w = \pi/2$. It is assumed that $\pi/2$ period can be generalized to complete $2\pi$.
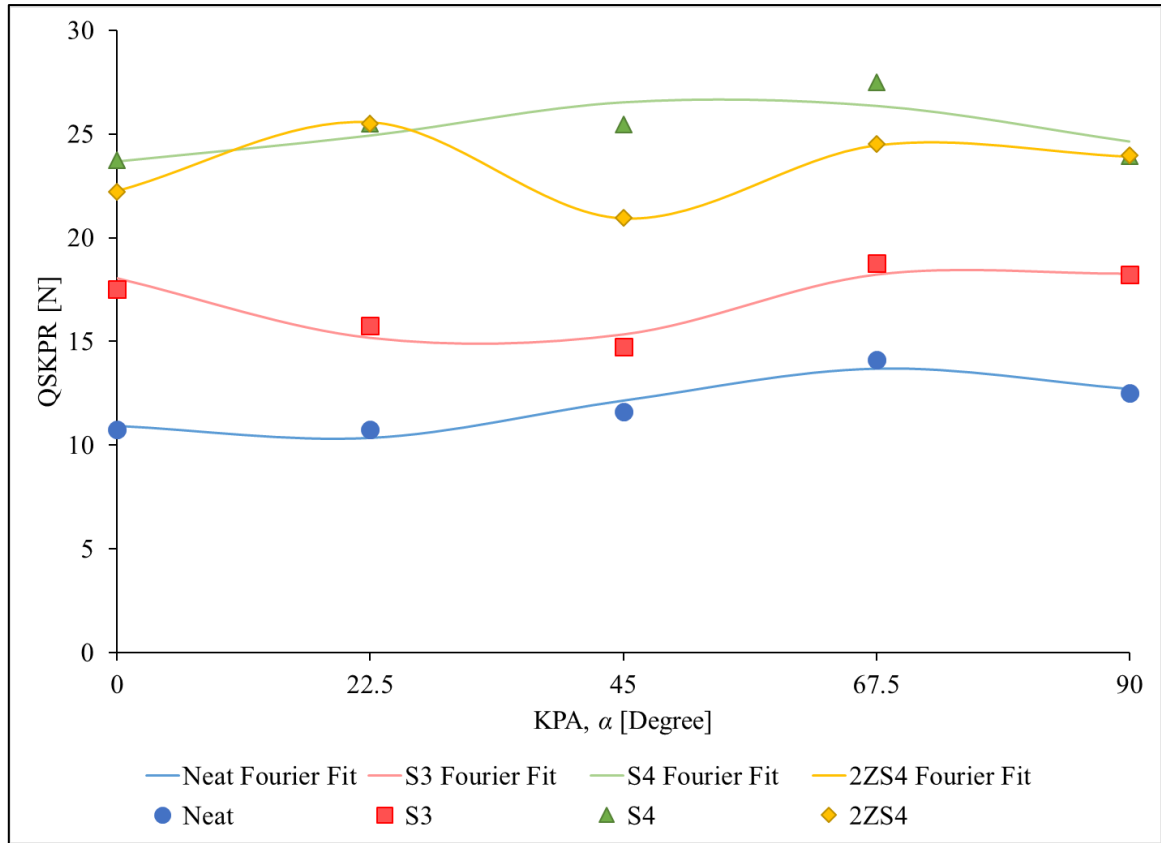
*Figure 46: Comparison of predicted and measured QSKPR of different fabrics as different KPAs.*

*Table 19: Fitted Coefficient of Fourier Function*

| Coefficients | Neat | S3 | S4 | 2ZS4 |
|:---:|:---:|:---:|:---:|:---:|
| $c_0$ | 11.96 | 16.75 | 25.18 | 23.29 |
| $c_1$ | -1.04 | 1.30 | -1.51 | -1.02 |
| $c_2$ | -1.39 | -1.63 | 0.26 | 2.26 |
| $w$ | 0.06 | 0.07 | 0.05 | 0.11 |

*Table 20: Goodness of fit for different fabrics*

| Fabric | SSE | RMSE | R-Square | Adj. R-Sq. | DFE | No. of Coefficients |
|:---:|:---:|:---:|:---:|:---:|:---:|:---:|
| Neat | 0.656 | 0.811 | 0.917 | 0.667 | 1 | 4 |
| S3 | 1.243 | 1.115 | 0.893 | 0.570 | 1 | 4 |
| S4 | 3.309 | 1.820 | 0.636 | -0.457 | 1 | 4 |
| 2ZS4 | 0.022 | 0.148 | 0.999 | 0.994 | 1 | 4 |

It is observable that nearly all fabric data fit well and explainable by Fourier function. However, it can be seen that the QSKPR response of S4 fabric have become distinctively homogenous which does not provide enough amplitude for complete fitting the function.

**5.8. Video Analysis**

To understand the interaction of knife and fabric the video of knife penetration, during quasi-static stab testing, was captured on CCD camera. The method and setup followed can be found in section 4.2.2.2. For comparison Neat and S4 fabric samples are analysed at 0° KPA.

The force-displacement curves are shown for Neat fabric in Figure 47 and for S4 fabric in Figure 49. These curves are labelled at different points mentioning fracture of certain yarns as numbered in Figure 48 for Neat fabric and in Figure 49 for S4 fabric.

The knife penetration can be viewed in two parts, first yarn is fracturing on blunt side and second sharp side of the knife. The yarn fracture on both sides are discussed below.

### 5.8.1. <u>Blunt side yarn fracture</u>

In both cases, of Neat and S4, as the knife starts to penetrate, the yarns interacting with blunt side of the knife are pushed aside, resulting a force like yarn pull out unless they are fractured. It is observable for yarn number 4 in Figure 48(B)-(D) and for yarn number 3 in Figure 50(B)-(D). After completion of first 6mm of knife penetration the blunt side get parallel to the length of knife, so further pressure from blunt side ends and only sharp side causes the pressure and yarn fracture. This initial fracture of yarn on blunt side is the major cause of higher peak in force-displacement curve.
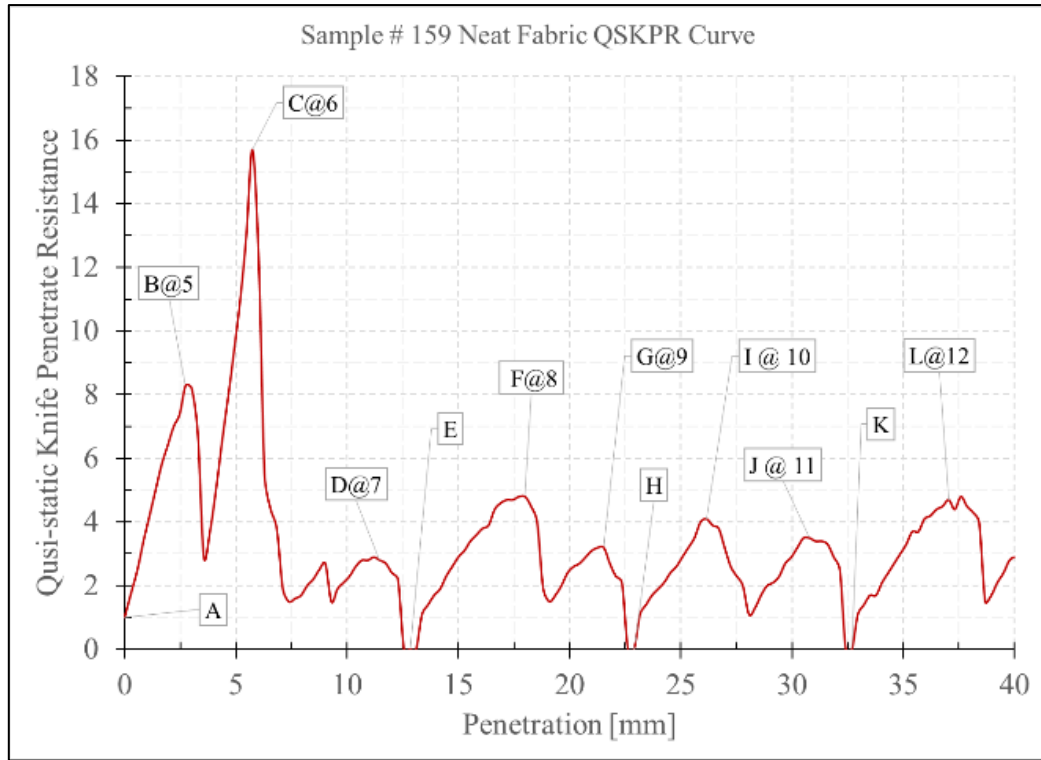
*Figure 47: Force-Displacement curve for Neat fabric at 0° KPA, label pointing fracture of different yarns*
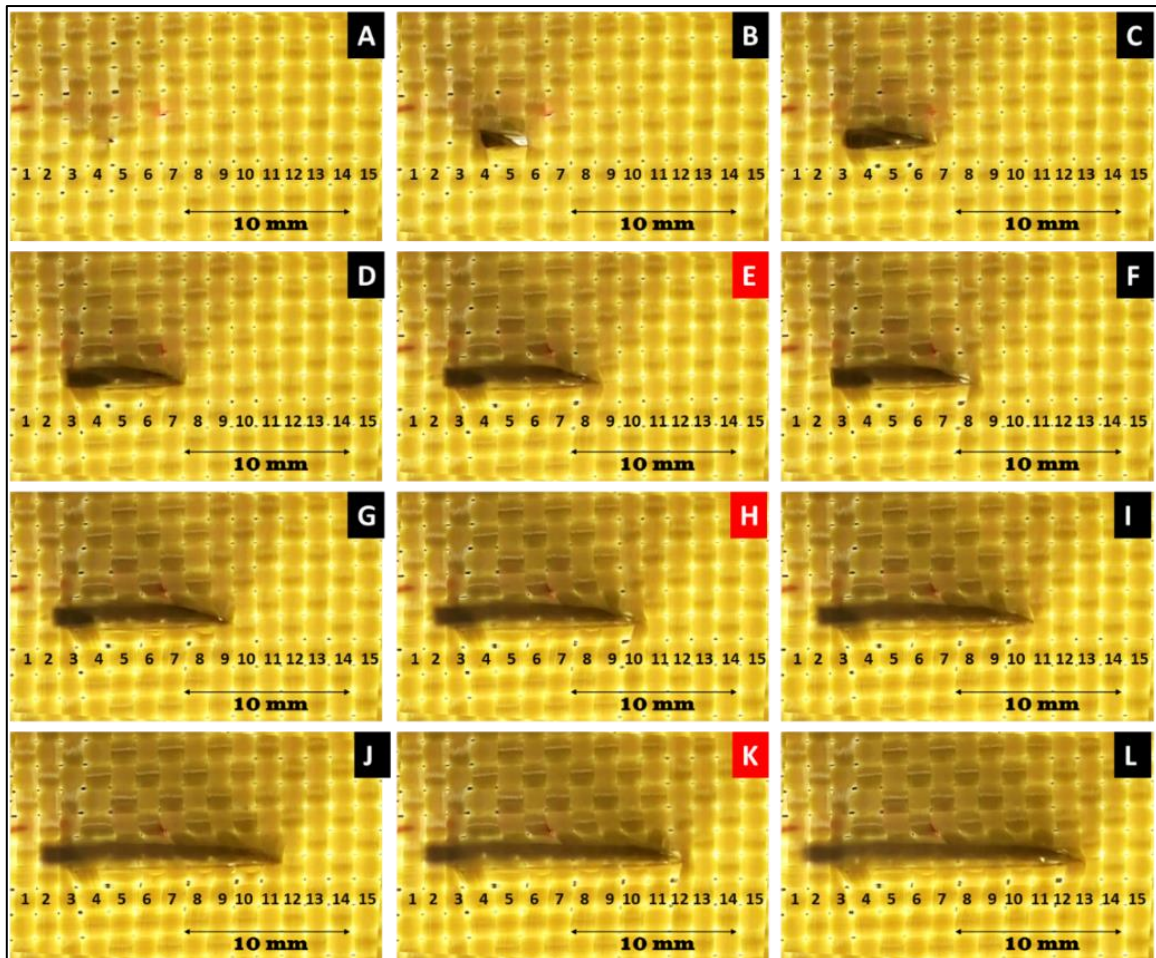


*Figure 48: Camera images showing knife penetration for Neat fabric at 0° KPA, different yarn fractures are labelled, at E, H and K knife penetrates without yarn fracture.*
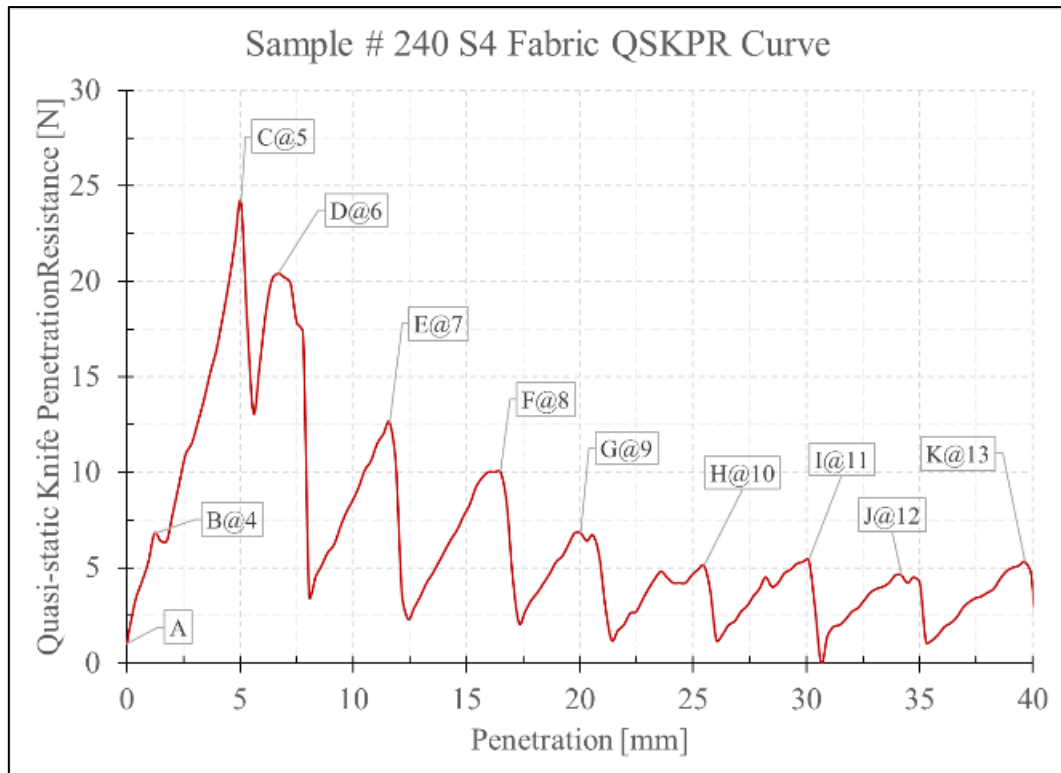
*Figure 49: Force-Displacement curve for S4 fabric at 0 KPA, showing point of different yarns fracture*
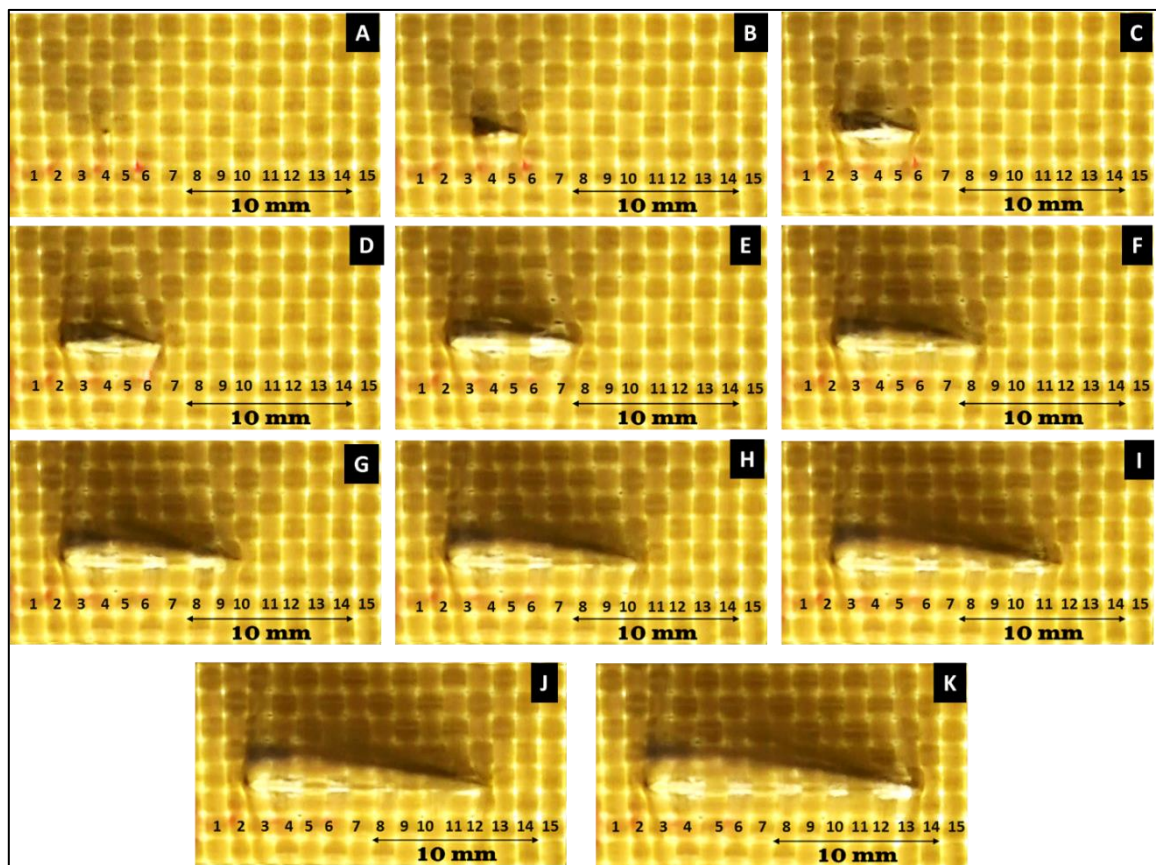


*Figure 50: Camera images showing knife penetration for S4 at 0° KPA, different yarn fractures are labelled.*

## 5.8.2. Sharp side yarn fracture

In Figure 47 and Figure 49 every peak is labelled with corresponding sub-figure and yarn number found in Figure 48 and Figure 50, respectively for Neat and S4 fabrics. Each peak is produced exactly before fracture of corresponding yarn. It can be seen that the fabric resistance falls to zero due to the gaps between yarns, for Neat fabric as mentioned at E, H and K in Figure 47 and Figure 48. While, for S4 fabric knife does not find a gap enough that resistance falls to zero. Moreover, the force-displacement curve's contours for Neat fabric are depicting inconsistent resistance from each individual yarn cutting, i.e. partial cutting of yarn which is also evident in recorded videos.



(a)



(b)



(c)
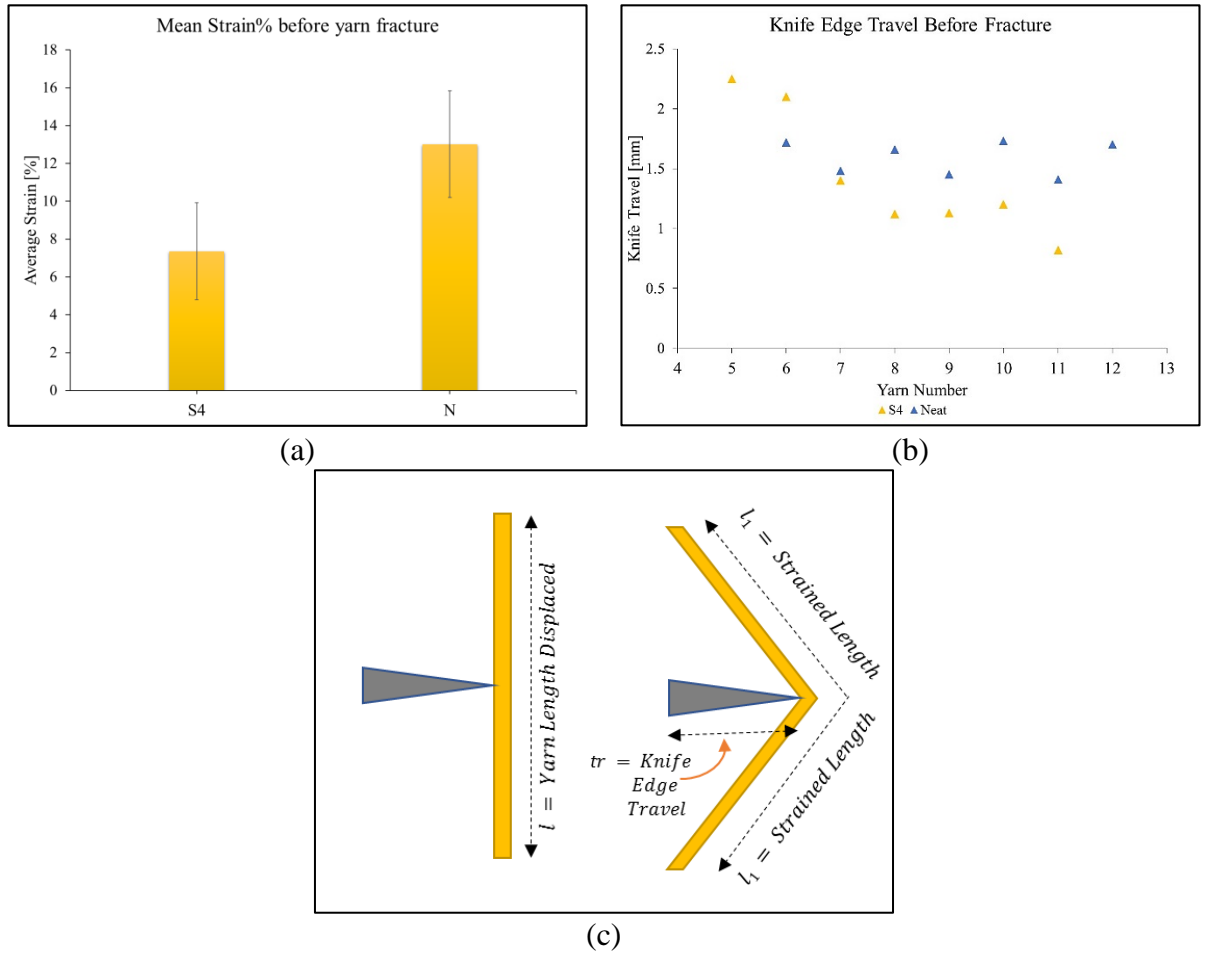
*Figure 51: (a) Mean Strain % of S4 and N analyzed from image analysis, (b) Travel of knife edge before each yarn rupture and (c) Illustration of yarn strain before fracture*

On the contrary the S4 yarn fracturing curves making clear peaks, as seen in Figure 49 at label C, D, E, F and G, that indicates the strong resistance offered by S4 individual yarns and complete yarn cut in one step without any partial cutting. This behaviour shows the intra-fibre cohesion that make filaments of the yarn behave as single assembly.

$$l_1 = \sqrt{\left(\frac{l}{2}\right)^2 + tr^2}$$

<div align="right">20</div>

$$Strain\% = \frac{(2l_1 - l)100}{l}$$

<div align="right">21</div>

Here $l$ is the length before straining, one half of the strained length is denoted with $l_1$ is calculated from Equation 20. $2l_1$ is the total length after straining and the percentage strain was measured using Equation 21.

The other reason of higher peak of S4 than Neat is the stiffer yarn behaviour of S4 yarns. The image analysis performed for the image-frames extracted from recorded video, as shown in Figure 51(c), proves this finding. Mean strain measured (by Equation 20 and 21) at rupture of S4 yarns was found to be lower than Neat yarns, as shown in Figure 51(a). Furthermore, the absorption of energy is higher for preceding yarns than following yarns, in case of S4 as shown for yarn number 5 and 6 in Figure 51(b).

## 5.9. Cutting Resistance of Individual Yarns

To examine how yarns behaviour against knife blade when no interlacement is there like in the fabric. The warp and weft yarns were removed from the treated and untreated fabrics. Their resistance against same (K1) knife edge was recorded as was used to penetrate the fabric. The details of device and procedure are already discussed in section 4.2.4.3.

The mean cutting resistance and energy versus knife vertical displacement and knife edge displacement was recorded for 10 yarns. The results are shown for Neat warp and weft in Figure 52 and Figure 53, and S4 warp and weft in Figure 54 and Figure 55 respectively. The shaded area in figures is indicating 95% confidence interval of mean resistance. Few things are noteworthy here:

1. Near about all yarn are completely fractured for same knife displacement, similar cut resistance and cut energy.

2. Both Neat (warp and weft) yarns and few S4 weft show partial fracture, Neat yarn around midway of complete fracture displacement at around 5 *mJ* cut energy and S4 weft later than midway at around 12 *mJ*.

3. S4 warp does not show partial fracture but cut in one go. And fracture of complete yarn completes earlier than Neat yarns, for both S4 warp and weft.
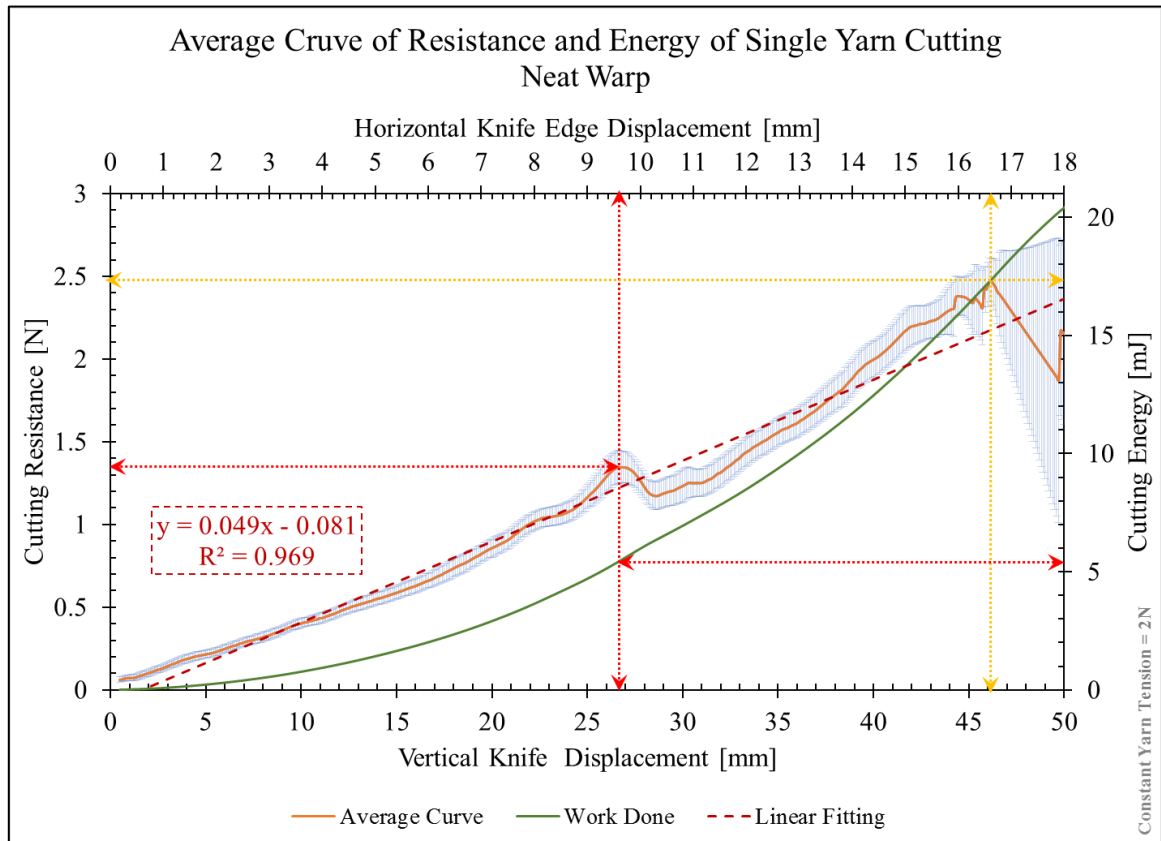


*Figure 52: Mean curve for cutting resistance and cutting energy verses vertical and knife edge displacement for Neat warp*
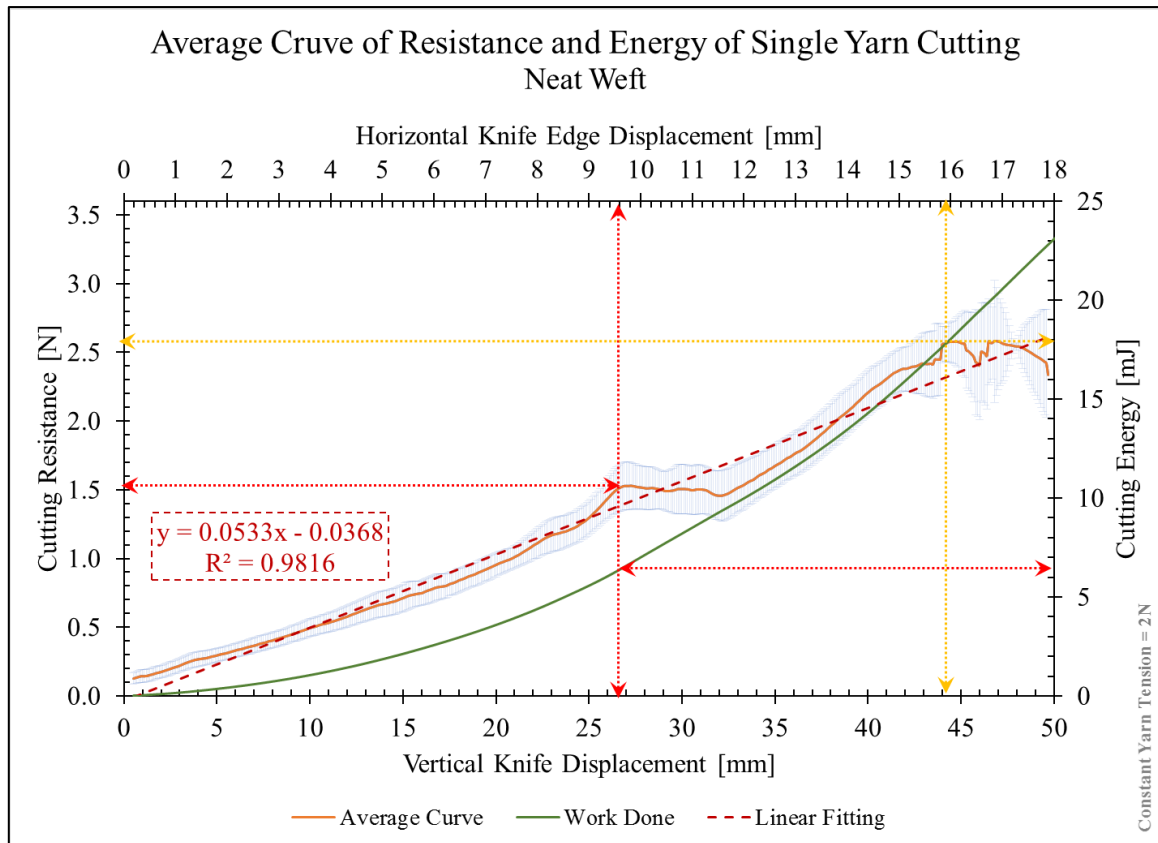
*Figure 53: Mean curve for cutting resistance and cutting energy verses vertical and knife edge displacement for Neat weft*
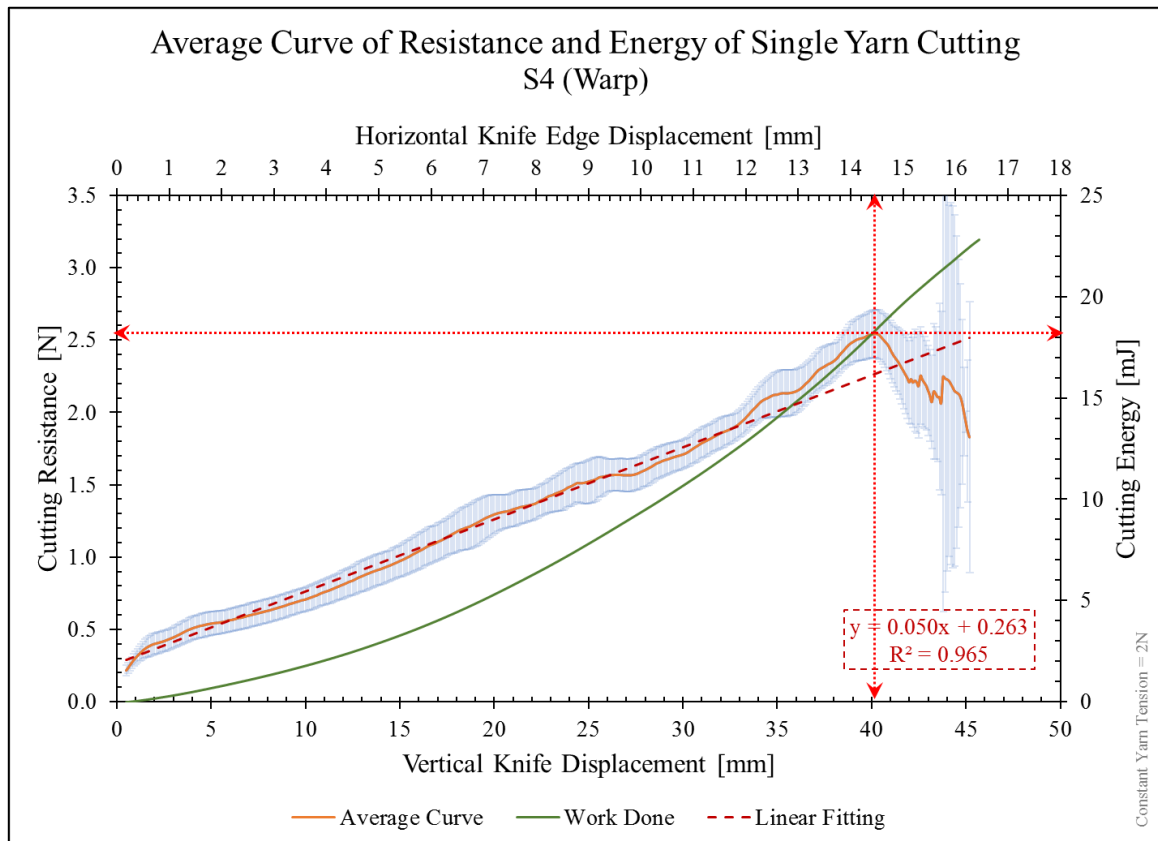


*Figure 54: Mean curve for cutting resistance and cutting energy verses vertical and knife edge displacement for S4 warp*

73
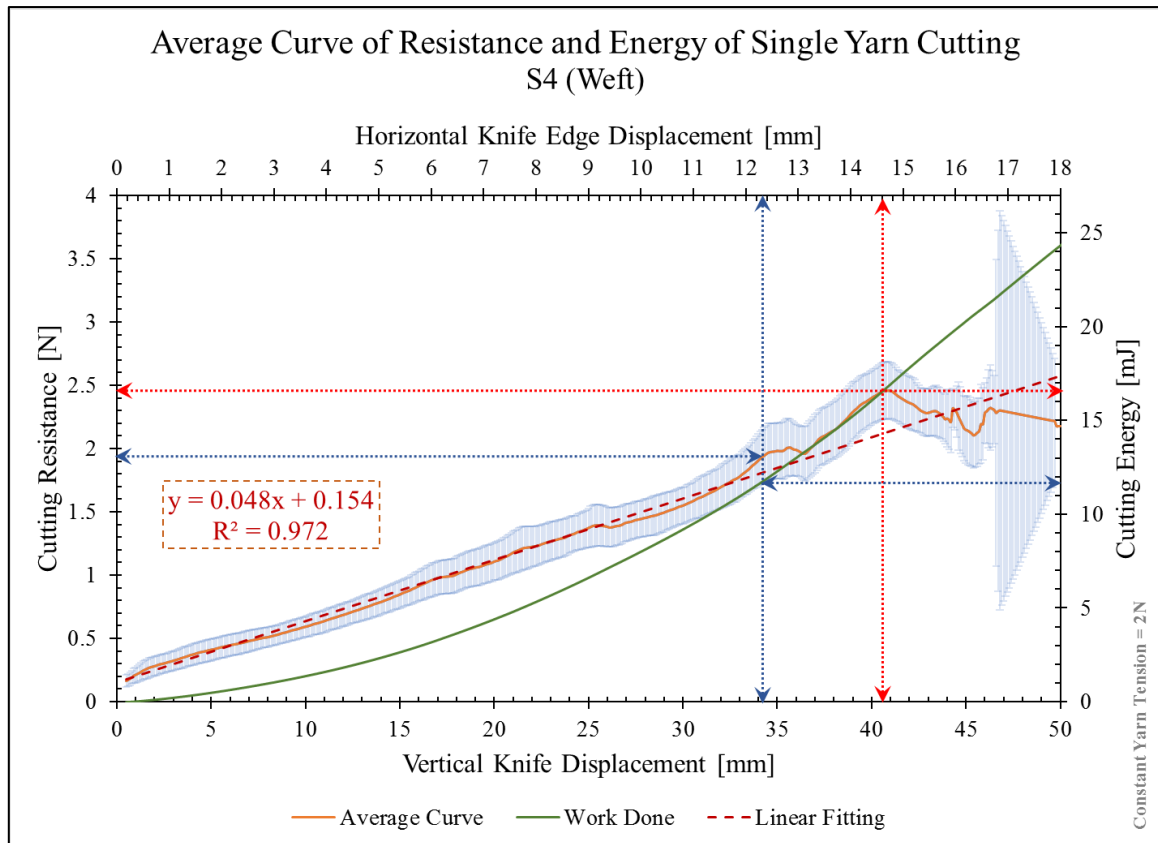
*Figure 55: Mean curve for cutting resistance and cutting energy verses vertical and knife edge displacement for S4 weft*
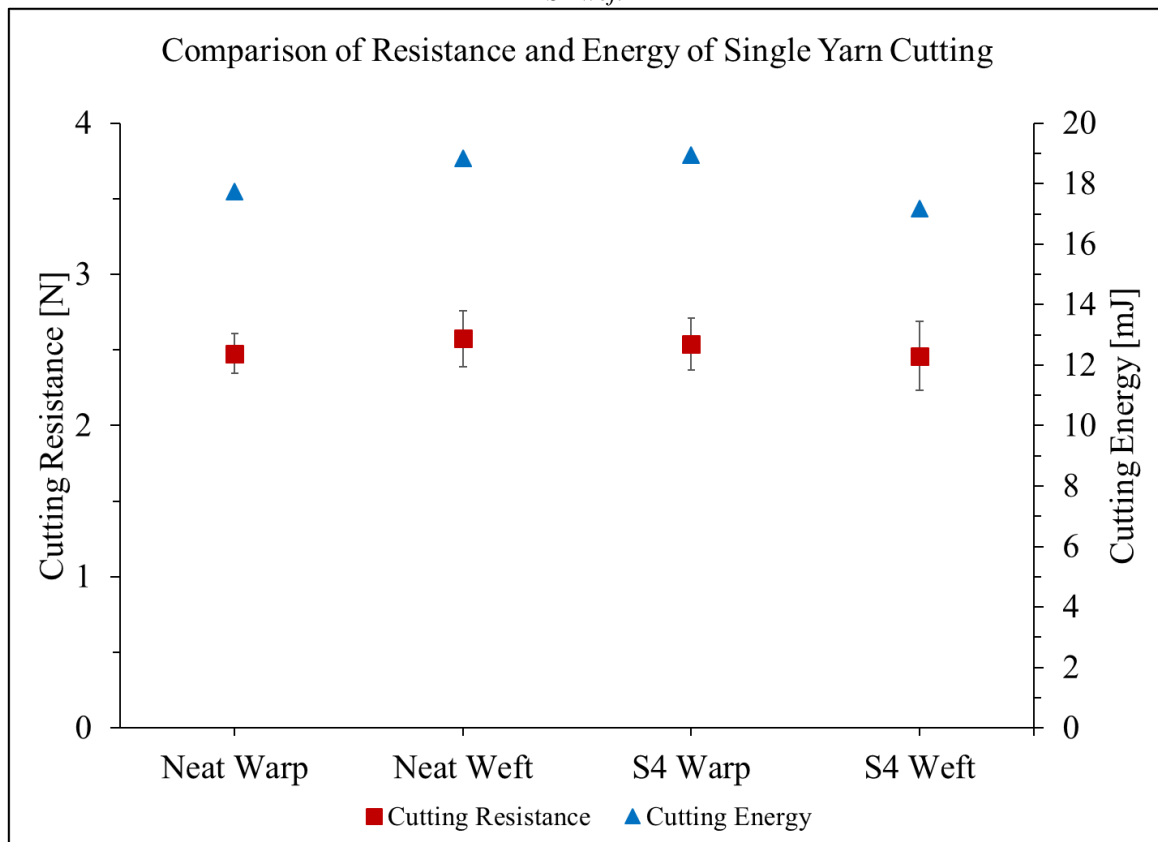


*Figure 56: Average Cut resistance and Cut Energy for different types of individual yarns*

These results are summarized in Table 21 and graphically represented in Figure 56.

*Table 21: Individual Yarn Cutting Statistics*

| Fabrics | Mean Cutting Resistance | Values at Peak Resistance for: | | |
| --- | --- | --- | --- | --- |
| | | Yarn Cutting Energy | Knife Edge Displacement | Knife Length Displacement |
| | [N] | [mJ] | [mm] | [mm] |
| Neat Warp | 2.48 (0.13) | 17.75 | 16.78 | 46.1 |
| Neat Weft | 2.58 (0.19) | 18.83 | 16.31 | 44.8 |
| S4 Warp | 2.54 (0.17) | 18.94 | 14.70 | 40.4 |
| S4 Weft | 2.46 (0.23) | 17.17 | 14.89 | 40.9 |

From these results it can be inferred that S4 yarns have developed enough inter-fibre cohesion that they persist partial yarn fracture to larger extent, than Neat yarns, but once cutting starts complete yarn cuts in one step. While Neat yarn individual filament resist against separately and yarns fracture by parts, showing absence of inter-fibre cohesive force.

## 5.10. Yarn pull out force

The force required to pull out yarn from the fabric can give an estimate of friction due to yarn to yarn sliding. Yarn pull out force was measured for warp and weft of Neat and S4 fabrics following the procedure as described in section 4.2.4.2.

Each yarn was pulled out for a total of 40 interlacement. For each interlacement yarn get lose and tight as free end passes over different interlacements, this is evident from pull out data shown in Figure 57. The peaks, from yarn pull out (force-displacement) data, were plotted and these peak points were fitted with linear regression, 2nd order polynomial as found in Equation 22. Table 22 and Table 23 show the coefficient of fitted model, goodness of fit and analysis of variance. Mean pull-out resistance was computed for every peak in measurement curve by dividing the interlacements contributing to the resistance. Then mean for every fabric direction was computed and shown in Table 24 and as found in

Figure 59.
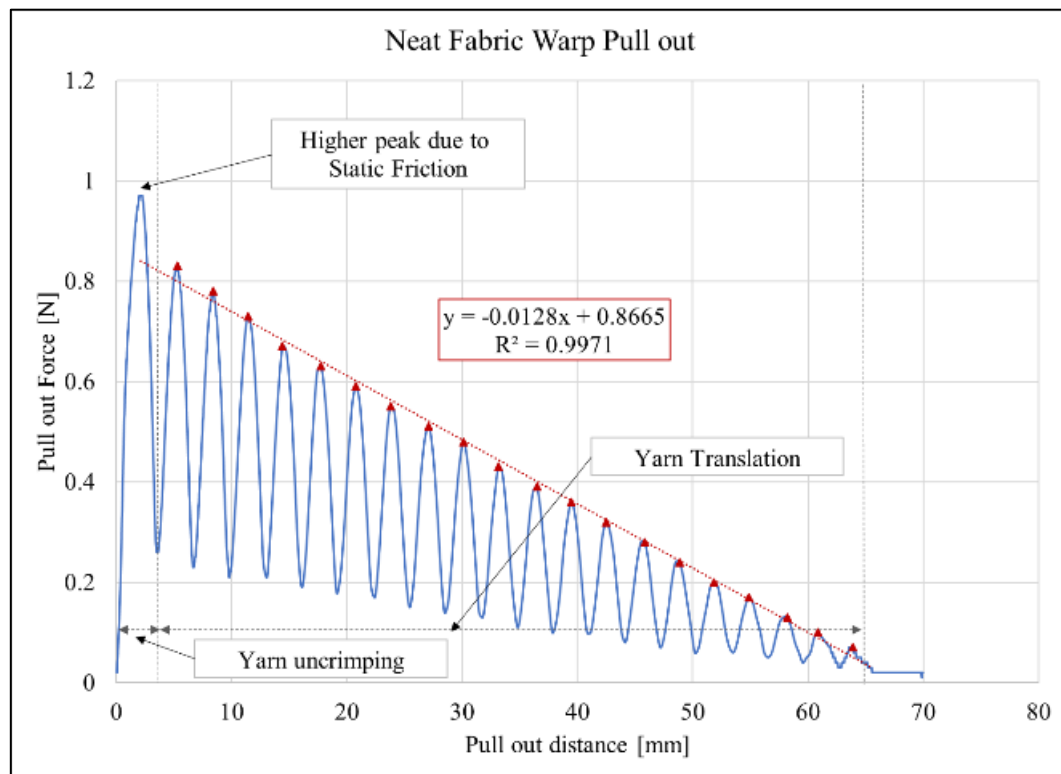


*Figure 57: Force-displacement curve of Yarn Pull-out test*
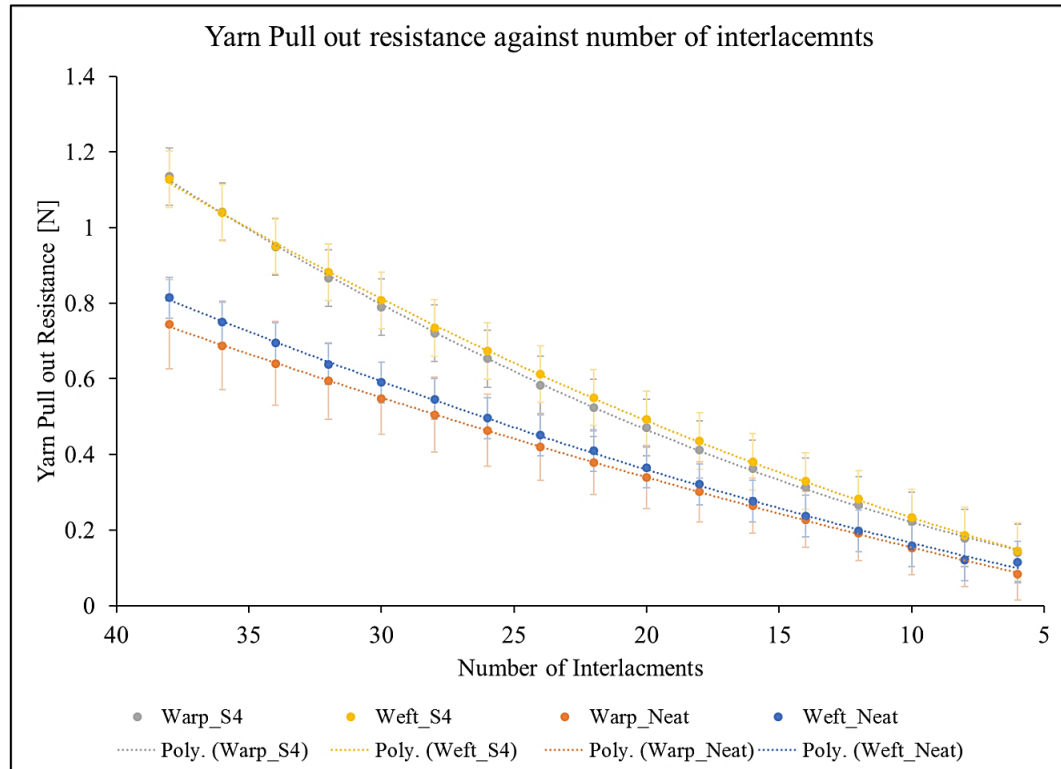


Figure 58: Yarn Pull-out resistance against opposing interlacements of yarns for warp and weft of Neat and S4 fabrics

$$f(x) = p_1 x^2 + p_2 x + p_3$$

Table 22: Yarn pull-out coefficients of fitted models

| Fabric | Pull-out direction | Equation Coefficients | | |
|--------|-------------------|-----------------------|-----------------------|------------------------|
| | | $p_1$ | $p_2$ | $p_3$ |
| Neat | Weft | 0.000197 (0.000042) | 0.0135 (0.0019) | 0.0115 (0.01837) |
| | Warp | 0.000128 (0.000016) | 0.0147 (0.0007) | -0.0055 (0.00723) |
| S4 | Weft | 0.000332 (0.000029) | 0.0157 (0.0013) | 0.0429 (0.01279) |
| | Warp | 0.000436 (0.000035) | 0.0114 (0.0016) | 0.0638 (0.01561) |

Table 23: Goodness of fit 2nd degree polynomial fit

| Fabric | Pull-out direction | SSE | R-Square | Degree of freedom | Adj. R-sq. | RMSE | # Coef. |
|--------|-------------------|-----|----------|-------------------|------------|------|---------|
| Neat | Weft | 6.55E-04 | 0.999189 | 14 | 0.999073 | 0.006838 | 3 |
| | Warp | 1.01E-04 | 0.99985 | 14 | 0.999829 | 0.002691 | 3 |
| S4 | Weft | 3.17E-04 | 0.99979 | 14 | 0.99976 | 0.004758 | 3 |
| | Warp | 4.73E-04 | 0.999694 | 14 | 0.999651 | 0.00581 | 3 |

S4 warp and weft show significantly higher mean resistance than Neat warp and weft.

Weft of both fabrics shows slightly higher resistance than respective warp, which may be related to higher crimp of weft than warp.
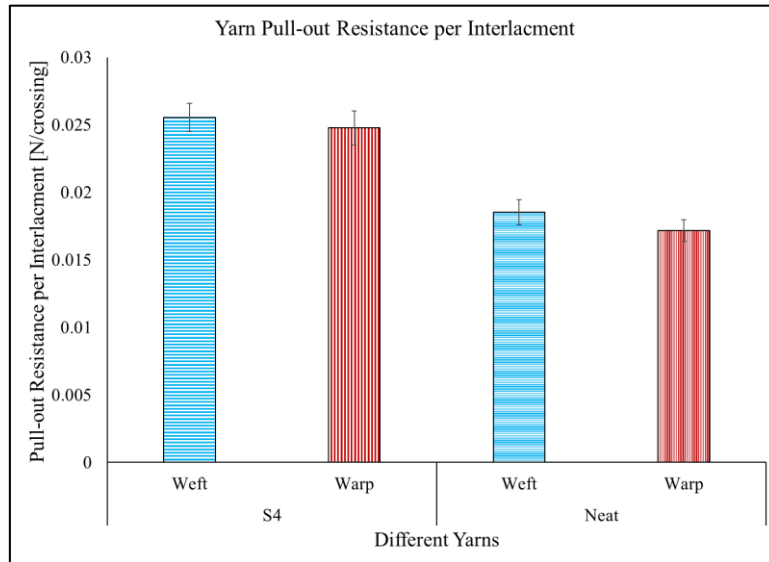


Figure 59: Mean Yarn pull-out resistance per interlacement for warp and weft direction of S4 and Neat fabrics

*Table 24: Mean pull-out resistance of each interlacement*

| Fabric | Pull-out Force per interlacement, [N] | |
|--------|------------------|------------------|
|        | **Warp**         | **Weft**         |
| Neat   | 0.0172 (0.0008)  | 0.0185 (0.0009)  |
| S4     | 0.0248 (0.0013)  | 0.0255 (0.0011)  |

## 5.11.    Yarn Sliding Resistance

In the video analysis it was observed that on average each yarn is displaced from 1-2 *mm* before it was cut by sharp edge of the knife, sliding over opposing yarns. Once this sliding resistance is known we can observe how it is contributing to the stab resistance of the fabric.

We can measure the resistance offered by the yarns of the fabric when they slide over opposite yarns. To measure this sliding resistance a setup was designed using a thin wire as photographed in Figure 60 and the procedure explanation is given in section 4.2.4.4. The results are shown in Figure 61, for warp and weft yarns of Neat and S4 fabrics.



(a)                                              (b)
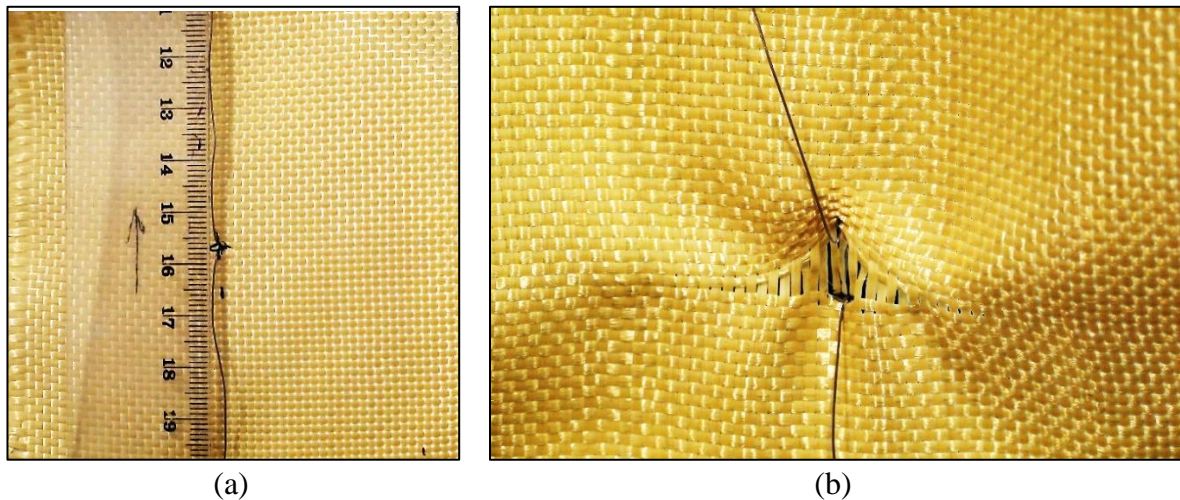
*Figure 60: Fabric samples installed on Universal Testing Machine, before (a) and after (b) yarn sliding resistance measurement.*

The sliding resistance for 10 *mm* was recorded for warp and weft of Neat and S4 fabrics, for 10 samples each. The interpolated mean values were plotted. The data was fitted with second degree polynomial (as in Equation 22) and mean resistance at 1 and 2 *mm* is shown in Table 25. The coefficient of fitted model, analysis of variance and

goodness of fitted data are shown in Table 26 and Table 27.

*Table 25: Yarn sliding resistance for different fabric in warp and weft direction*

| Fabric sliding resistance (N) | | | | |
|---|---|---|---|---|
| **Fabric** | **Direction** | **Warp** | | **Weft** | |
| | **Sliding Distance** | **1 mm** | **2 mm** | **1 mm** | **2 mm** |
| **Neat** | | 0.51 | 0.89 | 0.39 | 0.71 |
| **S4** | | 2.17 | 4.58 | 1.68 | 3.48 |
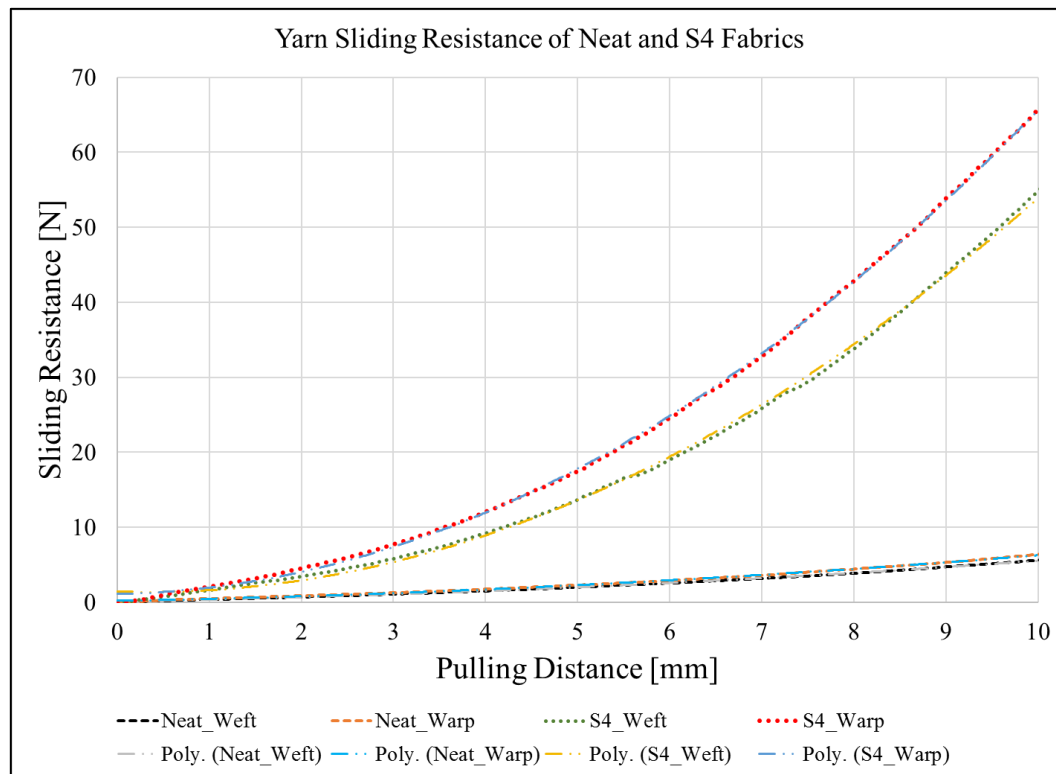


*Figure 61: Fabric Sliding resistance, measured using wire loop pull up, in warp and weft direction of Neat and S4 fabrics*

*Table 26: Parameters of fitted model*

| Fabric | Equation Parameters | | |
|---|---|---|---|
| | $p_1$ | $p_2$ | $p_3$ |
| **Neat Warp** | 0.623 (0.0048) | 0.225 (0.0498) | 1.12 (0.108) |
| **Neat Weft** | 0.562 (0.0073) | -0.374 (0.075) | 1.439 (0.163) |
| **S4 Warp** | 0.038 (0.00075) | 0.231 (0.0078) | 0.207 (0.0168) |
| **S4 Weft** | 0.033 (0.00051) | 0.211 (0.0053) | 0.131 (0.0114) |

*Table 27: Goodness of fit for 2ⁿᵈ degree polynomial fitted model for slide resistance of different fabrics*

| Fabric | SEE | R-Sq. | df | Adj. R-Sq. | RMSE | # Coef. |
|---|---|---|---|---|---|---|
| **Neat Warp** | 37.678 | 0.999 | 332 | 0.999 | 0.337 | 3 |
| **Neat Weft** | 85.633 | 0.999 | 332 | 0.999 | 0.508 | 3 |
| **S4 Warp** | 0.914 | 0.999 | 332 | 0.999 | 0.052 | 3 |
| **S4 Weft** | 0.421 | 0.999 | 332 | 0.999 | 0.036 | 3 |

## 5.12.     Effect of Layers orientation

The minimum requirement of penetration energy defined by stab resistance standard (NIJ Standard–0115.00) cannot be fulfilled by single layer of Neat fabric. Also, stab resistant textile must have sufficient thickness to resist against stab. Therefore, multiple-sheet textile was required. Since orientation of fabric with respect to knife changes for each stack when more than one sheet is stacked at different stacking angle (SA). Therefore, stacking angle was studied for two-layered textile. Stacking angle is the angle between warp direction of two consecutive layers.

Three different SA 0°, 90° and 45° were analysed for Neat fabric samples. The orientation of different stacking angles is shown in Figure 62. Each of this orientation was tested for QSKPR in five KPAs i.e. 0°, 22.5°, 45°, 67.5° and 90°.
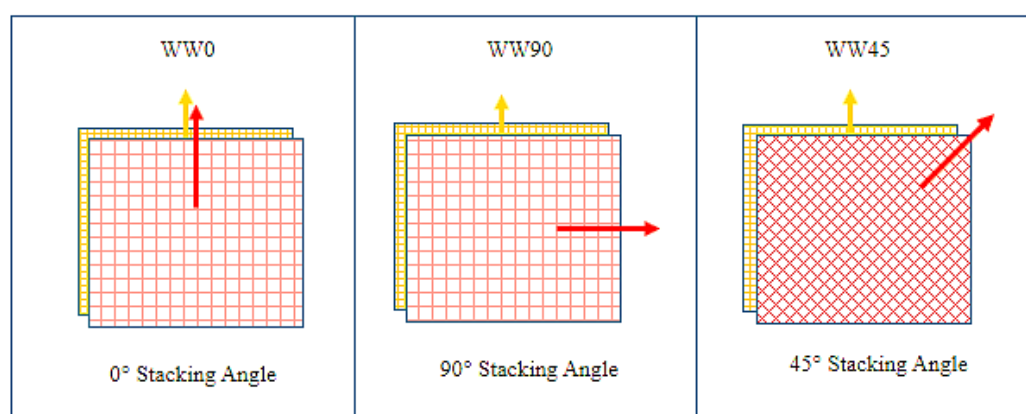


*Figure 62: Stacking of two sheets at different stacking angles, arrows representing warp direction of respective fabric*

### 5.12.1. Effect of Stacking

The QSKPR of different combinations of stacks is shown in Figure 63 and penetration energy in Figure 64. The mean QSKPR and mean Penetration Energy are represented by horizontal lines in each case. A comparison with Figure 40 discloses the fact that mean QSKPR of two sheets stack has arisen from 7 to 10 *times* than mean QSKPR of single sheet.  This evident the synergic effect of multi-sheet stack.
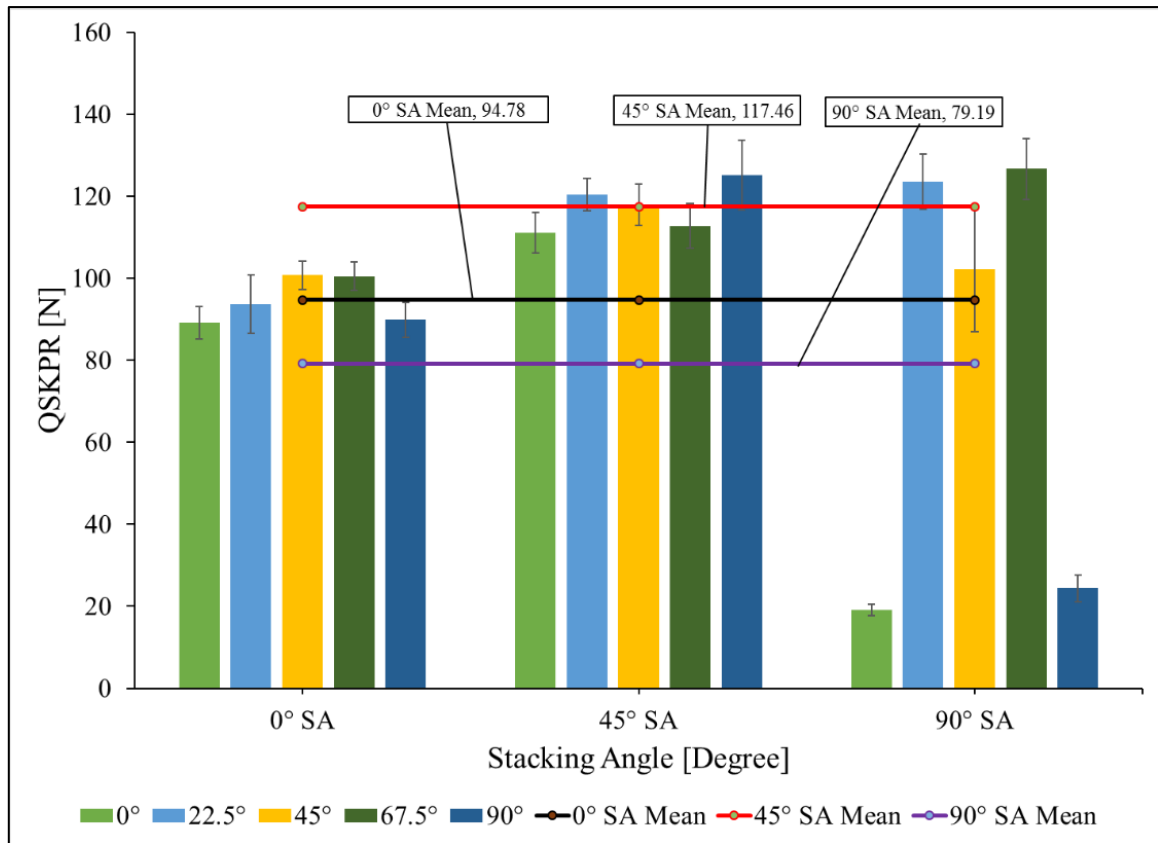
*Figure 63: Change in QSKPR of different fabrics with different Stacking Angles at different KPAs*
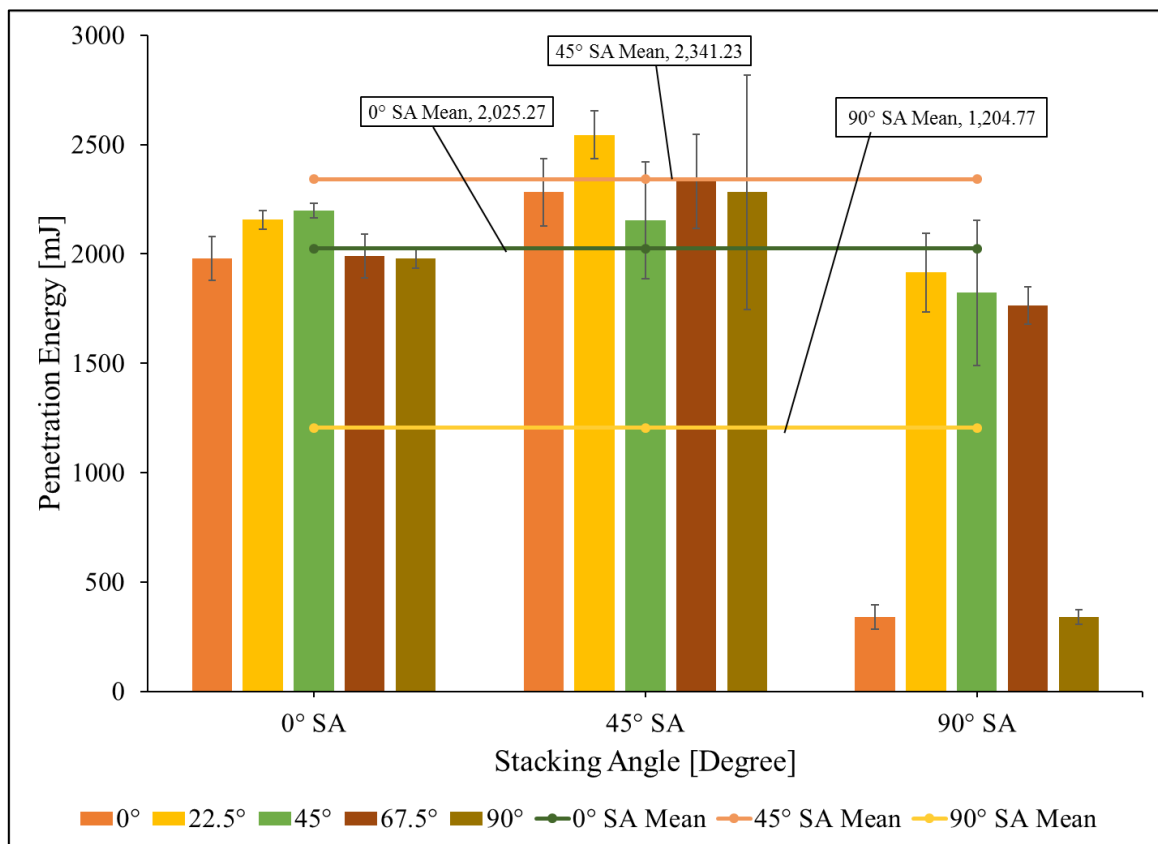


*Figure 64: Change in Penetration Energy of fabrics with different Stacking Angles at different KPAs*

5.12.2. <u>Effect of Stacking Angle and KPA on QSKPR and PE</u>

It is clear from these figures (Figure 63 and Figure 64) that change in SAs and KPAs is causing variation in QSKPR of different stacks. The error bars representing 95% confidence limits of each KPA examined. For definite understanding one-way analysis of variance (ANOVA) was performed to find significant difference of penetration angle within each set of samples (Figure 63 and Figure 64), as shown in Table 28. In all the cases F-statistics is higher than critical F value establishing statistically significantly different mean QSKPR for each KPA examined, within each stack orientation. That confirms the change of QSKPR with varying KPA for two-sheets stack.

*Table 28: One-way ANOVA for QSKPR for different SA*

| SA | Source of Variation | SS | df | MS | F | P-value | F-critical |
|----|---------------------|-----|----|----|----|---------|------------|
| | Between Groups | 748.31 | 4 | 187.08 | 5.50 | 0.003 | 2.76 |
| 0° | Within Groups | 849.73 | 25 | 33.99 | | | |
| | Total | 1598.05 | 29 | | | | |
| | Between Groups | 644.35 | 4 | 161.09 | 3.05 | 0.035 | 2.76 |
| 45° | Within Groups | 1318.75 | 25 | 52.75 | | | |
| | Total | 1963.10 | 29 | | | | |
| | Between Groups | 68261.87 | 4 | 17065.47 | 125.53 | 3.641E-16 | 2.76 |
| 90° | Within Groups | 3398.72 | 25 | 135.95 | | | |
| | Total | 71660.59 | 29 | | | | |

The mean QSKPR of different stacks is in increasing order from $90° < 0° < 45°$. To explain this order, we must consider the orientation of warp and weft yarns in different sheets of a stack. The warp and weft of two sheets are found to be aligned as illustrated in Figure 65. In earlier discussion, we have seen that the QSKPR of fabric is a complementary response (section 5.7.2) and warp dominates in load bearing. This trend has been magnified when warps of both sheets are aligned, as in case of SA of 0°, shown in Figure 65(a). If we compare the single sheet QSKPR of Neat fabric (Figure

40) and two-sheets stack results (Figure 63, 0° SA) a resemblance can be found for response at different KPAs.

In case of SA of 90° the warp of two sheets aligned perpendicular to each other, as shown in Figure 65(c) and that may be the reason of loss of QSKPR at 0° and 90° KPAs, at this SA. That is, when knife is penetrating parallel, to warps of one of the sheets, the stabbing resistance achieved is like as achieved by single sheet QSKPR. Also, when knife is not penetrating parallel to the warp direction of any sheet the strength exhibited is comparable to QSKPR shown at SA 0° or 45°.
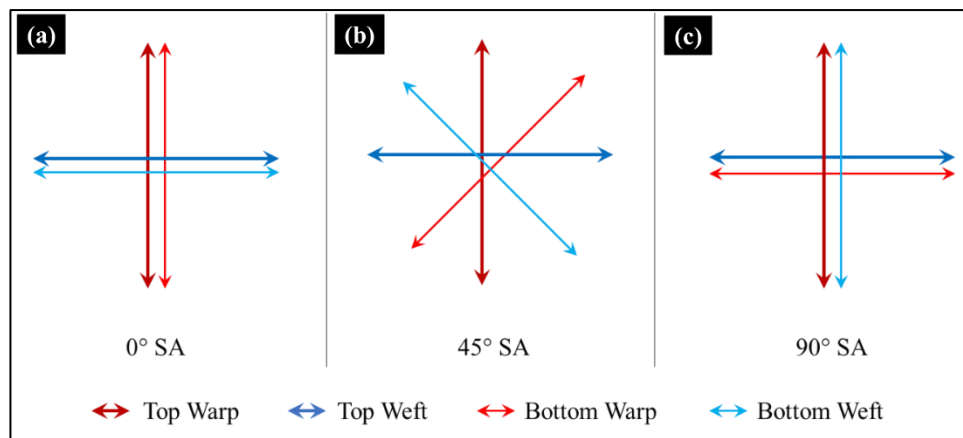


*Figure 65: Orientation of warps and wefts for different sheets at different SAs*

For the case of 45° SA mean QSKPR is found to be maximum in comparison to other SAs. Similar reason, as discussed earlier, is found to be present in this case also. The knife gets parallel to the yarns of one direction at 0°, 45° or 90° KPA, present in any one of the sheets.

KPA is measured from the top sheet that come first in contact with knife. At 45° KPA warp or weft of the bottom sheet is parallel to knife. In the case of warp, the QSKPR may reduce and in case of weft it may not reduce to that extent. That is the reason of much variation of PE at 45° KPA for 45° SA. Similarly, at 0° KPA warp of the top sheet and at 90° KPA weft of the top sheet is parallel to penetrating knife i.e. QSKPR and PE is achieved as is evident from the Figure 63 and Figure 64. For the

other two KPAs (i.e. 22.5° and 67.5°), we observe maximum PE and comparable QSKPR because no yarn is parallel to knife and cutting energy is distributed among all the yarns of both sheets leading to the best PE and one of the best QSKPR of all the results observed.

From all these discussion, it can be safe to infer that more the number of yarns resisting in multiple directions, for various sheets of stack, higher will be the distribution of stabbing energy and more resistance is offered by the textile.

### 5.12.3. Force-Displacement Curves of Different KPAs

Force-displacement curve of double sheet stack orientated at 0°, 45° and 90° SA are shown in Figure 66. Each column in this figure from top to bottom is showing, 0°, 90°, 22.5°,67.5° and 45° KPAs best sample's curve, a, d, g, j and m, for SA 0°, b, e, h, k and n for SA 45° and c, f, i, l and o for SA 90° respectively. One noticeable observation is that these curves are very different from the curve we observed in Figure 41, for single layer fabric. The single higher peak is now converted in jolting and mounting towards higher resistance (*N*) as penetration continuous. Therefore, the peak for each sample is obtained at deeper penetration in contrast to single layer where top peak was obtained at the start within 6 mm of vertical penetration. From these peaks it is observable that yarns from two sheets continuously remain in contact with knife and continuous resistance and knife edge does not find empty space like single layer where peak can fall to zero resistance (*N*).  The other noticeable finding is for 45° SA uniform response visible for KPAs.
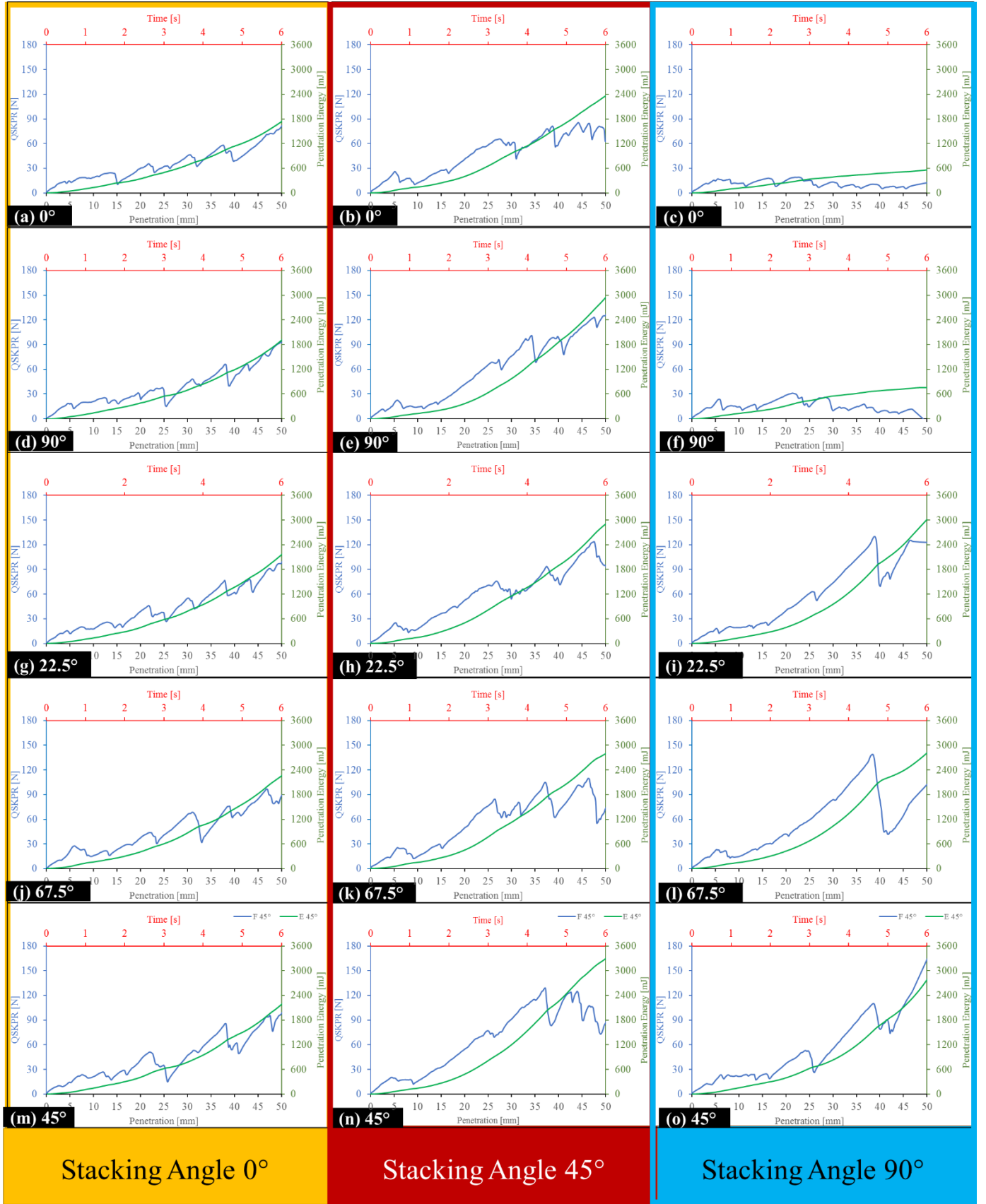
*Figure 66: Comparison of best curves observed for QSKPR (in blue color) and Penetration Energy (in green color) at different KPAs for two-layers stacked at 0°,45° and 90° SA*

5.12.4. Generalizing single quadrant QSKPR over 360°

Assuming similar response in all four quadrants, as in measured quadrant, and generalizing the results of QSKPR in all four quadrants, over complete 360°, results the Figure 67. A better understanding be seen of isotropic response of stabbing for different stacking orientations. The synergic output of different stacking orientations is observable. It is evident that 45° SA seems to be more resistant and isotropic than other SAs. This establishes the fact that at smaller stacking angle, as they distribute the yarn in multiple directions, can produces more homogenous stab resistance.
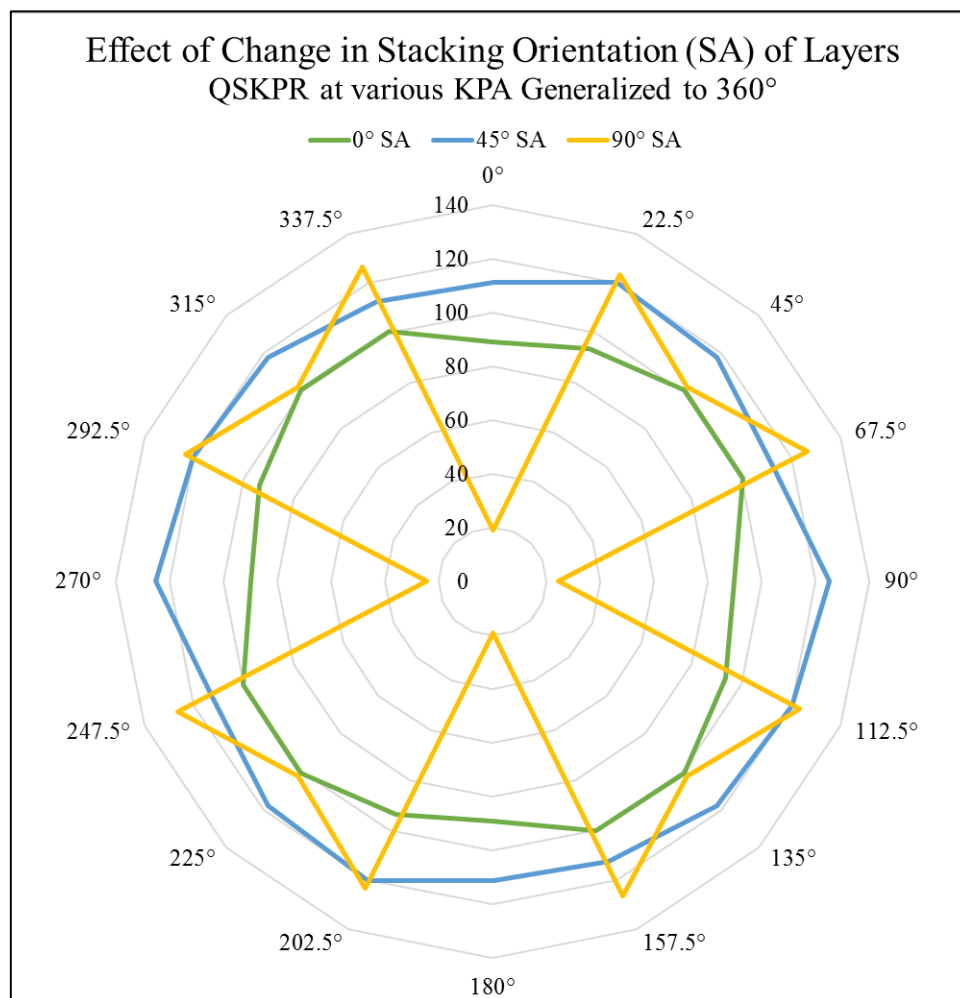


*Figure 67: Effect of change in SA on QSKPR of stack of two sheets, generalized to 360°*

5.12.5. <u>Effect of Thickness on QSKPR</u>

Adding more numbers of layers increases the surface area in contact with knife. Also, adding more number of layers will cause the increase of time-period of contact for which knife acceleration could be resisted and hence increases friction to produce immobility to the moving knife. The other benefit of having more numbers of layers is total number of yarns resisting against knife are multiplied and chances of distribution of penetration energy in multiple direction increases. However, adding more layers increases the mass and inertia of resisting textile that negatively affect the stab resistance, therefore, for certain material optimum design is required.

**5.13.    Dynamic Stab Resistance (DSR)**

The best result of QSKPR، in double sheet stack، was found for 45° SA. So, 45° SA was chosen for dynamic stab testing. Warp of each next sheet was turned 45° from warp of next sheet, for 8 sheets stack. The drop-tower was used to drop knife, under gravity, on to the fabric samples, mounted on backing material. The procedure is described in section 4.2.2.3. The sample being tested was tapped with backing material platform and it was rotated to allow knife drop in five different direction (KPAs) so that knife cutting axis make 0°, 22.5°, 45°, 67.5° or 90° with warp of the top most sheet.

The penetration depth was recorded by the machine and was also confirmed from cut produced in the paper sheets placed in backing material. The mean of penetration depth recorded for all KPAs is presented in Figure 68. Two penetration energies were examined.

From these results treated fabric, S4, has comparatively higher stab resistance than untreated fabric for both examined energies. Increasing the drop energy increases the depth of penetration in Neat fabric while S4 samples remain unchanged.
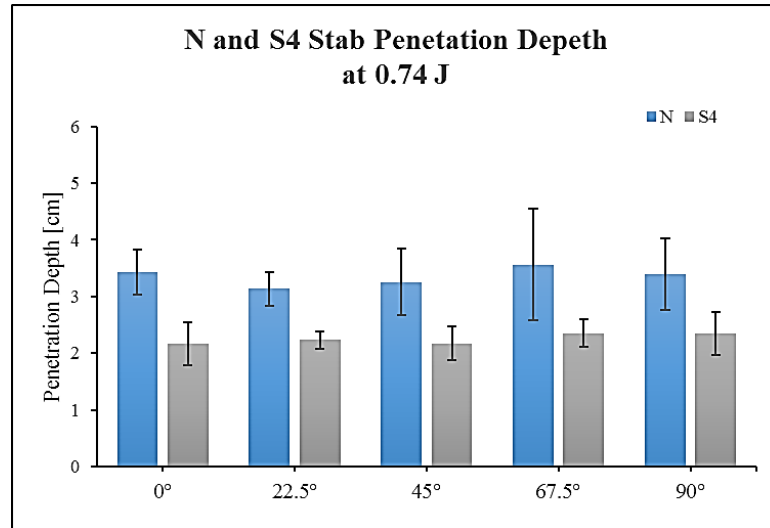
(a)
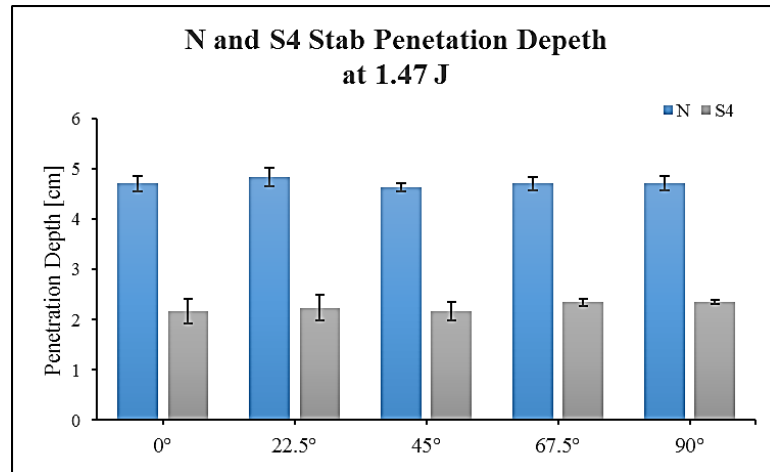


(b)

*Figure 68: Comparison of dynamic stab resistance in terms of knife penetration depth for Neat and S4 samples, (a) 0.74 J and (b) 1.47 J*

The other observation is for both the fabrics showing no effect of KPA for both penetrated energies. This may be attributed to the SA which cause distribution of impact energy in multiple directions and hence similar response in all penetration directions was achieved. This finding supports the fact that to achieve isotropic response, from multi-sheet stab resistance textile, the stacking angle should be small enough such that, it distributes the penetration energy in multiple directions.

# CHAPTER 6
# CONCLUSIONS, APPLICATIONS, AND FUTURE WORK

# 6. Conclusions, Applications and Future Work

## 6.1. Conclusions

This research investigated the quasi-static knife penetration resistance (QSKPR) and dynamic stab resistance (DSR) of single and stack of multiple sheets of woven fabric. The interaction of fabric and knife was studied when penetration was performed in different directions. The angle made between warp direction of the fabric and the knife cutting axis was called knife penetration angle (KPA). The KPA was change at five different angles i.e. 0°, 22.5°, 45°, 67.5°, and 90°. For multiple sheet stack, Stacking Angle (SA) is the angle made between warp of each consecutive sheet. For double sheet stack three SA (0°, 45°, and 90°) were investigated and best SA (45°) was investigated for DSR of eight sheets stack. To investigate the effect of change in friction, the surface of fabric was modified with $SiO_2$, $TiO_2$ and Ozone with $SiO_2$. The effect of KPA and SA was investigated on QSKPR and DSR. Treated and untreated fabrics was investigated for their comfort, mechanical and physical change on their surface.

A new approach to deposit $SiO_2$ using water glass (WG) as precursor was discovered. Light acidic medium used helped to deposit $SiO_2$ on the surface of fibres. $SiO_2$ deposition was confirmed using Scanning Electron Microscope (SEM), Fourier Transform Infra-red (FTIR) Spectroscopy and Energy-Dispersive X-ray (EDX) Spectroscopy. The deposited layer adds weight up to 8%, fills the pores, increases inter-fibre, inter-yarn and surface friction of the fabric. Increase in the fabric friction was found to be directly proportional to the concentration of WG. Ozone application improves the tensile strength and reduces the bending rigidity. Before depositing $SiO_2$ layer, pre-treatment with Ozone for 120 minutes achieves the similar frictional characteristics, with better comfort. tensile strength and flexibility properties. Presence of $TiO_2$ on fabric surface was observed under SEM. $TiO_2$ particle deposited on fibre surface from its aqueous solution require binding agent to fix with fibres surface. Without

binding agent, increasing concentration of aqueous solution of $TiO_2$ from 0.01 *g/l* to 0.5 *g/l* does not improve the stabbing performance of para-Aramid fabrics.

It was found that increasing amount of deposited $SiO_2$ increases the QSKPR and DSR. With 40% WG solution increase in QSKPR and DSR was found to increase about 200% for all KPAs. The response of fabric against QSKPR changed from partial yarn cutting to individual yarn cutting in fewer steps and load was distributed to larger area due to increase in inter-yarn friction and intra-yarn cohesion. The distance that cutting knife travelled for cutting consecutive yarns was changed with the change in knife penetration angle that inversely affected the QSKPR. The increase in friction of treated fabrics distributed the knife stabbing load to neighbouring yarns. This distribution was complementary between warp and weft yarns depending on knife penetration angle. The change in penetration angle changed the distribution of stabbing load among the warp and weft yarns. The higher QSKPR was resulted when the load was carried by both warp and weft yarns, at a penetration angle (67.5°) that actuated to induce more stresses in the yarns with higher tensile strength and yarn to yarn friction.

The model was developed from Fourier function for QSKPR ($R_{st}$) response of each fabric for various KPAs. The model fits well for all untreated and treated fabrics responses except for S4, which showed least variations in QSKPR for different KPAs. Video analysis unveiled that yarn present on blunt side of knife are fractured in yarn pull out while sharp edge of knife displaces the yarn first, sliding over other yarns, and then fracture it in parts. $SiO_2$ treated fabric exhibited presence of intra-yarn cohesion to persist partial yarn fracture to a larger extent than untreated yarn, that showed absence of such cohesive force. The yarns of $SiO_2$ treated fabric required significantly lower strain than untreated fabric, showing higher modulus of rigidity. Yarn to yarn friction was found to be higher in treated fabrics than untreated fabrics that required more pull out force or higher resistance of yarn sliding.

Stacked setup of multiple sheets produced higher response of QSKPR and DSR due to more contact area of fabrics interacting with knife and more time available to resist against the knife. Stacking also provided ability of resisting textile to distribute penetrating energy in multiple directions. Sheets stack at 45° SA was found to well distribute penetration energy and exhibit higher QSKPR and DSR and, also, improved isotropy of stab resistance.

## 6.2. Applications

The essence of this project can be applied to any impact resistance application for resisting against high energy sharp edged objects.

### 6.2.1. Knife stab evaluation

For knife stab testing, it is suggested that at least three cutting angles with small difference (of less than 45°) be examined for homogeneity of stabbing response, either from warp or weft of the woven fabric.

### 6.2.2. Stacking orientation

For the multiple-sheets stacks required for anti-stabbing systems, each sheet in the stack must be rotated to orient yarn of different sheets at different angle i.e. 45° SA.

### 6.2.3. Ozone treatment and $SiO_2$ deposition method

The benefit of this research can be obtained by employing the method developed in this research to deposit $SiO_2$ from WG. Ozone pre-treatment before $SiO_2$ deposition on the fabric, can enhance the tensile strength of the yarns without losing much air permeability and bending rigidity characteristics as compared to untreated fabrics.

## 6.3. Future Work

In future, SAs in more directions can be verified to optimize for best knife stabbing response. Upon, such knowledge a stab resistance solution may be developed.

# REFERENCES

[1] E. L. Thomas, "Opportunities in Protection Materials Science and Technology for Future Army Applications", in *Advances in Ceramic Armor VIII*, 2012, pp. 145-148.

[2] R. A. Scott, *Textiles for protection*. Elsevier, 2005.

[3] X. Chen, "Introduction", in *Advanced Fibrous Composite Materials for Ballistic Protection*, 2016, pp. 1–10.

[4] M. Hudspeth, W. Chen, and J. Zheng, "Why the Smith theory over-predicts instant rupture velocities during fiber transverse impact," *Text. Res. J.*, vol. 86, no. 7, pp. 743-754, (2015).

[5] S. Rebouillat, "ARAMIDS: 'disruptive', open and continuous innovation," in *Advanced Fibrous Composite Materials for Ballistic Protection*, X. Chen, Ed. 2016, pp. 11–70.

[6] E. G. Chatzi and J. L. Koenig, "Morphology and structure of kevlar fibers: A review," *Polym. Plast. Technol. Eng.*, vol. 26, no. 3–4, pp. 229–270, (1987).

[7] H. S. Hwang, M. H. Malakooti, B. A. Patterson, and H. A. Sodano, "Increased interyarn friction through ZnO nanowire arrays grown on aramid fabric," *Compos. Sci. Technol.*, vol. 107, pp. 75–81, (2015).

[8] K. K. Govarthanam, S. C. Anand, and S. Rajendran, "Development of Advanced Personal Protective Equipment Fabrics for Protection Against Slashes and Pathogenic Bacteria Part 1: Development and Evaluation of Slash-resistant Garments," *J. Ind. Text.*, vol. 40, no. 2, pp. 139–155, (2010).

[9] H. Kim and I. Nam, "Stab Resisting Behavior of Polymeric Resin Reinforced p-Aramid Fabrics," *J. Appl. Polym. Sci.*, vol. 123, pp. 2733–2742, (2012).

[10] C. Eades, "Knife Crime': ineffective reactions to a distracting problem," *A Rev. Evid. policy*, vol. 1, (2006).

[11] G. Nolan, S. V. Hainsworth, and G. N. Rutty, "Forces required for a knife to penetrate a variety of clothing types," *J. Forensic Sci.*, vol. 58, no. 2, pp. 372–379, (2013).

[12] J. R. Sorensen, M. D. Cunningham, M. P. Vigen, and S. O. Woods, "Serious assaults on prison staff: A descriptive analysis," *J. Crim. Justice*, vol. 39, no. 2, pp. 143–150, (2011).

[13] M. J. Decker, C. J. Halbach, C. H. Nam, N. J. Wagner, and E. D. Wetzel, "Stab resistance of shear thickening fluid (STF)-treated fabrics," *Compos. Sci. Technol.*, vol. 67, no. 3–4, pp. 565–578, (2007).

[14] J. Barker and C. Black, "Ballistic vests for police officers: using clothing comfort theory to analyse personal protective clothing," *Int. J. Fash. Des. Technol. Educ.*, vol. 2, no. 2–3, pp. 59–69, (2009).

[15] H. N. Choi, T. M. Hong, E. H. Lee, J. G. Paik, B. I. Yoon, S. G. Lee, and C. National, "Stab resistance of aramid fabrics reinforced with silica STF," in *18th international conference on composite materials*, 2011, pp. 1–4.

[16] K. Bilisik, "Impact-resistant fabrics (ballistic/stabbing/slashing/spike)", in *Engineering of High-Performance Textiles,* 2018, pp. 377-434.

[17] D. Grinevičiūtė, A. Abraitienė, A. Sankauskaitė, D. M. Tumėnienė, L. Lenkauskaitė, and R. Barauskas, "Influence of Chemical Surface Modification of Woven Fabrics on Ballistic and Stab Protection of Multilayer Packets," *Mater. Sci.*, vol. 20, no. 2, pp. 193–197, (2014).

[18] P. V. Cavallaro, "Soft Body Armor : An Overview of Materials , Manufacturing , Testing , and Ballistic Impact Dynamics" (No. NUWC-NPT-TR-12-057). NAVAL

UNDERSEA WARFARE CENTER DIV NEWPORT RI, 2011.

[19]   E. D. LaBarre, X. Calderon-Colon, M. Morris, J. Tiffany, E. Wetzel, A. Merkle, and M. Trexler, "Effect of a carbon nanotube coating on friction and impact performance of Kevlar," *J. Mater. Sci.*, vol. 50, no. 16, pp. 5431–5442, (2015).

[20]   S. Gürgen and M. C. Kuşhan, "The stab resistance of fabrics impregnated with shear thickening fluids including various particle size of additives," *Compos. Part A Appl. Sci. Manuf.*, vol. 94, pp. 50–60, (2017).

[21]   J. A. Bencomo-Cisneros, A. Tejeda-Ochoa, J. A. García-Estrada, C. A. Herrera-Ramírez, A. Hurtado-Macías, R. Martínez-Sánchez, and J. M. Herrera-Ramírez, "Characterization of Kevlar-29 fibers by tensile tests and nanoindentation," *J. Alloys Compd.*, vol. 536, no. SUPPL.1, pp. S456–S459, (2012).

[22]   S. V Kulkarni and J. S. R. V. V Rosen, "An investigation of the compressive strength of Kevlar 49 / epoxy composites," no. September, pp. 217–225, (1975).

[23]   M. Miraftab, *Fatigue failure of textile fibres*. CRC Press, 2009.

[24]   B. S. Wong and X. Wang, "Biaxial rotation fatigue in textile fibres," in *Fatigue failure of textile fibres*, M. Miraftab, Ed. CRC Press, 2009, pp. 73–91.

[25]   T. Aramid, "Ballistic materials handbook," 2018. [Online]. Available: https://www.teijinaramid.com/wp-content/uploads/2018/03/TEIJ_Handbook_Ballistics_2018_WEB.pdf. [Accessed: 16-Sep-2018].

[26]   Dupont, "Kevlar ® Reference Designs for Vests made with DuPont Kevlar XP," 2010. [Online]. Available: http://www.dupont.com/content/dam/dupont/products-and-services/fabrics-fibers-and-nonwovens/fibers/documents/DSP_KevlarXP_ReferenceDesigns_K23338.pdf.

[Accessed: 16-Sep-2018].

[27]    N. Benson, R. Oliveria Dos Santos, K. Griffiths, N. Cole, P. Doble, C. Roux, and L. Blanes, "The development of a stabbing machine for forensic textile damage analysis," *Forensic Sci. Int.*, vol. 285, p. 161, (2018).

[28]    M. Y. Yuhazri, N. H. C. H. Nadia, H. Sihombing, S. H. Yahaya, and A. Abu, "A review on flexible thermoplastic composite laminate for anti-stab applications," *J. Adv. Manuf. Technol.*, vol. 9, no. 1, p. 28, (2015).

[29]    M. D. Gilchrist, S. Keenan, M. Curtis, M. Cassidy, G. Byrne, and M. Destrade, "Measuring knife stab penetration into skin simulant using a novel biaxial tension device," *Forensic Sci. Int.*, vol. 177, no. 1, pp. 52–65, (2008).

[30]    J. Mayo and E. Wetzel, "Cut resistance and failure of high-performance single fibers," *Text. Res. J.*, vol. 84, no. 12, pp. 1233–1246, (2014).

[31]    B. N. Vu Thi, T. Vu-Khanh, and J. Lara, "Mechanics and mechanism of cut resistance of protective materials," *Theor. Appl. Fract. Mech.*, vol. 52, no. 1, pp. 7–13, (2009).

[32]    H. S. Shin, D. C. Erlich, J. W. Simons, and D. A. Shockey, "Cut Resistance of High-strength Yarns," *Text. Res. J.*, vol. 76, no. 8, pp. 607–613, (2006).

[33]    J. Mayo and E. D. Wetzel, "Cut Resistance and Fracture Toughness of High Perfomance Fibers," in *Dynamic Behavior of Materials, Volume 1*, 2011, pp. 167–173, (2011).

[34]    M. Hudspeth, D. Li, J. Spatola, W. Chen, and J. Zheng, "The effects of off-axis transverse deflection loading on the failure strain of various high-performance fibers," *Text. Res. J.* , (2015).

[35]    M. U. Javiad, J. Militky, J. Wiener, J. Salacova, A. Jabbar, and M. Umair, "Effect of

surface modification and knife penetration angle on the Quasi-Static Knife Penetration Resistance of para-aramid fabrics.," *J. Text. Inst.,* (2018).

[36]    J. L. Park, B. il Yoon, J. G. Paik, and T. J. Kang, "Ballistic performance of p-aramid fabrics impregnated with shear thickening fluid; Part I − Effect of laminating sequence," *Text. Res. J.*, vol. 82, no. 6, pp. 527–541, (2012).

[37]    S. Chocron, C. E. Anderson, K. R. Samant, E. Figueroa, A. E. Nicholls, and J. D. Walker, "Measurement of strain in fabrics under ballistic impact using embedded nichrome wires, part II: Results and analysis," *Int. J. Impact Eng.*, vol. 37, no. 1, pp. 69–81, (2010).

[38]    Bernard Knight and B. Knight, "The dynamics of stab wounds," *Forensic Sci.*, vol. 6, no. 3, pp. 249–255, (1975).

[39]    S. V. Hainsworth, R. J. Delaney, and G. N. Rutty, "How sharp is sharp? Towards quantification of the sharpness and penetration ability of kitchen knives used in stabbings," *Int. J. Legal Med.*, vol. 122, no. 4, pp. 281–291, (2008).

[40]    H. S. Shin, D. C. Erlich, and D. A. Shockey, "Test for measuring cut tesistance of yarns," *J. Mater. Sci.*, vol. 38, pp. 3603–3610, (2003).

[41]    I. Horsfall, C. Watson, S. Champion, P. Prosser, T. Ringrose, I. H. Ã, C. Watson, S. Champion, P. Prosser, and T. Ringrose, "The effect of knife handle shape on stabbing performance," *Appl. Ergon.*, vol. 36, no. 4 SPEC. ISS., pp. 505–511, (2005).

[42]    S. Gürgen, M. C. Kuşhan, and W. Li, "Shear thickening fluids in protective applications: A review," *Prog. Polym. Sci.*, vol. 75, pp. 48–72, (2017).

[43]    H. Rao, M. Hosur, J. M. Jr, S. Burton, and S. Jeelani, "Stab Characterization of Hybrid Ballistic Fabrics," *Proc. SEM Annu. Conf.*, (2009).

[44]    R. G. E. Jr, Y. S. Lee, J. E. Kirkwood, K. M. Kirkwood, E. D. Wetzel, and N. J. Wagner, ""Liquid armor ": Protective fabrics utilizing shear thickening fluids," *Chem. Eng.*, no. March 2016, pp. 1–8, (2004).

[45]    N. R. Council and others, *Opportunities in protection materials science and technology for future army applications*. National Academies Press, 2011.

[46]    S. Min, Y. Chu, and X. Chen, "Numerical study on mechanisms of angle-plied panels for ballistic protection," *Mater. Des.*, vol. 90, pp. 896–905, (2016).

[47]    DuPont, "PERFORMANCE INNOVATION & KEVLAR Realizing the power of performance," 2003. [Online]. Available: http://www.dupont.com/content/dam/dupont/products-and-services/fabrics-fibers-and-nonwovens/fibers/documents/Kevlar_LP_brand_brochure.pdf. [Accessed: 16-Sep-2018].

[48]    P. C. Dempsey, P. J. Handcock, and N. J. Rehrer, "Impact of police body armour and equipment on mobility," *Appl. Ergon.*, vol. 44, no. 6, pp. 957–961, (2013).

[49]    Y. Termonia, "Puncture resistance of fibrous structures," *Int. J. Impact Eng.*, vol. 32, no. 9, pp. 1512–1520, (2006).

[50]    E. K. J. Chadwick, A. C. Nicol, J. V. Lane, and T. G. F. Gray, "Biomechanics of knife stab attacks," *Forensic Sci. Int.*, vol. 105, no. 1, pp. 35–44, (1999).

[51]    R. Gadow and K. von Niessen, "Lightweight ballistic structures made of ceramic and cermet/aramide composites," *Ceram. Armor Armor Syst.*, vol. 151, pp. 1–18, (2006).

[52]    R. Gadow and K. von Niessen, "Lightweight ballistic with additional stab protection made of thermally sprayed ceramic and cermet coatings on aramide fabrics," *Int. J. Appl. Ceram. Technol.*, vol. 3, no. 4, pp. 284–292, (2006).

[53] P. G. Karandikar, G. Evans, S. Wong, M. K. Aghajanian, and M. Sennett, "A Review of Ceramics for Armor Applications," pp. 163–175, (2009).

[54] N. V. David, X.-L. Gao, and J. Q. Zheng, "Ballistic Resistant Body Armor: Contemporary and Prospective Materials and Related Protection Mechanisms," *Appl. Mech. Rev.*, vol. 62, no. 5, p. 050802, (2009).

[55] E. E. B. White, M. Chellamuthu, and J. P. Rothstein, "Extensional rheology of a shear-thickening cornstarch and water suspension," *Rheol. Acta*, vol. 49, no. 2, pp. 119–129, (2010).

[56] a. Srivastava, A. Majumdar, and B. S. Butola, "Improving the Impact Resistance of Textile Structures by using Shear Thickening Fluids: A Review," *Crit. Rev. Solid State Mater. Sci.*, vol. 37, no. 2, pp. 115–129, (2012).

[57] L. Chang, K. Friedrich, A. K. Schlarb, R. Tanner, and L. Ye, "Shear-thickening behaviour of concentrated polymer dispersions under steady and oscillatory shear," *J. Mater. Sci.*, vol. 46, no. 2, pp. 339–346, (2011).

[58] S. R. Raghavan, J. Hou, G. L. Baker, and S. A. Khan, "Colloidal Interactions between Particles with Tethered Nonpolar Chains Dispersed in Polar Media: Direct Correlation between Dynamic Rheology and Interaction Parameters," *Langmuir*, vol. 16, no. 3, pp. 1066–1077, (2000).

[59] R. G. Egres and N. J. Wagner, "The rheology and microstructure of acicular precipitated calcium carbonate colloidal suspensions through the shear thickening transition," *J. Rheol. (N. Y. N. Y).*, vol. 49, no. 3, pp. 719–746, (2005).

[60] A. K. Gurnon and N. J. Wagner, "Microstructure and rheology relationships for shear thickening colloidal dispersions," *J. Fluid Mech.*, vol. 769, pp. 242–276, (2015).

[61] N. J. Wagner and J. F. Brady, "Shear thickening in colloidal dispersions," *Phys.*

*Today*, vol. 62, no. 10, pp. 27–32, (2009).

[62]    X. Cheng, J. H. McCoy, J. N. Israelachvili, and I. Cohen, "Imaging the microscopic structure of shear thinning and thickening colloidal suspensions," *Science (80-. ).*, vol. 333, no. 6047, pp. 1276–1279, (2011).

[63]    M. Hasanzadeh and V. Mottaghitalab, "The role of shear-thickening fluids (STFs) in ballistic and stab-resistance improvement of flexible armor," *J. Mater. Eng. Perform.*, vol. 23, no. 4, pp. 1182–1196, (2014).

[64]    S. Gürgen, M. C. Ku\cshan, and W. Li, "The effect of carbide particle additives on rheology of shear thickening fluids," *Korea-Australia Rheol. J.*, vol. 28, no. 2, pp. 121–128, (2016).

[65]    B. a Rosen, C. H. N. Laufer, D. P. Kalman, E. D. Wetzel, and J. Norman, "Multi-Threat Performance of Kaolin-Based Shear Thickening Fluid ( Stf ) -Treated Fabrics," *Most*, no. June, pp. 1–11, (2007).

[66]    A. Khodadadi, G. H. Liaghat, and M. A. Akbari, "Experimental Analysis of Penetration into Targets Made of Kevlar Laminate with STF Fluids," pp. 85–94, (2013).

[67]    T. J. Kang, K. H. Hong, and M. R. Yoo, "Preparation and properties of fumed silica/Kevlar composite fabrics for application of stab resistant material," *Fibers Polym.*, vol. 11, no. 5, pp. 719–724, (2010).

[68]    W. Li, D. Xiong, X. Zhao, L. Sun, and J. Liu, "Dynamic stab resistance of ultra-high molecular weight polyethylene fabric impregnated with shear thickening fluid," *Mater. Des.*, vol. 102, pp. 162–167, (2016).

[69]    S. M. Hejazi, N. Kadivar, and A. Sajjadi, "Analytical assessment of woven fabrics under vertical stabbing - The role of protective clothing," *Forensic Sci. Int.*, vol. 259,

pp. 224–233, (2016).

[70] A. M. Sadegh and P. V. Cavallaro, "Mechanics of Energy Absorbability in Plain-Woven Fabrics: An Analytical Approach," *J. Eng. Fiber. Fabr.*, vol. 7, no. 1, pp. 10–25, (2012).

[71] B. J. Briscoe and F. Motamedi, "The ballistic impact characteristics of aramid fabrics: the influence of interface friction," *Wear*, vol. 158, no. 1–2, pp. 229–247, (1992).

[72] Y. Wang, X. Chen, R. Young, and I. Kinloch, "Finite element analysis of effect of inter-yarn friction on ballistic impact response of woven fabrics," *Compos. Struct.*, vol. 135, pp. 8–16, (2016).

[73] M. El Messiry and E. Eltahan, "Stab resistance of triaxial woven fabrics for soft body armor," *J. Ind. Text.*, vol. 45, no. 5, pp. 1062–1082, (2016).

[74] L. Wang, S. Zhang, W. M. Gao, and X. Wang, "FEM analysis of knife penetration through woven fabrics," *C. - Comput. Model. Eng. Sci.*, vol. 20, no. 1, pp. 11–20, (2007).

[75] J. Militký and C. Becker, "Selected Topics of Textile and Material Science," in *Selected Topics of Textile and Material Science*, D. Křemenáková, R. Mishra, J. Militký, and J. Šesták, Eds. Liberec: Publishing House of WBU, 2011, p. 404.

[76] X. Feng, S. Li, Y. Wang, Y. Wang, and J. Liu, "Effects of different silica particles on quasi-static stab resistant properties of fabrics impregnated with shear thickening fluids," *Mater. Des.*, vol. 64, pp. 456–461, (2014).

[77] D. B. Stojanović, M. Zrilić, R. Jančić-Heinemann, I. Živković, A. Kojović, P. S. Uskoković, and R. Aleksić, "Mechanical and anti-stabbing properties of modified thermoplastic polymers impregnated multiaxial p-aramid fabrics," *Polym. Adv. Technol.*, vol. 24, no. 8, pp. 772–776, (2013).

[78]    A. Ní Annaidh, M. Cassidy, M. Curtis, M. Destrade, and M. D. Gilchrist, "A combined experimental and numerical study of stab-penetration forces," *Forensic Sci. Int.*, vol. 233, no. 1–3, pp. 7–13, (2013).

[79]    W. Barnat and D. Sokołowski, "The study of stab resistance of dry aramid fabrics," *Acta Mech. Autom.*, vol. 8, no. 1, pp. 53–58, (2014).

[80]    Y. Wang, X. Chen, R. Young, I. Kinloch, and G. Wells, "A numerical study of ply orientation on ballistic impact resistance of multi-ply fabric panels," *Compos. Part B Eng.*, vol. 68, pp. 259–265, (2015).

[81]    NIST, "Stab Resistance of Personal Body Armor, NIJ Standard-0115.00," *Stab Resist. Pers. Body Armor, NIJ Stand.*, vol. JR000235, p. , 2000.

[82]    Y. Zhou, M. Ali, X. Gong, and D. Yang, "An overview of yarn pull-out behavior of woven fabrics," *Text. Res. J.*, no. 1, (2017).

[83]    D. Sun, X. Chen, and G. Wells, "Engineering and analysis of gripping fabrics for improved ballistic performance," *J. Compos. Mater.*, vol. 48, no. 11, pp. 1355–1364, (2014).

[84]    A. Majumdar and A. Laha, "Effects of fabric construction and shear thickening fluid on yarn pull-out from high-performance fabrics," *Text. Res. J.*, vol. 86, no. 19, pp. 2056–2066, (2016).

[85]    G. Angeloni, "Woven Fabric Data Sheet Gg 200 P," p. 1, 2016.

[86]    T. E. of Encyclopaedia Britannica, "Water Glass," *The Editors of Encyclopædia Britannica*, 2014. [Online]. Available: https://www.britannica.com/science/water-glass. [Accessed: 24-Feb-2017].

[87]    Y. Sun, T. Song, and W. Pang, "Synthesis of β-zeolites using water glass as the silicon

source," Sep-(1996).

[88] AEROXIDE, "TiO2 P25 Hydrophilic fumed titanium dioxide Characteristic physico-
chemical data," 2014. [Online]. Available:
https://www.aerosil.com/www2/uploads/productfinder/AEROXIDE-TiO2-P-25-
EN.pdf. [Accessed: 20-Mar-2017].

[89] Evonik, "AEROXIDE®, AERODISP® and AEROPERL® titanium dioxide as
photocatalyst," pp. 1–12, 2013.

[90] C. Guo, L. Zhou, and J. Lv, "Effects of expandable graphite and modified ammonium
polyphosphate on the flame-retardant and mechanical properties of wood flour-
polypropylene composites," *Polym. Polym. Compos.*, vol. 21, no. 7, pp. 449–456,
(2013).

[91] T. T. Li, R. Wang, C. W. Lou, and J. H. Lin, "Static and dynamic puncture behaviors
of compound fabrics with recycled high-performance Kevlar fibers," *Compos. Part B
Eng.*, vol. 59, pp. 60–66, (2014).

[92] J. Y. Hu, L. Hes, Y. Li, K. W. Yeung, and B. G. Yao, "Fabric Touch Tester: Integrated
evaluation of thermal-mechanical sensory properties of polymeric materials," *Polym.
Test.*, vol. 25, pp. 1081–1090, (2006).

[93] Y. Wang, J. Wiener, J. Militký, R. Mishra, and G. Zhu, "Ozone Effect on the
Properties of Aramid Fabric," *Autex Res. J.*, vol. 0, no. 0, (2016).

[94] S. Inoue, K. Morita, K. Asai, and H. Okamoto, "Preparation and Properties of Elastic
Polyimide-Silica Composites using Silanol Sol from Water Glass," *J. Appl. Polym.
Sci.*, vol. 92, no. 4, pp. 2211–2219, (2004).

[95] N. Pan and X. Zhang, "Shear Strength of Fibrous Sheets: An Experimental
Investigation," *Text. Res. J.*, vol. 67, no. 8, pp. 593–600, (1997).

**Publications and CV**

CURRICULUM VITAE

**Muhammad Usman Javaid**
E-34/1 Street Number 1 Firdous Park, Lahore Pakistan,
+420773876164, muhammad.usman.javaid@tul.cz

**Education**

**PhD (In progress) Technical University Liberec, Czech Republic**
Major: Textile Technics and Material Engineering
**MIT (2012) Virtual University, Pakistan**
Major: Information Technology
**BSc Engineering (2004) National Textile University, Faisalabad, Pakistan**
Major: Fabric Manufacturing

**Work Experience**

**Lecturer (2009-Present)**
Department of Fabric Manufacturing
National Textile University, Faisalabad, Pakistan

**Fabric Designer and Developer (2008-2009)**
Zephyr Textile Limited, Lahore, Pakistan

**Lecturer (2006-2008)**
Department of Fabric Manufacturing
National Textile University, Faisalabad, Pakistan

**Assistant Weaving Manager (2004-2005)**
Nishat Chunian Mills Limited, Kasur, Pakistan

**Related Journal Publications**

**M. U. Javaid**, et al. "Effect of surface modification of para-Aramid fabrics with Water Glass on their Quasi-Static Knife Penetration Resistance." Journal of Textile Institute, DOI:10.1080/00405000.2018.1496988

**Related Conference Publications**

**M. U. Javaid**, et al. "Effect of Surface Modification of Para-Aramid Fabric on Its Quasi-Static Knife Penetration (QSKP) With Water Glass and Ozone Treatments." Proceedings of workshop Billa Voda, September 2016

**Other Journal Publications**

- Ali, Azam, V. Baheti, **M. U. Javaid**, and J. Militky. "Enhancement in ageing and functional properties of copper-coated fabrics by subsequent electroplating" Applied Physics A, 2018 Vol. 124, No. 9, pp. 651
- M. S. Naeem, S. Javed, V. Baheti, J. Wiener, **M. U. Javaid**, S. Z. Hassan, A. Mazari, and J. Naeem. "Adsorption Kinetics of Acid Red on Activated Carbon Web Prepared from Acrylic Fibrous Waste" Fiber and Polymer, 2018 Vol. 19, No. 1, pp. 71-81
- Jabbar, J. Militky, J. Wiener, **M. U. Javaid**, and S. Rawawiire "Tensile, surface and thermal characterization of jute fibres after novel

treatments" Indian Journal of Fibre & Textile Research Vol. 41, September 2016, pp. 249-254

- K. Shaker, Y. Nawab, **M. U. Javaid**, M. Umair, and M. Maqsood. "Development of 3D Woven Fabric Based Pressure Switch" AUTEX Research Journal, Vol. 15, No 2, June 2015.
- M. Maqsood, Y. Nawab, **M. U. Javaid**, K. Shaker, and M. Umair. "Development of seersucker fabrics using single warp beam and modelling of their stretch-recovery behavior" The Journal of The Textile Institute, 2015 Vol. 106, No. 11, pp. 1154–1160

|            |            |
|------------|------------|
| **Book Chapter** | • A. Jabbar, J. Militky, A. Ali, **M. U. Javaid**, "Investigation of Mechanical and Thermomechanical Properties of Nanocellulose Coated Jute/Green Epoxy Composites" Advances in Natural Fiber Composites, 2018, pp. 175-194, DOI: http://doi.org/10.1007.978-3-319-664641-1_16 |
| **Conference Publications** | • M. Zubair, M. Z. Ahmed, **M. U. Javaid**. "Influence of Fabric Architecture and Material on Physical Properties of 3D Multilayer Woven Fabrics.", Proceedings of 9th Central European Conference 2017, 14th September 2017, Liberec Czech Republic, pp. 135-138<br>• **M. U. Javaid**, et al., "Radiation distribution characterization of fluorescent dyed polyester fabrics at 633 nm wavelength.", Proceedings of workshop Svetlanka, 22-25 September 2015, pp. 73-76.<br>• **M. U. Javaid**, et al. "Viscose Fiber Strength and Degree of Polymerization", Conference: First International Young Engineers Convocation, At University of Engineering, Lahore, April 2014. |
| **Research Projects** | • Member of student grant competition (SGS) project 2017 titled," Development of electrically conductive textile materials (composites) for multi-functional applications", Faculty of Textile, Technical University of Liberec, Czech Republic.<br>• Member of student grant competition (SGS) project 2016, titled, "Nano-basalt filler nanocomposites based on natural fibers: Characterization of mechanical, impact, thermo-mechanical and fire properties.", Faculty of Textile, Technical University of Liberec, Czech Republic.<br>• Leader of the student grant competition (SGS) project 2015, titled, "materials for photodynamic therapy", Faculty of Textile, Technical University of Liberec, Czech Republic. |